University of Colorado, Boulder
Center for Integrated Plasma Studies
and Department of Physics

October 15, 2004

Prof. Richard Temkin
MIT NW16-186
Plasma Science & Fusion Center
167 Albany Street
Cambridge, MA 02139
Phone (617) 253-5528

Fax (617) 253-6078

Re: Nomination of *Kiran Sonnad* for the Outstanding Doctoral Thesis Research in Beam Physics Award

It is a pleasure to nominate Kiran Sonnad for the Outstanding Doctoral Thesis Research in Beam Physics Award of the Division of the Physics of Beams of the American Physical Society. I have known Kiran since he joined my research group in 1999, and in that time I have seen him grow into a mature researcher with in-depth knowledge of accelerator physics. His thesis research meets the established, high standards of excellent beam physics in that it is inventive, novel, and comprehensive. His thesis revolves around the area of nonlinear focusing systems. This work is inventive in that a method for using nonlinearity to mitigate halo formation has been proposed. The novelty is seen in the discovery of a new class of nonlinear accelerator focusing systems that have good integrability properties. The comprehensiveness is seen in the development of analysis of beams with significant space charge. I believe this work will be instrumental in halo mitigation in intense beams.

The first topic (of Ch. 3) of Kiran's thesis grew out of using the constant-focusing, particle-core model for understanding beam halos. In this theory, advanced by O'Connell, Wangler, Mills, and Crandall, the bulk of the beam is represented by an envelope equation that includes the external focusing through a constant term (rather than oscillating, as is actually the case for alternating-gradient focusing). It adds in the defocusing effects of emittance and space charge through other terms. This equation can be solved to find the envelope oscillations that occur when a beam is injected into a focusing system. When the beam is matched, the envelope remains at constant width, but if the focusing is too large or small given the emittance and space charge of the beam, the envelope undergoes

Boulder, Colorado 80309-0390 • (303) 492-1489 • FAX: (303) 492-0642
CARY@COLORADO.EDU

oscillations, and these lead to an electric potential oscillation at twice the betatron frequency.

Halo is understood by injecting test particles into the system – having them evolve in that oscillating potential. One finds that there exist chaotic orbits in this system that can start oscillating at small radii, but then transition to large trajectories, thus creating a halo. In the first part of his thesis, Kiran recaps this work through his own calculations.

Having understood the mechanism of halo generation, Kiran then went on to study a method for eliminating the halo. There had previously been suggestions that one could eliminate halo through collimation, but this proved difficult. Collimation removes the particle instantaneously at large radius, but as long as the oscillation remains, new particles on chaotic trajectories in the interior at the point of collimation move out to large radii. Thus, the halo is regenerated after collimation, and so eliminating halo requires elimination of the core oscillation that leads to chaotic, halo particles.

Kiran's doctoral research proposed to do this through use of a nonlinear focusing channel. With nonlinearity, we know that beam particles of different amplitudes will oscillate with different frequencies. This will lead to phase mixing that will damp away the oscillations. To demonstrate this effect, Kiran developed his own code for calculating how the collection of cylinder making up the beam oscillation self consistently. A sample result is shown in his Fig. 4.1, where one sees clearly how nonlinearity causes the mode to damp away.

The benefit is shown in Fig. 4.2, where test particle trajectories are seen to no longer have large oscillations away from the core. Later in this chapter a full particle-in-cell simulation is presented, and this shows that nonlinear damping of the oscillations followed by collimation can effectively remove the halo. This work has been submitted for publication in Phys. Rev. ST/AB, where it is currently under review.

With the above result, it remained to find systems where one could have strong nonlinear focusing not marred by particle loss through chaotic dynamics. In previous work, Weishi Wan and I had given one approach to this problem. However, Kiran decided to look at the problem from another angle – using Lie

transform perturbation theory. This turned out to be fruitful. Kiran was able to derive a condition for improved integrability. When this condition is satisfied, the Hamiltonian in the transformed system, while being nonlinear, is azimuthally symmetric (to the calculated order) and so integrable to that order. Follow-up numerical calculations have shown that systems satisfying this condition have dramatically larger dynamic apertures than systems that strongly violate this condition. This work has been published in Phys, Rev. E.

The final result of Kiran's thesis is in understanding the self-consistent propagation of beams through such nonlinear, alternating gradient focusing systems. His inspiration was the earlier work of Channel and Davidson in this area. Kiran's work was based on Hamiltonian, Lie-transform theory, which makes it easier to go to higher order. Regardless, an important result of Kiran's work is that the favorable integrability properties of the systems he found are not destroyed by space-charge effects.

Kiran's thesis has the above many results, but it also illustrates a number of theoretical techniques. In doing so, it illustrates Kiran's mastery of these techniques, and it also provides a reference for others to learn from. For example, his thesis illustrates particle-in-cell computations methods for azimuthally symmetric systems. It shows how one can use advanced perturbation methods (Lie transform methods) for studying beam physics problems. Finally, his thesis shows how one can use the methods of nonlinear dynamics, such as surfaces of section, for studying beam physics.

Kiran's work was rewarded by his selection for an invited talk on his work at the 2005 Particle Accelerator Conference to be held in Knoxville. He has also achieved a stable home in the beam physics community by obtaining a job at SLAC.

A good thesis is one that brings new ideas to the field. Kiran's use of Lie-transform perturbation methods for finding integrable systems and for analyzing space-charge effects in such systems has done just that. A great thesis, however, is one that is also timely and leads to new research directions that others pick up on. The letter of Curt Bohn shows that Kiran's work was both timely (NIU had considered pursuing similar ideas) and led to new research directions (that NIU intends to pursue in the future).

In closing, I want to add a personal note that it was been a pleasure to have Kiran in my research group. He required little direction, as he is highly motivated and self-directed. But most importantly, I highly recommend Outstanding Doctoral Thesis Research in Beam Physics Award.

Sincerely yours,

John R. Cary
Professor of Physics

University of Colorado, Boulder
Center for Integrated Plasma Studies
and Department of Physics

October 15, 2004

Contents of the nomination of

Kiran Sonnad

for the

Outstanding Doctoral Thesis Research in Beam Physics Award

Prof. Cary's letter of nomination

Prof. Bohn's seconding letter

Dr. Colestock's seconding letter

Biographical sketch of Dr. Sonnad

List of publications of Dr. Sonnad

Dr. Sonnad's Ph. D. Thesis

Reprint: K. Sonnad and J. R. Cary, "Finding a nonlinear lattice with improved integrability using Lie transform perturbation theory," Phys. Rev. E. 69, 056501 (2004).

Preprint: K. Sonnad and J. R. Cary, "Control of beam halo formation through nonlinear damping and collimation," Phys. Rev. ST/AB (2004) in review.

Boulder, Colorado 80309-0390 • (303) 492-1489 • FAX: (303) 492-0642
CARY@COLORADO.EDU

NORTHERN
ILLINOIS
UNIVERSITY

DEPARTMENT OF PHYSICS

DEKALB, ILLINOIS
60115-2854

(815) 753-1772

Dr. Richard Temkin
MIT NW16-186
Plasma Science & Fusion Center
167 Albany Street
Cambridge, MA 02139
12 October 2004

Dear Dr. Temkin:

I enthusiastically second the nomination of Kiran G. Sonnad for the Outstanding Doctoral Thesis Research in Beam Physics Award. Dr. Sonnad's dissertation, entitled "Nonlinear Focusing in Particle Accelerators: An Application and Its Associated Dynamics" presents an intriguing idea for controlling beam halo. The idea is purposely to impose a nonlinear external focusing force on the beam that establishes a large population of chaotic orbits. These orbits phase-mix rapidly, thereby damping global collective oscillations in the beam that are relics of beam generation. Because these global oscillations are largely responsible for producing beam halo via parametric resonance, their damping would lead one to anticipate no further halo will be produced. The idea is to strip the halo after the global modes have largely damped, after which point the beam is expected to remain halo-free. Sonnad demonstrates the idea by way of numerical simulations, and he also computes semi-analytically the distribution function of the equilibrium beam in the nonlinear focusing force.

I must confess that this novel idea had also occurred to one of my postdoctoral research associates and me some 18 months ago in the course of our research on the dynamics of nonequilibrium beams. Because a nonlinear force also leads to emittance growth and we were concerned with preserving high beam quality, we did not pursue this avenue. Our decision was auspicious in that we did not know at that time that people at Colorado were pursuing it. I think Kirin has done an excellent job pointing out the potential benefits of the idea for halo control. I also believe that there are further questions to investigate before the idea can be considered to be mature, and Kirin's dissertation and related publications will certainly motivate further investigation. In fact, I will soon have one of my graduate students start exploring an aspect of this idea. When an idea triggers further exploratory work, that is a sure sign it is both important and well presented.

In summary, I believe Dr. Sonnad's dissertation is outstanding and is well qualified to be formally recognized as such. I urge the Selection Committee to choose this work for the 2004 Award.

Sincerely,

Courtlandt L. Bohn
Professor of Physics

Los Alamos
NATIONAL LABORATORY

Patrick L. Colestock
H851
Los Alamos National Lab
Los Alamos, NM 87545
Oct 15th, 2004

Thesis Award Selection Committee
Prof. Richard Temkin, Chair

Dear Sirs:

I am writing in support of Kiran Sonnad for the Outstanding Doctoral Thesis Research in Beam Physics Award. This work is exemplary in several ways. It is well-written and comprehensive; it is self-contained and forms an excellent reference for others interested in nonlinear focusing and related mathematical techniques, such as Lie transform methods; and most importantly, it addresses an outstanding issue, perhaps one of the most important issues today, in beam physics: the production of halo in intense beams.

The production of beam halo has been shown both experimentally and theoretically to be an important potential limitation to intense beam operation due to significant uncontrolled particle losses, or to the consequent cost of increasing beam apertures to accommodate unusually large beam sizes created by the combined effects of betatron and space charge-induced oscillations. It has been a topic of considerable study in recent years driven by the need to manage beam transport in such devices as the Spallation Neutron Source. While progress has been made on understanding the causes of halo production, up until the work of this thesis, very little has been done to devise means by which the halo could be controlled, or even eliminated. This work offers the first description of methods that can be pursued to solve this issue.

The particular benefit of this work is the demonstration of systematic analytical techniques that can be applied to ensure adequate dynamic aperture. It comes as somewhat of a surprise that the favorable integrability of the system persists even in the presence of strong space charge forces. This is a key new result. A consequence of his analytical and numerical work is a clear demonstration that beam halo can be minimized under the influence of nonlinear focusing elements. Kiran has devised a clean way of assembling such a focusing system. It is appropriate and laudable that he was selected for an invited paper at the forthcoming Particle Accelerator Conference.

Another aspect of this dissertation that I particularly appreciate is the clear and insightful way it is written. I found the structure logical and complete, the language precise and the explanations comprehensive. In particular I appreciate the combination of analytical and numerical work he brought together to achieve his new results.

In summary, I find this work to be both timely and innovative, addressing a very important issue in beam physics. I support him with no reservations for this award.

Sincerely,

Patrick L. Colestock

Patrick L. Colestock

SHORT BIO of Kiran Sonnad

Education

Ph. D., Physics, University of Colorado, Boulder, CO. (2004)
(Thesis advisor - Prof. John R. Cary)
M.S., Physics, University of Missouri, Rolla, MO. (1998)
BSc. in Physics and Mathematics, The National College, Bangalore, India

Employment History

10/04- Staff Member, Stanford Linear Accelerator Laboratory
1999-2004, Graduate Research Assistant, University of Colorado

RECENT PUBLICATIONS of Kiran Sonnad

K. Sonnad and J. R. Cary, "Finding a nonlinear lattice with improved integrability using Lie transform perturbation theory," Phys. Rev. E 69, 056501 (2004).

K. Sonnad and J. R. Cary, "Control of beam halo formation through nonlinear damping and collimation," Phys. Rev. ST/AB (2003) in review, draft available.

K. Sonnad and J. R. Cary, "A Lie transform perturbation scheme for Hamiltonian averaging in self-consistent systems," Proc. Part. Accel. Conf., Vol 3, p. 1536-1538 (Portland, 2003).

K. Sonnad and J. R. Cary, "The effect of nonlinear transport on beam halo formation," Proc. Part. Accel. Conf., Vol 4, p. 2997-2999 (Chicago, 2001).

Nonlinear Focusing in Particle Accelerators: An application and its associated dynamics

by

Kiran G. Sonnad

B.Sc., National College, Bangalore, India 1995

M.S., University of Missouri, Rolla, MO 1998

A thesis submitted to the

Faculty of the Graduate School of the

University of Colorado in partial fulfillment

of the requirements for the degree of

Doctor of Philosophy

Department of Physics

2004

This thesis entitled:
Nonlinear Focusing in Particle Accelerators: An application and its associated dynamics
written by Kiran G. Sonnad
has been approved for the Department of Physics

John R. Cary

Prof. Scott Robertson

Date

The final copy of this thesis has been examined by the signatories, and we find that both the content and the form meet acceptable presentation standards of scholarly work in the above mentioned discipline.

Sonnad, Kiran G. (Ph.D., Physics)

Nonlinear Focusing in Particle Accelerators: An application and its associated dynamics

Thesis directed by Prof John R. Cary

The use of nonlinear focusing in particle accelerators has been proposed in a variety of applications. This work proposes and studies yet another application and analyzes the dynamics associated with nonlinear focusing. To begin with, it is proposed that beam halos can be controlled by combining nonlinear focusing and collimation, which is verified by numerical simulations. The study relies on a one dimensional, continuous focusing Particle-in-Cell (PIC) model and a Particle-Core model. Results from the PIC simulations establish the importance of reducing the mismatch of the beam in order to reduce halo formation. It is then shown that nonlinear focusing leads to damping of the beam oscillations thereby reducing the mismatch. This damping is accompanied by emittance growth causing the beam to spread in phase space. To compensate for this, the beam is collimated, and further evolution of the beam shows that the halo is not generated. The use of the idealized, one-dimensional, continuous focusing model is justified by analyzing nonlinear alternate gradient focusing systems. The Lie Transform perturbation theory is used to derive an equivalent continuous focusing system for the alternate gradient focusing channel by canonically averaging over the lattice or fast oscillating time scale. The analysis shows the existence of a condition in which the system is azimuthally symmetric in the canonically transformed, slowly oscillating frame. Numerical results show that this condition leads to reduced chaos and improved confinement in the charged particle motion. The Lie Transform analysis is then extended to include space charge effects which enables one to calculate a near equilibrium distribution function which is azimuthally symmetric in the nonlinear lattice.

Acknowledgements

This work has been made possible as a result of the guidance and support of many individuals during and before beginning my doctoral work. Professor John Cary, my thesis advisor, has been the primary source of guidance, support and inspiration not only for this work but also in my overall professional development. I wish to offer my sincere gratitude to Professors Scott Parker, Scott Robertson, James Miess and William Ford for serving in my thesis committee. I also had useful discussions through courses and informally with Professor Raul Stern on basic plasma physics, Professor Scott Parker on computational physics, Dr James Howard on nonlinear dynamics, Professor Scott Robertson on experimental plasma physics and Professor Leo Radzihovsky on statistical mechanics. The courses taught by Dr Steve Holmes, Dr John Banard and Dr Steve Lund at the US Particle Accelerator School were invaluable in providing a basic understanding of accelerator physics. Discussions on and/or beyond the subject matter with colleagues Jinhyung Lee, Rodolfo Giacone, Chet Nieter, Brent Goode, Samuel Jones, Charlson Kim, Srinath Vadlamani and Zoltan Sternovsky were directly beneficial to this work and in making my stay in Boulder more enjoyable. Help on administrative matters from Carolyn James made many things easier. Last but not the least, I wish to acknowledge my Masters degree thesis advisor Prof. John Carstens at the University of Missouri, Rolla who first introduced me to research.

This work would not have been possible without the financial support from the Department of Energy.

Contents

Tables

Table

Figures

Figure

Chapter 1

Introduction

Particle accelerators find applications in almost every branch of physics. They are used not only in the analysis of physical, chemical and biological samples but also modification of the physical, chemical and biological properties of matter in applications varying from material sciences to medical physics. The most energetic beams are used in subatomic physics research. A rapidly growing application of particle accelerators is synchrotron radiation sources. New applications under active development include spallation sources, X-ray emitting Free Electron Lasers and heavy ion fusion. Improvement in the current applications and realizing future applications demand the need for improved performance of the accelerating systems. This would mean improved confinement of the particles, higher energies, more intense beams, improved dynamic aperture, higher luminosity etc. The various challenges to be overcome to meet these demands include space charge effects, energy loss due to synchrotron radiation, beam halos, non-linear effects, production of electron clouds, instabilities, beam-beam interactions etc. These demands have made the theoretical understanding of the dynamics of charged particles and the study of collective effects of beams in particle accelerators increasingly important.

The common accelerators such as cyclic and linear accelerators and storage rings rely upon alternating gradient quadrupole magnets for the purpose of focusing in the direction transverse to the motion of the beam. This system and other models which

incorporate linear focusing have been studied extensively. It is clear that linear focusing forces are desirable because nonlinear oscillations of the particles lead to chaotic motion and loss in confinement. Despite this, nonlinear focusing of various forms are gaining importance in a variety of applications and are being proposed for a number of current and future projects. This thesis will present yet another proposal for applying nonlinear focusing to beam halo mitigation and also make a detailed analysis of the dynamics associated with such a system. This analysis will be extended to examine the equilibrium properties in the nonlinear focusing channel. These studies can in turn prove useful to other applications of nonlinear focusing as well.

Since nonlinear focusing systems have not been studied extensively, it becomes important that whenever an application of such a system is proposed, all the problems associated with it are systematically analyzed and the results verified through numerical computations before being considered for experiments. With such a broad goal, this thesis brings together aspects of computational physics, nonlinear dynamics and perturbation analysis making this work of interest to other areas of physics as well where such tools are used.

To begin with, an overview of some of the established theories related to linear focusing systems with respect to transverse motion of the particles is presented in Chapter 2. In general, none of these theories are valid when a nonlinear term is added to the respective focusing force. Chapter 3 will first describe the mechanism behind beam halo formation in space charge dominated beams. This will be followed by a study of applying a combination of nonlinear focusing and collimation to control the beam halo. The study relies on a continuous focusing model and the calculations use a radial particle-in-cell (PIC) code as well as a particle-core model. Chapter 5 will introde Lie Transform perturbation analysis which will be used to derive a condition for designing a nonlinear alternate gradient focusing transport system with improved integrability in chapter 6. This condition will provide a relationship between a nonlinear

alternate gradient lattice (arrangement of the focusing components) and an equivalent azimuthally symmetric, continuous focusing channel that was used as a model in the previous chapter. Numerical calculations are performed in order to track the motion of the particles which show that confinement dramatically improves with improved integrability. The Lie transform analysis is extended to high intensity beams in chapter 7. High intensity beams are self consistent systems. In other words, they include space charge forces. Using the analysis developed in this chapter, an equilibrium distribution is derived which retains the conditions of near integrability and azimuthal symmetry when the same conditions of lattice design derived in the previous chapter are satisfied. Distributions that are perturbed from equilibrium distributions are of use in analyzing different modes of oscillations, stabilities and resonances.

The results are summarized in chapter 8 along with a conclusion and possible future directions in which this work can be extended and applied. Appendix A and B provide details of the numerical schemes used in the calculations performed in this work. The emphasis in this thesis is broad even within the domain of beam physics and is intended to have a lasting appeal to researchers and students interested in a variety of areas within and beyond beam physics.

Chapter 2

Some Aspects of Linear Focusing

This chapter provides a brief overview based on some pioneering work related to linear focusing models in particle accelerators. It will begin with the Courant-Snyder theory associated with the dynamics of a single particle satisfying Hill's equation. This will show the existence of a closed form solution for the trajectory of a charged particle in an alternate gradient quadrupole channel. The analysis will then move to beams with space charge effects in which the rms envelope equation, and the Kapchinskij-Vladmirskij (KV) equilibrium distribution will be derived. All of the analysis in this chapter deals with motion transverse to the propagation of the beam. The material in this chapter is based on some popular books on accelerator physics [22, 66, 16, 50] and from notes provided in courses at the US Particle Accelerator Schools [33, 3].

2.1 Transverse Motion of Single Charged Particles

2.1.1 Alternate Gradient Quadrupoles and Focusing

Focusing in accelerators is required to keep the particles from drifting away from the desired trajectory which is usually called the reference orbit. Particle beams are made up of collections of particles and it is impossible to have a system in which they all travel along the intended direction all the time. In storage rings, it is required to keep the particles from wandering away for hundreds of thousands of revolutions. Such a focusing is accomplished with the help of quadrupole magnets.

A quadrupole magnet has a nonuniform magnetic field that is proportional to the distance from the center. It is impossible to obtain a magnetic field in vacuum that produces restoring forces in both transverse degrees of freedoms simultaneously. However, it is still possible to obtain a stable, net focusing system from magnets with alternating polarities or gradients. Alternate gradient focusing was discovered in 1952 by Courant, Livingstone, Snyder and Christofilos [15, 14, 13].

In the absence of any current density, the magnetic field satifies the condition $\nabla \times \vec{B} = 0$ which leads to

$$\frac{\partial B_y}{\partial x} = \frac{\partial B_x}{\partial y} \tag{2.1}$$

where x and y are the coordinates transverse to the propagation of the beam. For displacements that are small from the reference orbit, the magnetic field may be expressed as

$$\vec{B} = B_x\hat{x} + B_y\hat{y} = \left(B_x(0,0) + \frac{\partial B_x}{\partial y}y + \frac{\partial B_x}{\partial x}x\right)\hat{x} + \left(B_y(0,0) + \frac{\partial B_y}{\partial x}x + \frac{\partial B_y}{\partial y}y\right)\hat{y} \tag{2.2}$$

In quadrupole magnets, the dipole terms $B_x(0,0)$ and $B_y(0,0)$ are zero. Assuming that the particle is moving in the z direction, it is easy to see that the last term of each component of the magnetic field produces a force that is perpendicular to the displacement and cannot be regarded as a restoring force. The remaining coefficients of x and y are equal according to Eq. (2.1). From the Lorentz force, one can easily see that if one of these coefficients produces a focusing, or restoring force, the other one produces a defocussing force. A quadrupole magnet can be produced by hyperbolic pole shapes as shown in Fig. 2.1 The magnetic field produced by these magnets to a good approximation is given by,

$$B_y = B_0\frac{x}{a} \tag{2.3}$$

$$B_x = B_0\frac{y}{a} \tag{2.4}$$

where B_0 is the magnetic field at a characteristic distance a from the center.

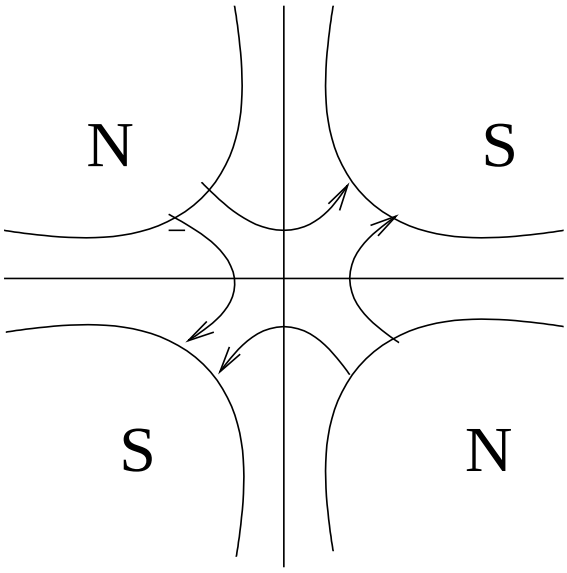

Figure 2.1: Design of a quadrupole magnet

From an analogy with optics, one can associate a focal length to a quarupole magnet using the thin lens approximation. We imagine a charged particle moving through the quadrupole at a distance x from the magnet's axis of symmetry. The thin lens approximation implies that the length of the magnet, l, is short enough that the displacement x is unaltered as the particle passes through the magnet and hence the magnetic field experienced by the particle, $B_y = B_0 x/a$, is constant along the particle trajectory. The paraxial approximation assumes the angle with respect to the direction along the reference orbit is equal to the slope of the particle's trajectory, ie, $x' = dx/ds$ where s is the distance measured along the reference orbit. As shown in Figure 2.2, the slope of the particle's trajectory will be altered by an amount

$$\Delta x' = -\frac{l}{\rho} = -l\left(\frac{eB_y}{p}\right) = -\left(\frac{eB_0 l}{pa}\right)x \tag{2.5}$$

where ρ is the radius of curvature of the trajectory and p the momentum of the particle along the axial direction.

Since a ray parallel to the optic axis will be bent toward the focal point of the lens, as shown in Figure 2.3, the change in slope is simply $\Delta x' = -x/f$, where f is the

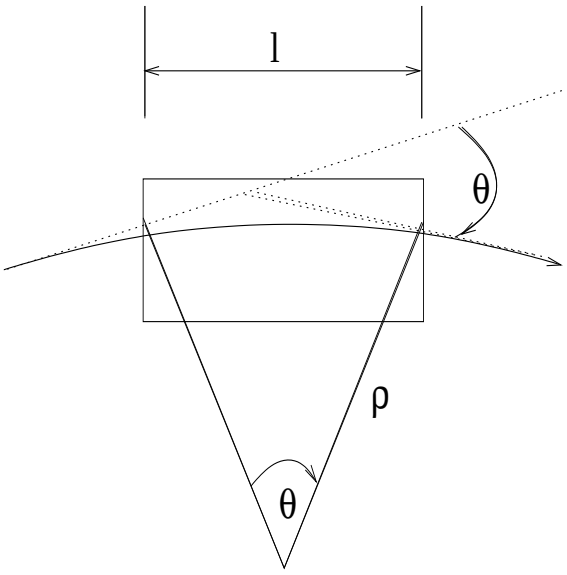

Figure 2.2: Deflection of a particle across a thin quadrupole

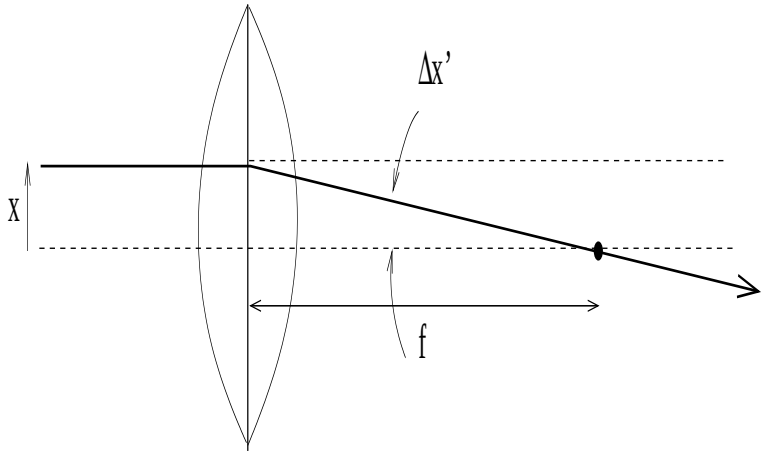

Figure 2.3: Ray initially parallel to the optic axis that bends and passes the focal point

focal length of the quadrupole lens. The focal length is thus given by

$$\frac{1}{f} = \frac{eB_0 l}{pa} \tag{2.6}$$

Equation 2.5 may be expressed in matrix form as

$$\left| \begin{array}{c} x \\ x' \end{array} \right|_{out} = \left| \begin{array}{cc} 1 & 0 \\ -\frac{1}{f} & 1 \end{array} \right| \left| \begin{array}{c} x \\ x' \end{array} \right|_{in} \tag{2.7}$$

For a defocussing (concave) lens, the focal length is of opposite sign. The motion in

free space, between two lenses is referred as a drift. For a drift along a length L, the transformation matrix is ,

$$\begin{vmatrix} x \\ x' \end{vmatrix}_{out} = \begin{vmatrix} 1 & L \\ 0 & 1 \end{vmatrix} \begin{vmatrix} x \\ x' \end{vmatrix}_{in} \tag{2.8}$$

It is well known from geometrical optics that a combination of equal strength convex and concave lenses will produce net focusing. As an example, one can calculate the transfer matrix across a lattice which consists of equally spaced focusing and defocussing lenses which begins with a focusing lens, then a drift of length L, third a defocussing lens, and finally another drift of length L. This is often referred to as a FODO lattice. This transformation matrix may be evaluated to give,

$$M = \begin{vmatrix} 1 - \frac{L}{f} - \left(\frac{L}{f}\right)^2 & 2L + \frac{L^2}{f} \\ -\frac{L}{f^2} & 1 + \frac{L}{f} \end{vmatrix} \tag{2.9}$$

At least in the case where L is small when compared to f, it is clear that there is net focusing by comparing with Eq. 2.7. In this approximation the resulting matrix is that of a thin lens of net focal length $f^2/L > 0$. If the two lenses were interchanged, the net result would still be focusing. Hence a system of alternating gradient thin quadrupole magnets, could in principle, focus in both degrees of freedom simultaneously. Moreover, it is possible to show that the motion is stable provided the focal length is greater than half the lens spacing [22]. That is,

$$\left|\frac{L}{2f}\right| \leq 1 \tag{2.10}$$

2.1.2 Equations of Motion

It is now straight forward to write the equations of motion for a particle with constant axial momentum. Consider a particle passing through a quadrupole lens along a distance Δs. Then from Equation 2.5, we have

$$\frac{\Delta x'}{\Delta s} = -\left(\frac{eB_0(s)}{pa}\right) x \tag{2.11}$$

Taking the limit as $\Delta s \to 0$, we obtain the second order differential equation

$$x'' + \left(\frac{eB_0}{pa}\right) x = 0. \tag{2.12}$$

This equation arises in the special case where the design trajectory is a straight line. Suppose the path along the reference orbit has a local curvature ρ_0, which is the case in the presence of a dipole magnet, then the equations would be modified to [22]

$$\frac{d^2x}{ds^2} + \left[-\frac{1}{\rho_0} + \frac{eB_0}{pa}\right] x = 0 \tag{2.13}$$

and

$$\frac{d^2y}{ds^2} - \left[\frac{eB_0}{pa}\right] y = 0 \tag{2.14}$$

The curvature term $1/\rho_0$ is generally very small when compared to the focusing term. These equations may be expressed in the form

$$x'' + \kappa_x(s)x = 0 \tag{2.15}$$

$$y'' + \kappa_y(s)y = 0 \tag{2.16}$$

where,

$$\left.\begin{aligned} \kappa_x(s) &= \tfrac{1}{\rho_0^2} \\ \kappa_y(s) &= 0 \end{aligned}\right\} \text{ in dipole} \tag{2.17}$$

$$\kappa_x(s) = \kappa_y(s) = 0\} \quad \text{in drift} \tag{2.18}$$

$$\left.\kappa_x(s) = -\kappa_y(s) = \frac{eB_0}{pa}\right\} \quad \text{in quadrupoles} \tag{2.19}$$

These differential equations are homogeneous as long as the particles do not have a momentum that is offset from the reference orbit. The equation of motion for x looks like a harmonic oscillator with a time varying spring constant, a form of Hill's equation. To solve this equation, we look for a solution of the form

$$x(s) = A_x\sqrt{\beta_x(s)}\cos(\phi_x(s) - \phi_0) \tag{2.20}$$

Differentiating this with respecting to s gives

$$x'(s) = \frac{A_x}{2\sqrt{\beta_x(s)}}\frac{d\beta_x}{ds}\cos(\phi_x(s)-\phi_0) - A_x\sqrt{\beta_x(s)}\frac{d\phi_x}{ds}\sin(\phi_x(s)-\phi_0) \tag{2.21}$$

and the second derivative is,

$$\begin{aligned} x'' &= -\frac{A_x}{4\beta_x^{3/2}}\left(\frac{d\beta_x}{ds}\right)^2\cos(\phi_x(s)-\phi_0) \\ &+ \frac{A_x}{2\beta_x^{1/2}}\frac{d^2\beta_x}{ds^2}\cos(\phi_x(s)-\phi_0) \\ &- \frac{A_x}{2\beta_x^{1/2}}\frac{d\beta_x}{ds}\frac{d\phi_x}{ds}\sin(\phi_x(s)-\phi_0) \\ &- \frac{A_x}{2\beta_x^{1/2}}\left(\frac{d\beta_x}{ds}\right)\left(\frac{d\phi_x}{ds}\right)\sin(\phi_x(s)-\phi_0) \\ &- A_x\beta_x^{1/2}\left(\frac{d\phi_x}{ds}\right)^2\cos(\phi_x(s)-\phi_0) \\ &- A_x\beta_x^{1/2}\frac{d^2\phi_x}{ds^2}\sin(\phi_x(s)-\phi_0) \end{aligned} \tag{2.22}$$

Substituting this into Eq. 2.15 and collecting the sin and cosine terms, we get

$$\begin{aligned} & A_x[-\frac{1}{4\beta_x^{3/2}}\left(\frac{d\beta_x}{ds}\right)^2 + \frac{1}{2\beta_x^{1/2}}\frac{d^2\beta_x}{ds^2} \\ - \;& \beta_x^{1/2}\left(\frac{d\phi_x}{ds}\right)^2 + \kappa_x\beta_x^{1/2}]\cos(\phi_x(s)-\phi_0) \\ + \;& A_x[-\frac{1}{\beta_x^{1/2}}\left(\frac{d\beta_x}{ds}\right)\left(\frac{d\phi_x}{ds}\right) - \beta_x^{1/2}\frac{d^2\phi_x}{ds^2}]\sin(\phi_x(s)-\phi_0) = 0 \end{aligned} \tag{2.23}$$

Each coefficient has to equal to zero.

We look at the coefficient of $\sin(\phi_x(s)-\phi_0)$ first. This gives,

$$\left(\frac{d\beta_x}{ds}\right)\left(\frac{d\phi_x}{ds}\right) + \beta_x\frac{d^2\phi_x}{ds^2} = 0 \tag{2.24}$$

Combining these leads to,

$$\frac{d}{ds}\left(\beta_x\frac{d\phi_x}{ds}\right) = 0, \tag{2.25}$$

which gives,

$$\beta_x\frac{d\phi_x}{ds} = \text{constant} = 1. \tag{2.26}$$

So,

$$\frac{d\phi_x}{ds} = \frac{1}{\beta_x} \tag{2.27}$$

Equating the coefficients of $\cos(\phi_x(s) - \phi_0)$, we obtain

$$-\frac{1}{4\beta_x^{3/2}}\left(\frac{d\beta_x}{ds}\right)^2 + \frac{1}{2\beta_x^{1/2}}\frac{d^2\beta_x}{ds^2} - \beta_x^{1/2}\left(\frac{d\phi_x}{ds}\right)^2 + \kappa_x\beta_x^{1/2} = 0 \tag{2.28}$$

or, from Eq. (2.27) this may be rewritten as,

$$2\beta_x\frac{d^2\beta_x}{ds^2} - \left(\frac{d\beta_x}{ds}\right)^2 + 4\beta_x^2\kappa_x = 4 \tag{2.29}$$

It may be noted that since $\kappa_x \neq \kappa_y$, β_x is different from β_y. The differential equation for β_x (or β_y) is not easily solvable as it stands. This can be solved using matrix techniques, which will not be done here.

2.1.3 Courant-Snyder Invariant

Let us define

$$\alpha_x(s) = -\frac{1}{2}\frac{d\beta_x}{ds} \tag{2.30}$$

We know that the motion is of the form

$$x(s) = A_x\sqrt{\beta_x(s)}\cos(\phi_x(s) - \phi_0) \tag{2.31}$$

Differentiating this with respect to s yields,

$$\frac{dx}{ds} = \frac{1}{2}\frac{A_x}{\beta_x^{1/2}}\frac{d\beta_x}{ds}\cos(\phi_x(s) - \phi_0) - A_x\beta_x^{1/2}\frac{d\phi_x}{ds}\sin(\phi_x(s) - \phi_0) \tag{2.32}$$

Simplifying this by using Eq. 2.30, Eq. 2.31 and Eq. 2.27, we get

$$x'(s) = -\frac{\alpha_x}{\beta_x}x + \frac{A_x}{\beta_x^{1/2}}\sin(\phi_x(s) - \phi_0), \tag{2.33}$$

which may be rewritten as,

$$\beta_x x' + \alpha_x x = A_x\sqrt{\beta_x}\sin(\phi_x(s) - \phi_0). \tag{2.34}$$

So,

$$x^2 + (\beta_x x' + \alpha_x x)^2 = A_x^2 \beta_x [\cos^2(\phi_x(s) - \phi_0) + \sin^2(\phi_x(s) - \phi_0)] \tag{2.35}$$

or,

$$A_x^2 = \frac{x^2 + (\beta_x' + \alpha_x)^2}{\beta_x} = \text{constant of motion} \tag{2.36}$$

This constant is known as the Courant-Snyder invariant. Figure 2.4 shows a graphical representation of the trajectory of a particle satisfying the equation of motion in a quadrupole focusing channel. This proves the existence of a closed form solution for the motion of a particle in a quadupole focusing channel.

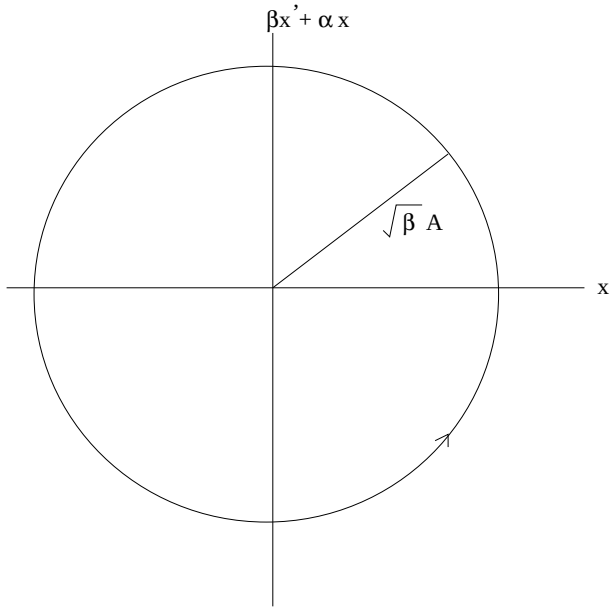

Figure 2.4: Graphical representation of particle trajectory

2.2 Beams with Space Charge Effects

This section will deal with high intensity beams where the effect of space charges cannot be neglected. In general, problems associated with such a system involves solving the implicit Vlasov-Poisson equations which is usually done computationally with the help of a Vlasov-fluid code, or Particle-in-cell (PIC) simulation. However, two re-

markable analytical results exist which form the basis of a lot of analysis of beams with space charge effects under linear focusing.

2.2.1 The RMS Envelope Equation

Consider a beam moving in the s direction, where individual particles satisfy the equations of transverse motion

$$x'' + \kappa(s)x - F_{sc} = 0 \tag{2.37}$$

The linear external force is given by $-\kappa(s)x$, and F_{sc} is the space-charge force term, which is in general nonlinear and includes both the self electric and self magnetic forces. It is assumed that the beam is very long compared to its characteristic width, and there are no forces along the s direction. For the sake of simplicity, we assume that the particles are distributed about a mean position at $x = y = 0$. First we write the equations of motion for the second moments of the distribution. These are,

$$\frac{d\langle x^2\rangle}{ds} = 2\langle xx'\rangle \tag{2.38}$$

$$\frac{d\langle xx'\rangle}{ds} = \langle x'^2\rangle + \langle xx''\rangle = \langle x'^2\rangle - \kappa(s)\langle x^2\rangle + \langle xF_{sc}\rangle \tag{2.39}$$

where the angle brackets $\langle \ldots \rangle$ represents an average over the particle distribution in position space. If the rms size of the beam is denoted by $a_x = \sqrt{\langle x^2\rangle}$, then by using Eq. (2.38) we have

$$a_x a_x' = \langle xx'\rangle \tag{2.40}$$

Differentiating this and using Eq. (2.39) gives

$$a_x'' - \frac{\langle x^2\rangle\langle x'^2\rangle - \langle xx'\rangle^2}{a_x^3} - \frac{\langle xx''\rangle}{a_x} = 0 \tag{2.41}$$

At this point, we define a quantity ϵ_x known as the rms emittance which is given by

$$\epsilon_x = 4\sqrt{\langle x^2\rangle\langle x'^2\rangle - \langle xx'\rangle^2} \tag{2.42}$$

The properties of ϵ_x will be analyzed in the next section. Eliminating x'' by combining Eq. (2.37) and Eq. (2.41) yields

$$a'' + \kappa(s)a - \frac{\epsilon_x^2}{a^3} - \frac{\langle xF_{sc}\rangle}{a} = 0 \tag{2.43}$$

For a bean with uniform distribution over an ellipse, the x and y components of the Electric field inside the ellipse can be computed by Gauss' law and are given by

$$E_x = \frac{I}{\pi\epsilon_0 v(R_x + R_y)}\frac{x}{R_x} \tag{2.44}$$

$$E_y = \frac{I}{\pi\epsilon_0 v(R_x + R_y)}\frac{y}{R_x} \tag{2.45}$$

where R_x and R_y are the semiaxes of the ellipse, related to the rms beam sizes by $R_x = 2a_x$ and $R_y = 2a_y$, v is the velocity of the particle along s, I is the beam current, ϵ_0 is the free space permitivity. Using these expressions for electric fields, in Eq. (2.43), we get

$$R_x'' + \kappa(s)R_x - \frac{\epsilon_x^2}{R_x^3} - \frac{K_p}{2(R_x + R_y)} = 0 \tag{2.46}$$

$$R_y'' + \kappa(s)R_y - \frac{\epsilon_y^2}{R_y^3} - \frac{K_p}{2(R_x + R_y)} = 0 \tag{2.47}$$

where the quantity K_p is a constant called the generalized perveance. The force arising from a magnetic field has the same form as the electric field, which can be verified by solving Ampere's law instead of Gauss' law. This introduces an additional factor in the expression for K_p. Taking into account this additional effect, the perveance is given by

$$K_p = qI/2\pi\epsilon_0 m\gamma^3 v^3, \tag{2.48}$$

where, q is the charge of the particles, ϵ_0 is the free space permitivity, m is the mass of the particle, γ is the relativistic Lorentz factor and v is the axial velocity of the particle. These equations were derived by Kapchinsky and Vladmirsky [38] and are known as the K-V envelope equations. It was later proved by Lapostolle [41] and independently by Sacherer [54] that these equations are valid not only for uniform distributions but for all distributions with elliptical symmetry with a beam "Radius" of $R_x = 2a_x$ and $R_y = 2a_y$.

2.2.2 Properties of Beam Emittance

We now examine the properties of the beam rms emittance. To start with, we show that when the particle equation of motion is $x'' = \kappa(s)x$, the rms emittance is a conserved quantity. Beginning with the definition of emittance, given by Eq. 2.42, we have,

$$\epsilon_x^2 = 16[\langle x'^2\rangle\langle x^2\rangle - \langle xx'\rangle^2] \tag{2.49}$$

Differentiating this, we get

$$\frac{d\epsilon_x^2}{ds} = 16[\frac{d\langle x'^2\rangle}{ds}\langle x^2\rangle + \langle x'^2\rangle\frac{d\langle x^2\rangle}{ds} - 2\langle xx'\rangle(\langle xx''\rangle + \langle x'^2\rangle)] \tag{2.50}$$

This may be simplified to

$$\frac{d\epsilon_x^2}{ds} = 16[2\langle x'x''\rangle\langle x^2\rangle + 2\langle x'^2\rangle\langle xx'\rangle - 2\langle xx'\rangle\langle xx''\rangle - 2\langle xx'\rangle\langle x'^2\rangle] \tag{2.51}$$

where the second and fourth terms cancel. Using $x'' = \kappa(s)x$, and the fact that $\kappa(s)$ can be factored out of the averaging, we get

$$\frac{d\epsilon_x^2}{ds} = 64\kappa(s)[\langle xx'\rangle\langle x^2\rangle - \langle xx'\rangle\langle x^2\rangle] = 0 \tag{2.52}$$

Thus, the emittance is a conserved quantity as long as the the forces on the particles are linear. The space charge force is linear for a uniform distribution elliptical beam as shown in Eq. (2.44). Thus, the emittance can be regarded as a conserved quantity in the envelope equation under certain restrictions. The envelope equation has been used extensively to study beams with space charge effects.

2.2.3 The Kapchinskij-Vladmirskij Beam Equilibria

It is often important to determine an equilibrium beam distribution. Beams that are perturbed from this equilibrium distribution are analyzed to study different modes of oscillations, instabilities and resonances. The only known equilibrium distribution

for a linear focusing system is the Kapchinskij-Vladmirskij (KV) [38] distribution which has been used extensively to study high intensity beams.

An equilibrium here refers to a phase space distribution function that depends upon the invariants of the motion. This is known as a Vlasov equilibrium which is a stationary solution to the Vlasov equation. The Vlasov equation in Hamiltonian formalism is given by

$$\frac{\partial f}{\partial s} = \{f, H\} \tag{2.53}$$

where, f is the phase space density, H is the Hamiltonian, and $\{\ \}$ represents the Poisson bracket. Any phase space function of the invariants of the motion commutes with the Hamiltonian, *ie* is equal to zero in a Poisson bracket operation giving a stationary solution of the Vlasov equation which corresponds to a Vlasov equilibrium.

In this section, it will be shown that a beam with a uniform charge distribution over an ellipse is indeed such an equilibrium under linear focusing. The Hamiltonian of a long beam with space charge effects and neglecting longitudinal effects is given by

$$H = \frac{1}{2}(x'^2 + y'^2) + \frac{1}{2}\kappa_x(s)x^2 + \frac{1}{2}\kappa_y(s)y^2 + \psi(x, y, s) \tag{2.54}$$

The term $\psi(x, y, z)$ arises due to the effect of the space charge perveance. In the specific case of a uniform charge distribution over an ellipse $(x^2/R_x^2 + y^2/R_y^2) < 1$, Eqs. (2.44 and 2.45) can be used to show that

$$\psi(x, y, s) = -[K_p/(R_x + R_y)](x^2/R_x + y^2/R_y) \tag{2.55}$$

and this Hamiltonian may now be rewritten as

$$H = \frac{1}{2}(x'^2 + y'^2) + \frac{1}{2}K_x(s)x^2 + \frac{1}{2}K_y(s)y^2 \tag{2.56}$$

where

$$K_x = \kappa_x(s) - \frac{K_p}{R_x(R_x + R_y)} \tag{2.57}$$

and

$$K_y = \kappa_y(s) - \frac{K_p}{R_y(R_x + R_y)} \tag{2.58}$$

A canonical transformation is now performed by introducing a generating function of the second kind, $F_2(x, y, X', Y')$. This transformation simplifies the Hamiltonian which in turn helps identify constants of motion. At this point, we define functions $w_x(s) = R_x/\epsilon_x^{1/2}$. $w_y(s) = R_y/\epsilon_y^{1/2}$. The function F_2 that will be used is,

$$F_2(x, y, X', Y') = \frac{x}{w_x(s)}\left[X' + \frac{1}{2}x\frac{dw_x(s)}{ds}\right] + \frac{y}{w_y(s)}\left[Y' + \frac{1}{2}y\frac{dw_y(s)}{ds}\right] \tag{2.59}$$

The new phase space variables will satisfy the following,

$$\begin{aligned} X &= \frac{\partial F_2}{\partial X'} = \frac{x}{w_x}, \\ Y &= \frac{\partial F_2}{\partial Y'} = \frac{y}{w_y}, \\ x' &= \frac{\partial F_2}{\partial x} = \frac{1}{w_x}\left[X' + x\frac{dw_x}{ds}\right], \\ y' &= \frac{\partial F_2}{\partial y} = \frac{1}{w_y}\left[Y' + y\frac{dw_y}{ds}\right]. \end{aligned} \tag{2.60}$$

Solving for X' and Y' gives,

$$\begin{aligned} X' &= w_x x' - x\frac{dw_x}{ds}, \\ Y' &= w_y y' - y\frac{dw_y}{ds}. \end{aligned} \tag{2.61}$$

The transformed Hamiltonian is given by $K = H + \partial F_2/\partial s$. From the envelope equations (2.46) and (2.47) it can be seen that the second derivatives of $w_x(s)$ and $w_y(s)$ are given by

$$\begin{aligned} \frac{d^2}{ds}w_x(s) + K_x(s)w_x(s) &= \frac{1}{w_x(s)} \\ \frac{d^2}{ds}w_y(s) + K_y(s)w_y(s) &= \frac{1}{w_y(s)} \end{aligned} \tag{2.62}$$

Using these to calculate the new Hamiltonian, we get

$$K(X, Y, X', Y') = \frac{1}{2w_x^2(s)}[X'^2 + X^2] + \frac{1}{2w_y^2(s)}[Y'^2 + Y^2] \tag{2.63}$$

The equations of motion may now be determined for the new variables. They are,

$$\begin{aligned}
\frac{d}{ds}X' &= -\frac{1}{w_x^2(s)}X(s), \\
\frac{d}{ds}Y' &= -\frac{1}{w_y^2(s)}Y(s), \\
\frac{d}{ds}X &= \frac{1}{w_x^2(s)}X'(s), \\
\frac{d}{ds}Y &= \frac{1}{w_y^2(s)}Y'(s).
\end{aligned} \tag{2.64}$$

Solving these equations gives,

$$\begin{aligned}
X(s) &= X_0 \cos[\psi_x(s, s_0)] + X_0' \sin[\psi_x(s, s_0)] \\
Y(s) &= Y_0 \cos[\psi_y(s, s_0)] + Y_0' \sin[\psi_y(s, s_0)],
\end{aligned} \tag{2.65}$$

where,

$$\psi_x(s, s_0) = \int_{s_0}^{s} \frac{ds}{w_x^2(s)}. \tag{2.66}$$

In Eq. (2.65), $X(s)$ and $X'(s)$ are the particle orbits which pass through the phase-space point (X_0, X_0') at $s = s_0$, ie., $X'(s = s_0) = X_0'$ and $X(s = s_0) = X_0$. The solutions for $Y(s)$ and $Y'(s)$ are identical in form with $\psi_x(s, s_0)$ replaced by $\psi_y(s, s_0)$ which is evaluated in a similar manner. An important feature of these solutions is that one can obtain two natural constants of motion.

$$X'^2 + X^2 = constant, \tag{2.67}$$

$$Y'^2 + Y^2 = constant. \tag{2.68}$$

These are analogous to the Courant-Snyder invariants, A_x and A_y derived in section 1.2.

A self-consistent Vlasov equilibrium including space charge effects can now be constructed from the constants of motion $X'^2 + X^2$ and $Y'^2 + Y^2$. The KV equilibrium corresponds to a distribution function

$$f = \frac{N_b}{\pi^2 \epsilon_x \epsilon_y} \delta \left[\frac{1}{\epsilon_x}(X'^2 + X^2) + \frac{1}{\epsilon_y}(Y'^2 + Y^2) - 1 \right]. \tag{2.69}$$

This corresponds to a hyperellipsoidal shell in the (X, Y, X', Y') space.

From the transformations given by Eqs (2.61) and (2.60), it follows that

$$\begin{aligned} dxdy &= (w_x w_y) dX dY, \\ dx'dy' &= (w_x w_y)^{-1} dX' dY' \end{aligned} \tag{2.70}$$

and, the constants of motion may be expressed in terms of (x, y, x', y') as

$$\begin{aligned} X'^2 + X'^2 &= w_x \left(x' - \frac{x}{w_x} \frac{dw_x}{ds} + \frac{x^2}{w_x^2} \right), \\ Y'^2 + Y'^2 &= w_y \left(y' - \frac{y}{w_y} \frac{dw_y}{ds} + \frac{y^2}{w_y^2} \right) \end{aligned} \tag{2.71}$$

The density profile may now be determined from

$$n_b(x, y, s) = \int dx'dy' f_b = (w_x w_y)^{-1} \int dX'dY' f_b. \tag{2.72}$$

Using the expressions, $R_x = \sqrt{\epsilon_x} w_x$ and $R_y = \sqrt{\epsilon_y} w_y$, we obtain

$$n_b(x, y, s) = \begin{cases} \frac{N_b}{\pi a(s) b(s)}, & 0 \le x^2/R_x^2 + y^2/R_y^2 < 1 \\ 0, & x^2/R_x^2 + y^2/R_y^2 > 1 \end{cases} \tag{2.73}$$

which proves that a uniform distribution over an ellipse is a Vlasov equilibrium state. The evolution of R_x and R_y are determined by the envelope equations, (2.46) and (2.47).

The following chapters will deal with identical systems modified with nonlinear focusing terms. None of the theories mentioned in this chapter will be valid if nonlinear terms in the focusing cannot be neglected. The tools that will be used to study the modified systems will include PIC codes, Particle-Core models in the absence of an envelope equation, and finally Lie transform perturbation theory. The Lie transform analysis will be used to derive adiabatic invariants and also near equilibrium distributions in a nonlinear focusing channel.

Chapter 3

Mechanism of Beam Halo Formation

This chapter will explain the mechanism of beam halo formation in space charge dominated beams, *ie*, beams with a low emittance. The analysis and results presented in this chapter are based on the work of O'Connell, Wangler, Mills and Crandall [44]. A simplified model is used with the purpose of providing some physical insight into beam halos formed by a parametric resonance between the oscillation of the particles and the envelope oscillations. The term "Halo" describes a low density distribution of particles that surrounds a beam in phase space.

3.1 Dynamics of a Uniform-Density Core

Consider a zero emittance beam with uniform charge distribution and a circular cross-section of radius R that is propagating through a constant focusing channel. The beam is assumed to be very long compared to its width so that longitudinal effects may be neglected. The transverse equation of motion of the beam radius is given by the envelope equation, Eq. (2.46). Under these conditions this is,

$$\frac{d^2R}{ds^2} + \omega_0^2 R - \frac{K_p}{R} = 0 \tag{3.1}$$

where ω_0 is a constant and represents a continuous focusing force that is linear and is directed radially inward. The parameter K_p is the space charge perveance described in chapter 2. The emittance ϵ_r is zero which represents a cold beam. In this model, this

system represents the "core" of the beam. For a matched core $d^2R/ds^2 = 0$, and the corresponding radius is $R_0 = \sqrt{K_p}/\omega_0$. The transverse equation of motion of a single test particle is

$$\frac{d^2x}{ds^2} + \omega_0^2 x - F_{sc} = 0 \tag{3.2}$$

where F_{sc} is the space charge force, give for a uniform density core by

$$F_{sc} = \begin{cases} K_p x/R^2, & x < R \\ K_p/x, & x > R \end{cases} \tag{3.3}$$

For a small, perturbation δR from the matched radius R_0, the envelope equation can be linearized to give the solution $\delta R/R_0 = A \sin \Omega s$ where $\Omega = \sqrt{2}\omega_0$. With this perturbation, a particle lying within the beam, *ie*, $x < R$, will satisfy the equation of motion,

$$\frac{d^2x}{ds^2} + A\Omega^2 x \sin \Omega s \simeq 0. \tag{3.4}$$

This approximate result is a special case of the Mathieu equation, which suggests periodic solutions in x for particle frequencies below half the core frequency Ω. The rate of gain/loss of the particle energy due to the core oscillation is

$$\frac{dU}{ds} = \vec{F}\vec{x}' = -A\Omega^2 x x' \sin \Omega s \tag{3.5}$$

It is clear that when the frequency of oscillation of the particle is half that of Ω, *ie*, for example, if $x \sim \sin(\Omega s/2)$, then $dU/ds \sim \sin^2(\Omega s)$ which results in a nonzero average. This leads to a resonant interaction between the particle oscillation and the envelope oscillation of the core where particles can either gain energy, loose energy, or have no energy change depending on the relative phases of the particle displacement, the transverse velocity and the core radius oscillation. When a particle is moving in and out of the core, its oscillation is highly nonlinear due to the different forms taken by the space charge force F_{sc} for $x < R$ (inside the core) and $x > R$ (outside the core) respectively. As a result, there is a loss of phase coherence which creates a limit to

continued resonance and can result at different times in gain, loss or no net change in the energy of the particle. In the following section, a connection between beam halos and this resonant interaction will be analyzed.

3.2 Classification of Particle Trajectories

The model described in the previous section will be applied to numerically calculate the trajectories of particles with different initial conditions. The initial mismatch of the core is assumed to be $M = R/R_0 = 1.5$ with $dR/ds = 0$, $\omega_0 = 1.0$, and $K_b = 1$. The particles were launched with various initial conditions shown in Fig. 3.1. These conditions are identical to those used in Ref. [44]. The core radius oscillation is also shown in the first figure.

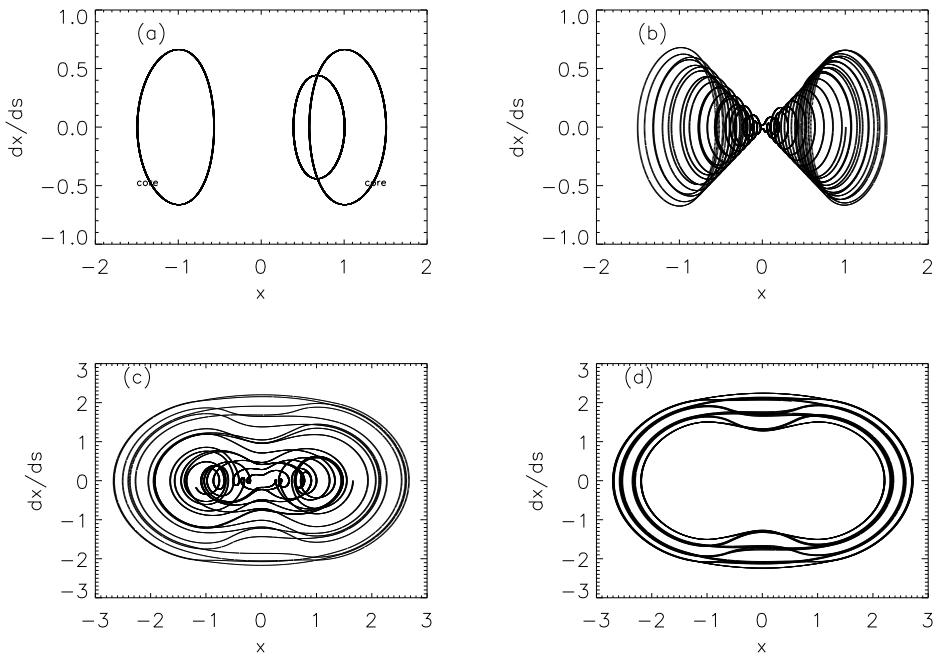

Figure 3.1: Particle trajectories in phase space with initial conditions $x' = 0$ and (a) $x = 1.0$, (b) $x = 1.55$, (c) $x = 1.65$, (d) $x = 2.2$.

With these conditions, the trajectories of particles can be classified into three distinct categories as follows: (1) For $x < 1.5$, the particles oscillate in phase with the

core radius about their own equilibrium radius. These are known as plasma trajectories. (2) For $x > 2.0$ the particles oscillate about the origin with an orbit that looks like an ellipse that is pinched inward along the velocity axis due to the space charge force. The amplitudes are variable and each orbit is confined to a narrow band in phase space. These particles occupy the halo region and their orbits are called betatron trajectories. (3) Finally, for $1.5 < x < 2.0$ the particles execute a more complex motion. They may initial spend part of the time executing plasma-like oscillations within the core, after which they enter a phase relationship with the core such that they gain energy and move into the halo region executing betatron-like oscillations. These particles can also reverse the procedure and lose energy to the core. As a result they return to execute plasma-like oscillations. Their orbits are referred to as hybrid trajectories, which are strongly affected by the resonant energy transfer analyzed in the previous section.

The discovery of hybrid trajectories are important because they suggest the formation of beam halos in a beam with no initial halo. In a real beam, the conditions are not as idealized as in the model used in the present analysis. Particles once lying within the core can be kicked into a hybrid trajectory due to real focusing effects like imperfections in the focusing system. Particles can also drift into resonance due to thermal diffusion. This would not be observable in the current model because a cold beam was used. Finally, it is impossible to produce a beam with a uniform distribution. One would always expect the presence of a tail in the particle distribution that extends beyond what can be viewed as a "core". All these situations can produce halos in beams that did not have any particles in the halo region initially.

Hybrid trajectories also indicate the limitations of collimation of the beam halo. Suppose at a given time the beam is collimated to remove the existing halo. Any such collimation procedure, even if carried out under the most ideal circumstances, would remove particles with betatron trajectories and those with hybrid trajectories, which at that time populate the halo region. However, particles with hybrid trajectories which lie

within the core at the time of collimation can gain energy at a later time and repopulate the halo. In the next chapter, a combination of nonlinear focusing and collimation as a mechanism to eliminate beam halos has been proposed and studied through numerical simulations.

Chapter 4

Control of Beam Halos through Nonlinear Damping and Collimation

4.1 Introduction

This work demonstrates that beam halos can be controlled by combining nonlinear focusing and collimation. The study relies on a one dimensional, constant focusing Particle-in-Cell model and a Particle-Core model. Calculations with a linear focusing force show that the extent and density of the halo depend strongly upon the initial mismatch of the beam, establishing the importance of obtaining a reduced mismatch. Nonlinear focusing is then introduced in the calculations to study damping in the beam oscillations thereby reducing the mismatch. Although the nonlinear force reduces the mismatch of the beam through a damping mechanism, it is accompanied by emittance growth. This process is very rapid and happens within the first 2-3 envelope oscillations. After this, the halo is collimated, and further evolution of the beam shows that the halo is not regenerated. It has also been shown that a one-time collimation with linear focusing is ineffective since the halo is regenerated after collimation. While the same was not true when nonlinear focusing was used, it resulted in a greater loss of particles during collimation due to the initial emittance growth, especially for higher initial mismatches of the beam. However, the elimination of the beam halo would result in a larger physical aperture thus allowing a beam of higher current that could more than compensate for this loss of particles.

A major issue facing the functioning of high current accelerators is beam halo

formation. High current accelerators find applications in heavy ion fusion, nuclear waste treatment, production of tritium, production of radio isotopes for medical use and spallation neutron sources [37]. The halo is formed by a small intensity distribution of particles surrounding the core of the beam. When such particles drift far away from the characteristic width of the beam, their loss will lead to the production of residual radioactivity of the accelerating system. Many of the above applications require that the number of particles lost to the system must be less that one part in 10^5 - 10^6. With such a stringent requirement, methods to control the beam halo can prove very useful. However there has been relatively less effort spent on devising such methods when compared to the extensive study that has already been done to understand the physics of beam halo formation. The methods employed to study beam halos include analytic models and multiparticle simulations using mainly the particle-core model, some PIC simulations, [29, 44, 39, 40, 12, 53, 45, 32, 23, 35, 65, 67, 48, 31, 30, 58, 46] and experimental studies [1, 51]. Batygin [5] showed that nonlinear forces can be used to obtain a better match with a prescribed charge distribution leading to reduced halo. The method suggested in this chapter does not require a specific initial charge distribution.

The dependence of the extent of beam halos and the initial beam mismatch has been studied by Wangler *et al*, [67], where it been shown that the maximum dimensionless particle amplitude X_{max}, which is the distance with respect to the matched beam width, can be described by an approximate empirical formula, which is,

$$X_{max} = A + B|ln(\mu)|. \tag{4.1}$$

Here, A and B are weak functions of the tune depression ratio approximately given by $A = B = 4$ [67], and μ is the initial beam mismatch ratio. This result is not a good estimation for maximum amplitude for μ close to 1. It has also been shown [36] that in addition to increased halo extent, the number of halo particles grows with increased initial mismatch ratio.

O'Connell *et al* [44] traced the trajectories of various test particles with different initial conditions. This led to the discovery of hybrid trajectories, which undergo a resonant interaction with the core which was later analyzed by Gluckstern [29]. This discovery of hybrid trajectories reveals the limitations on the effectiveness of a one time beam collimation, an issue that will be addressed in this paper. The removal of a halo using a multicollimator system has been studied previously [36] for a periodic linear focusing system.

Thus, it is already well established that reducing the beam mismatch can be an important factor in halo mitigation. In the this chapter, we propose reducing mismatch by damping the transverse oscillations of the beam by inducing nonlinear focusing before collimation to avoid the need for repeated collimation. Collimation still becomes essential in this process due the emittance growth accompanying the nonlinear damping. These studies are based on a radial Particle-in-cell (PIC) code along with some preliminary studies using a modified particle core model. This chapter describes the particle core model for nonlinear focusing and examines the effect of nonlinear focusing on beams through this model. The PIC algorithm and the physical model used to represent the beam has been described and simulation results of beam halo formation with different initial mismatches has been presented. In addition, results showing damping and emittance growth due to nonlinear focusing are presented. The regeneration of halo after collimation in a linear focusing channel is shown. It is finally shown that halos can be controlled by combining nonlinear focusing and collimation.

4.2 Results from a Particle-Core Model

The particle core model in this paper serves the purpose of obtaining a qualitatively similar result with a simpler model, thus exhibiting the general nature of the phenomena of damping and emittance growth due to nonlinear focusing. For a linear focusing system, the core is generally represented by the envelope equation, which is

not valid for a nonlinear focusing system. Since nonlinear focusing is used in this study, the core is simulated using a different method.

The envelope equation will still be used as a reference to determine parameters such as mismatch ratio and tune depression ratio. Consider a uniform, round, thin beam moving in the axial direction and with a constant axial velocity in a linear and constant focusing channel. Under these conditions, the envelope equation describes the oscillation of R, the radius of the beam with respect to the axial distance s which is a time like variable. This can be expressed as (see for example [16, 66]).

$$\frac{d^2R}{ds^2} + k_0 R - \frac{\epsilon^2}{R^3} - \frac{K}{R} = 0. \tag{4.2}$$

The focusing force is represented by k_0, K is the space charge perveance which depends upon the intensity, axial velocity and charge to mass ratio of the particles [16, 66]. The rms emittance of the beam ϵ_x is given by

$$\epsilon_x = 4\sqrt{\langle x\rangle^2\langle v_x\rangle^2 - \langle x v_x\rangle^2}, \tag{4.3}$$

where the angle bracket represents an average over the particle distribution in position space, x is displacement along the horizontal axis and $v_x = dx/ds$. For a matched beam, the radius remains constant at $R = R_0$. It was shown by Sacherer [54] that the envelope equation can be generalized to even nonuniform distributions having elliptic symmetry (in this case, azimuthal symmetry). In such a model, the beam radius and matched radius are given by $R = 2a$ and $R_0 = 2a_0$ respectively, where a is the rms width of the beam, and a_0 is the matched rms width. We define a dimensionless displacement by $X = x/a_0$, a dimensionless velocity by $V_x = v_x/\sqrt{k_o}a_0$, a dimensionless axial distance given by $S = \sqrt{k_0}s$ and a dimensionless rms width given by $M = a/a_0$. The initial mismatch ratio, which is the initial value of M is represented as μ. All calculations will be made with respect to these dimensionless quantities.

The tune depression ratio $\eta = \epsilon/\sqrt{k_0}R_0^2$ is a dimensionless quantity which gives a measure of the ratio between the wave numbers (or equivalently, frequencies) of a

particle oscillating with and without the effect of space charge respectively. While this ratio is exact for any in-core particle in a uniform distribution core, the definition may be extended to provide information on a general beam, especially to determine if a beam is space charge dominated or emittance dominated. A tune depression ratio close to unity represents an emittance dominated beam while if η is much less than unity is is a space charge dominated beam.

In this paper, the core was simulated through a series of infinitely long charged cylindrical "sheets" which could move radially inward or outward. The field on test particles and the sheets of the core were calculated from Gauss' law using a flux weighted averaging scheme [7]. The test particles did not contribute to the field. The sheets representing the core were advanced in the radial direction while the test particles were moved along the "x" and "y" coordinates. In both the cases, a leap frog scheme was used.

The sheets that represent the core and the test particles satisfy the following equation,

$$\frac{d^2r}{ds^2} = F + F_{sc}, \tag{4.4}$$

where r is the radial distance and s is the distance along the axis. F is the focusing force and F_{sc} is the space charge force. The purely linear focusing force had the form

$$F = -k_o r, \tag{4.5}$$

while the focusing force with the nonlinearity included had the form

$$F = -k_1 r - k_2 r^3. \tag{4.6}$$

The corresponding space charge densities that balance the focusing force will then be equal to

$$\rho = \frac{\epsilon_0}{e} 2k_0 \tag{4.7}$$

and

$$\rho = \frac{\epsilon_0}{e}(2k_1 + 4k_2 r^2) \tag{4.8}$$

respectively for $r < R_0$, and equal to zero for $r > R_0$. Here, e is the charge on the particle and ϵ_0 is the permitivity in free space. A mismatch is introduced by expanding or contracting the core and uniformly scaling the charge density to ensure conservation of charge. In performing the calculations in this section, we used a core which was expanded to 1.35 times its matched width. All the sheets comprising the core were initially at rest. In the absence of a nonlinearity, the density of the core is uniform, corresponding to a Kapchinskij-Vladmirskij (KV) distribution [38].

Based on the parameter a_0, the matched rms width of the beam, we set the linear and nonlinear focusing parameters such that they satisfied the condition,

$$k_0 a_0 = k_1 a_0 + k_2 a_0^2. \tag{4.9}$$

This equation indicates that the linear and nonlinear focusing forces were equal at the characteristic distance a_0 and also gives a measure as to how much the linear force was reduced before introducing the nonlinear component. The nonlinear term in Eq. 4.6 was four times the corresponding linear term at $r = a_0$. Thus,

$$\frac{k_1}{k_2 a_0^2} = 4. \tag{4.10}$$

This gives a measure of how strong the contribution of the nonlinearity is to the net focusing.

Figure 4.1(a) shows that the oscillations of the rms width of the core are sustained in the linear focusing case. This is because all the sheets in the core are oscillating in phase and at the same frequency. When nonlinearity is introduced, not only does the density become nonuniform, but the frequency distribution of the oscillations of the charged sheets for a mismatched beam also becomes nonuniform. This is expected to lead to damping of the oscillation in the rms width of the core as shown in Fig. 4.1(b).

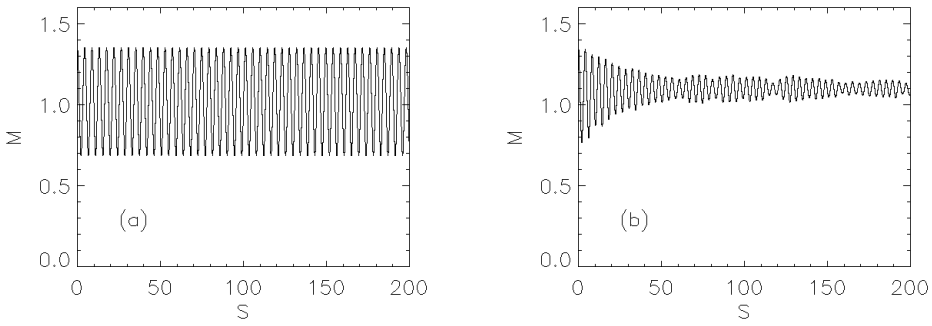

Figure 4.1: Oscillation of the rms width of the beam with respect to the matched rms width at μ =1.35 for (a)linear and (b)nonlinear focusing

The mechanism is well known in many branches of physics as Landau damping. In the damping process, the beam obtains a velocity distribution which is equivalent to heating of the beam.

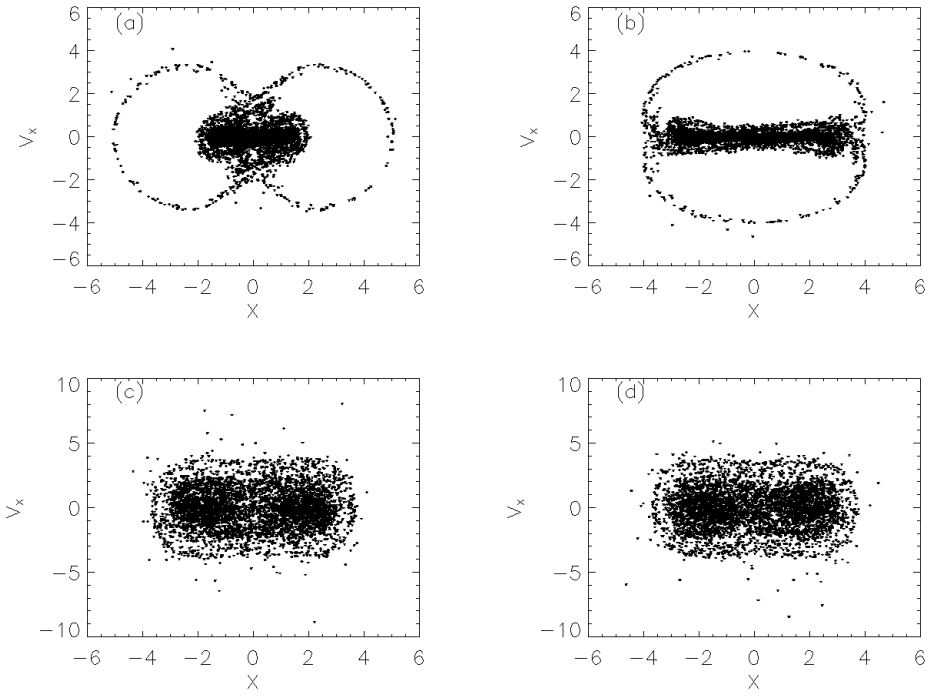

Figure 4.2: Phase space distribution of test particles. Linear oscillations at (a) minimum rms width (b) maximum rms width. Nonlinear oscillations at (c) minimum rms width and (d) maximum rms width.

Figure 4.2 shows the corresponding phase space distribution of test particles moving under the influence of this core at the end of about 40 core oscillations. In Fig 4.2(a), the distribution was plotted when the core was at a maximum rms width, and in Fig 4.2(b), the core had a minimum rms width, both with linear focusing. Both the distributions were plotted after about 40 core oscillations. For these calculations, 5000 test particles were used which had an initial Gaussian distribution with an rms width equal to half the initial radius of the core. In the linear case, this makes the core and particle distribution equivalent according to the envelope equation. The initial distribution was identical for the linear and nonlinear case corresponding to a tune depression of 0.1 in the linear focusing channel.

Figure 4.2(c) shows the final distribution resulting from nonlinear focusing. It can be seen clearly that the beam spreads out in velocity space, while the spread in position space is comparable to the linear focusing case. This is a because the nonlinear component of the focusing force increases rapidly as the particle moves away from the center. Thus, the particles having higher kinetic energy must also overcome a stronger potential gradient as they drift away from the core. It will be seen later that this plays an important role in restricting the radius of collimation in position space.

4.3 Results from PIC Simulations

The evolution of the beam is now simulated using a radial PIC code. In these calculations, the charge distributions and forces used were azimuthally symmetric, a simplified model for which a one-dimensional field solver is sufficient. Since the fields vary along the radial direction, they are solved using Gauss's law over a radial grid. The particles however, are advanced using the leap frog scheme in cartesian coordinates along the 'x' and 'y' axis. This helps avoid problems arising due to singularities at the origin if radial and azimuthal motion was was used [25]. The particles are distributed over the grid using area weighted averaging while the fields were assigned to the particles

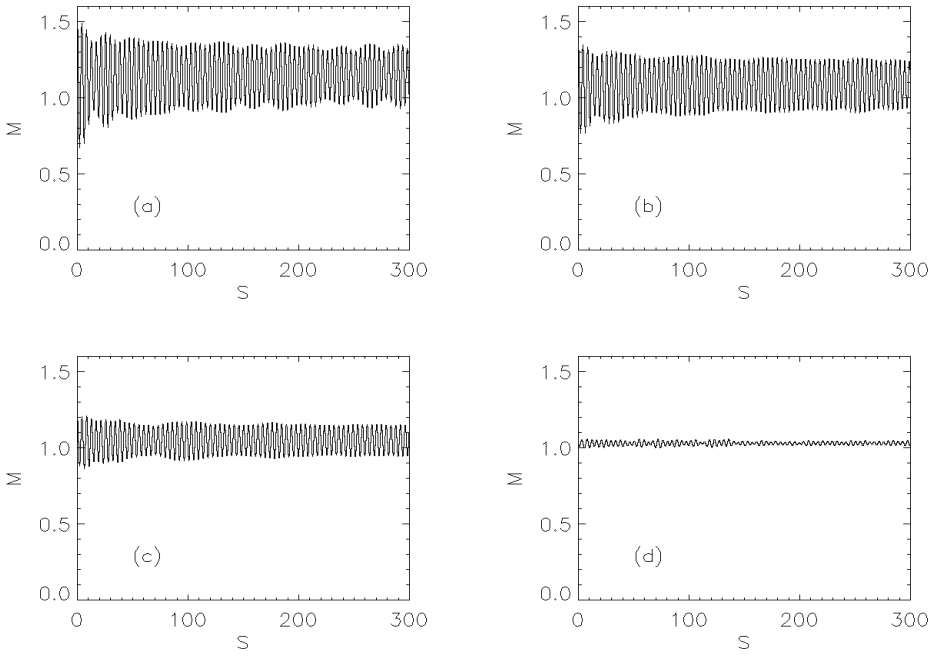

Figure 4.3: Oscillation of the dimensionless rms width of the beam for μ = (a) 1.5, (b) 1.35, (c) 1.2, (d) 1.02

using flux weighted averaging [7].

We examine the halo generated for beams with different initial mismatch ratios. The beam had an initial Gaussian distribution in position and velocity space. The tune depression calculated from the corresponding envelope equation was chosen to be 0.1 for all the cases, which implies that the beam is space charge dominated. We used 100,000 particles in all the PIC simulations, which was large enough for the particle distributions to retain the desired azimuthal symmetry.

Figure 4.3 shows the oscillation of the normalized rms width of the beam with an rms mismatch ratio μ of (a) 1.5, (b) 1.35, (c) 1.2 and (d) 1.02. For (a),(b) and (c), where the mismatch ratio is more significant, it may be noticed that there is some initial damping of the oscillations after which a steady pattern emerges. The small initial damping could be attributed to the fact that a Gaussian distribution does not correspond to a Vlasov-Poisson equilibrium, so in the initial stage of the beam oscillation, one could

expect some remixing of the distribution in phase space. In case of (d), the oscillation is not very regular and this is because the mismatch is not significantly large so other phenomena like density oscillations become more prominent. Density oscillations occur because an rms matched beam in this case still does not correspond to a Vlasov-Poisson equilibrium.

To examine the halo formation in these beams, the phase space distribution of the particles is then taken toward the end of the oscillations for two cases, which are (1) when the rms width of the distribution is a minimum and (2) when it is a maximum. It can be seen in Fig. 4.4 and 4.5 that the extent and intensity of the halo increases with increased mismatch, which confirms the need to obtain a reduced mismatch in order to control halo formation.

Figure 4.6 shows the damping of the oscillation of the rms width of beams with nonlinear focusing. The nonlinear focusing is of the same form as Eq. (4.6) with $k_0 a_0 =$

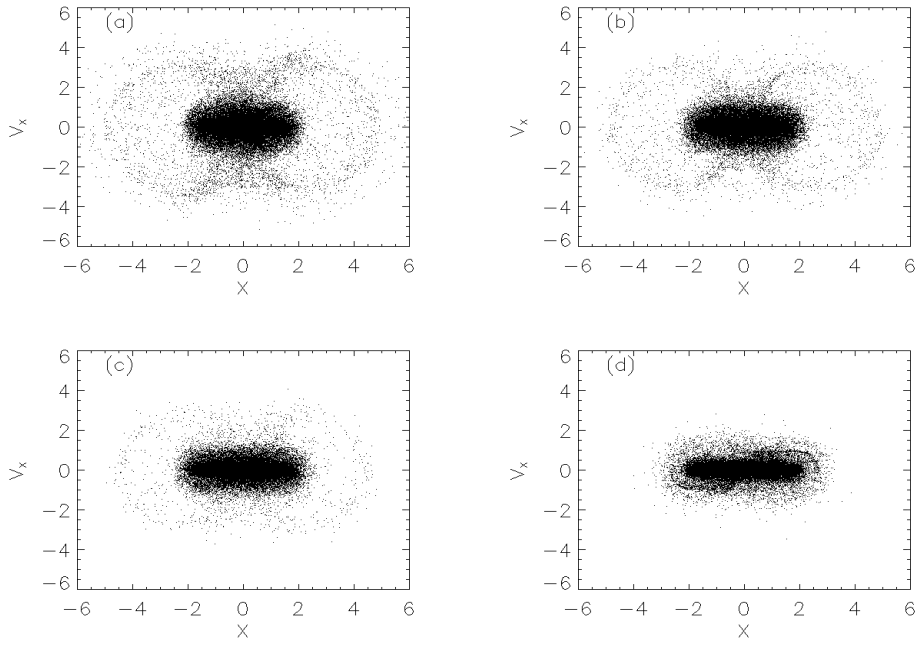

Figure 4.4: Phase space distribution at minimum rms width for μ = (a) 1.5, (b) 1.35, (c) 1.2, (d)1.02

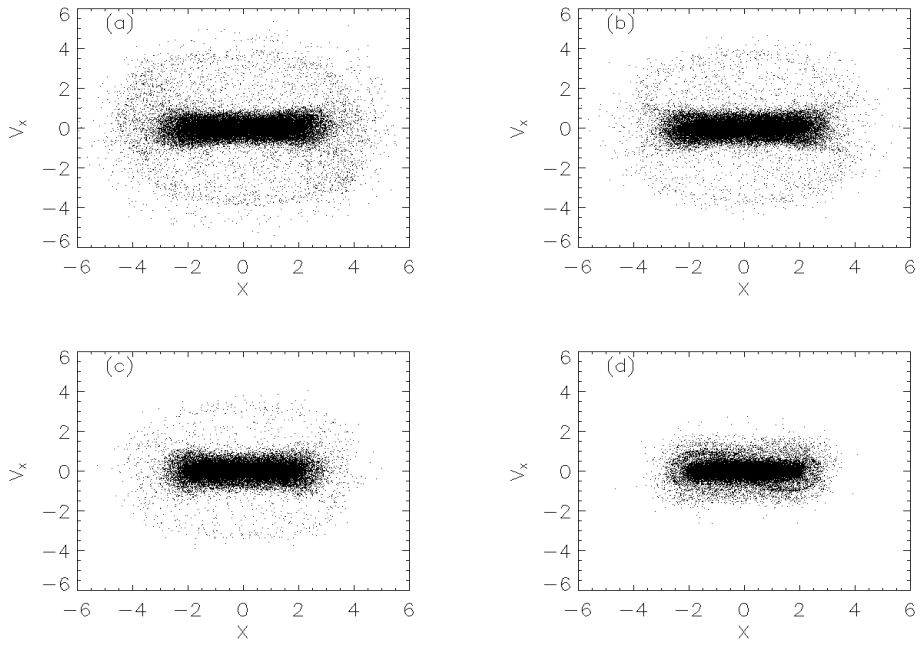

Figure 4.5: Phase space distribution at maximum rms width for μ = (a) 1.5, (b) 1.35, (c) 1.2, (d)1.02

$k_1 a_0 + k_2 a_0^3$ and $k_1/(k_2 a_0^2) = 4$, with a_0 being the matched rms width of the beam as predicted by the envelope equation. The initial distributions were identical to the ones used in the linear focusing case. The parameter μ when defined for a nonlinear focusing case corresponds to the mismatch ratio in the linear focusing channel for the same initial distribution.

Figures 4.7 and 4.8 show the corresponding phase space distribution of the particles for $\mu = 1.5$ and 1.2. They were taken toward the end of the nonlinear oscillations shown in Fig. 4.6 when the beam width is a minimum and a maximum respectively. It may be noticed that the rms width of the beam does not change significantly while oscillating as a consequence of the damping. Similar to the particle core model results, these figures show that the particles spread far in velocity space while their spread in position space is comparable to the linear focusing case.

The PIC simulation results show a similar response to nonlinear focusing as the

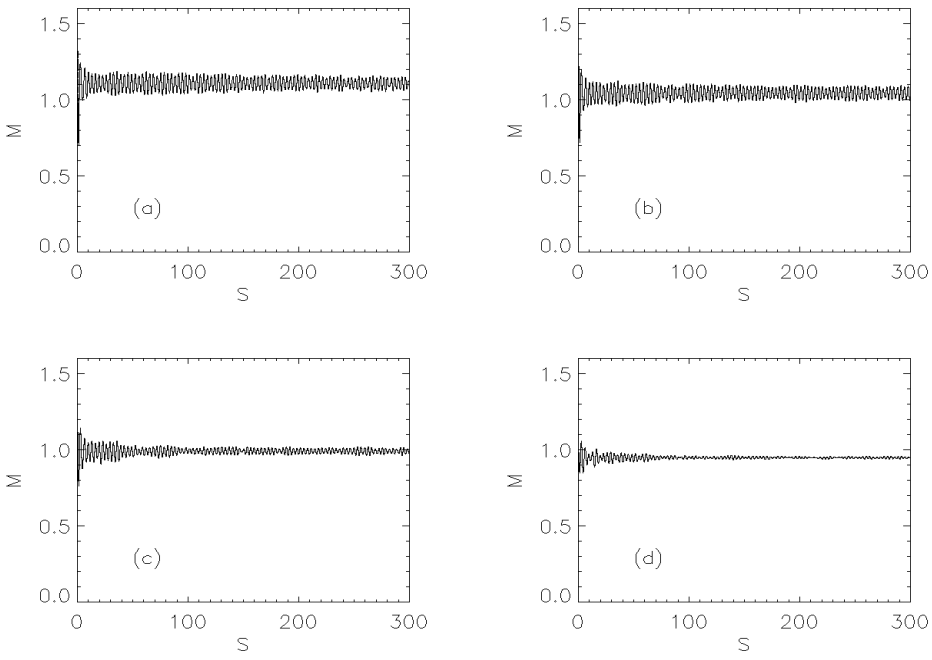

Figure 4.6: Oscillation of the dimensionless rms width of the beam with nonlinear focusing for μ = (a)1.5, (b) 1.35, (c)1.2, (d)1.02

particle-core model does, which is damping accompanied by emittance growth. However, we see in Fig. 4.6 that the damping is more rapid in the PIC simulations. It takes place in the first $1-2$ rms oscillations while it takes about $5-6$ oscillations in the particle core model. In the particle core model, we see a gap between the halo particles and the core for linear focusing which is not seen in the PIC simulation. This could be attributed to the fact that the particles in the particle-core model do not contribute to the field due to which they are influenced only by the perfectly linear oscillations of the core. With the same initial conditions used in both the models, the extent of the halo was the same for linear and nonlinear focusing.

4.4 Collimation with Linear Focusing

Our results show that a one time collimation is ineffective in the presence of linear focusing. At the initial process, the beam undergoes some emittance growth and then

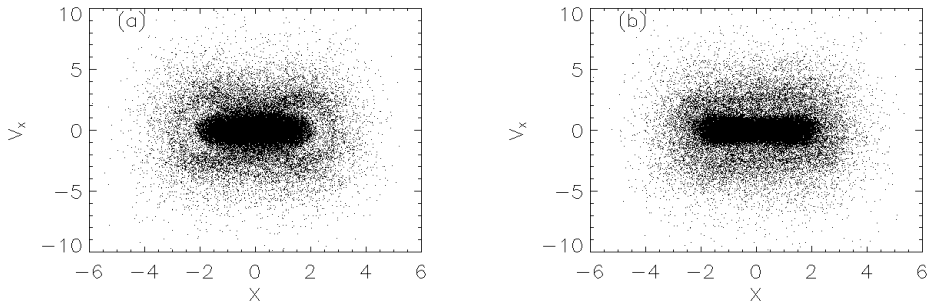

Figure 4.7: Phase space distribution for nonlinear oscillations, $\mu = 1.5$ at (a) minimum rms width (b) maximum rms width

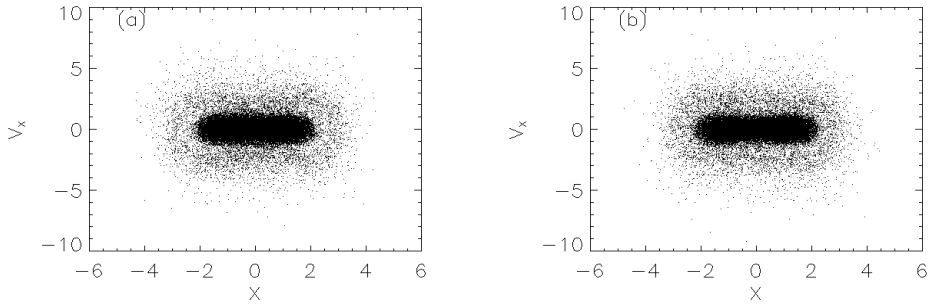

Figure 4.8: Phase space distribution for nonlinear oscillations, $\mu = 1.2$ at (a) minimum rms width (b) maximum rms width

settles into a steady state of oscillations. At this point, the halo was visually identified and collimated in phase space. There is no established quantitative definition as yet of a beam halo although recent efforts are being made to quantify such a halo [2]. The beam was collimated over an ellipse that satisfied the equation $X^2 + Y^2/c^2 + V_x^2 + V_y^2/d^2 = 1$. Here c and d are expressed in units of a_0 and $a_0\sqrt{k_0}$ respectively. The values of c and d used in the simulation were different for different values of μ and they are given in table 4.1. This was done for an initial mismatch ratio μ = (a)1.5, (b)1.35 and (c)1.2 for the same initial distributions used in Sec.4.3. For the sake of consistency, the collimation was always done when the beam radius was a maximum.

Figure 4.9 shows that the oscillations are sustained even after the collimation.

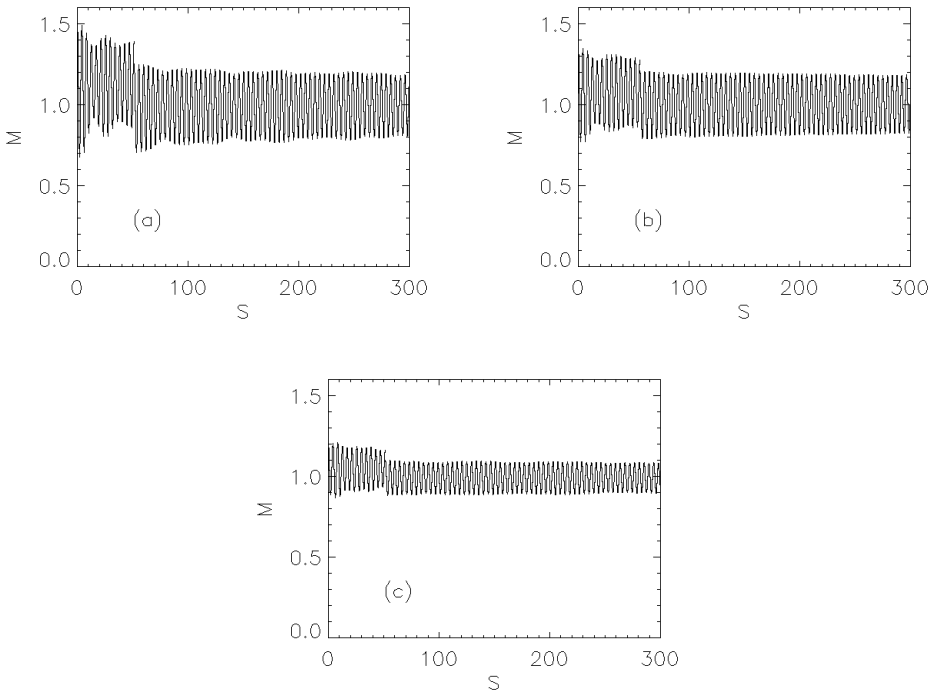

Figure 4.9: Oscillation of the dimensionless rms width of the beam showing collimation for $\mu =$ (a) 1.5, (b)1.35, (c)1.2

This is expected to cause continuous production of halo particles due to the resonant interaction of some particles with these oscillations. Thus, a one time collimation is ineffective and needs to be done periodically. The process can lead to continued beam loss and interference in the performance in the accelerator. Moreover, halo particles can still be generated between two collimating stations and lost to the accelerating system. All this demands the need to introduce a scheme that addresses the mechanism of beam halo formation itself.

Figure 4.10 shows that the halo is indeed regenerated. The phase space distribution was taken when the rms width of the beam was at a minimum toward the end of the oscillations shown in Fig. 4.9. In order to show the halo particles more clearly, the particles are made to appear a little wider in these plots. Although the halo intensity is smaller than that seen in Fig. 4.4, it is large enough to cause radio activity of the

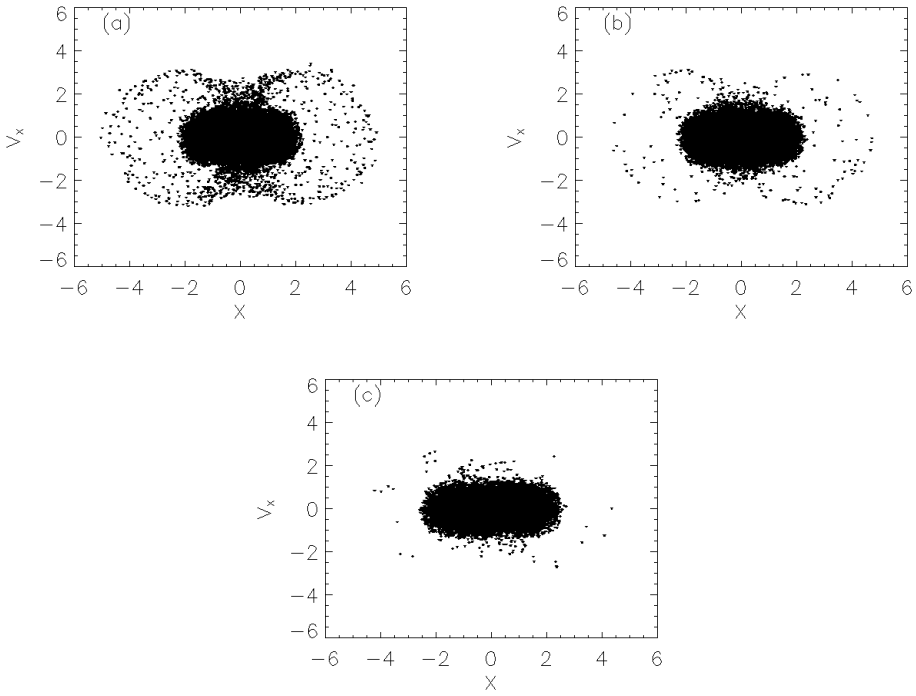

Figure 4.10: Phase space distribution of particles after initial collimation of beam with linear focusing at minimum rms width for $\mu =$ (a) 1.5, (b)1.35, (c) 1.2

walls given that the tolerance to fractional loss in many machines to the number of halo particles is one in $10^4 - 10^5$. It may be noticed that Figs.4.4 and 4.5 show that some particles go a little beyond a relatively dense peanut distribution and do not satisfy the maximum amplitude given by Eq. 4.1. On the other hand, such particles are not seen in Fig. 4.10. Otherwise the maximum extent of the peanut shape distribution is the same in both the plots for the corresponding mismatch and agree well with Eq. 4.1. Thus, it is clear that these distant particles in Fig.4.3 are produced only in the initial stage, a result of Vlasov mixing in phase space. Moreover, the boundary of the peanut shape distribution in Fig. 4.10(b) overlaps with that obtained in Fig. 4.2(a) using the particle core model and having the same initial mismatch of 1.35. This confirms the findings of Wangler *et al* [67] that the halo particles produced purely by a resonant interaction have a normalized maximum amplitude that depends only upon the initial

Table 4.1: Table specifying the collimation of beam with linear focusing

μ=1.5	c=3.5	d=1.5	particle loss = 6.1%
μ=1.35	c=3.5	d=1.5	particle loss = 4.32%
μ=1.2	c=3.0	d=1.5	particle loss = 3.98%

mismatch and not on the specific model used to simulate the beam. The results also show that for an rms mismatched, self-consistent Gaussian beam, some halo particles are produced at the initial stage by an additional mechanism that go beyond the given maximum amplitude.

4.5 Collimation with Nonlinear Focusing

This section will show that the combination of nonlinear damping and collimation eliminates the beam halos permanently. Figure 4.11 shows the oscillation of the beam along with the collimation. It may be noticed that the damping is sustained even after the collimation is performed which is an important phenomenon that ensures that the halo is not reproduced. The halo was once again visually identified and collimated in phase space over an ellipse that satisfied the equation,

$$\frac{X^2 + Y^2}{c^2} + \frac{V_x^2 + V_y^2}{d^2} = 1. \tag{4.11}$$

The values of c and d are given in table 4.2. These were chosen by careful examination of enlarged figures of the distribution, so that the high density area constituting the core was not scraped off. The table also shows that the number of particles lost due to collimation reduces with reduced mismatch. Thus, having a small initial mismatch is still an advantage but this is not possible to achieve in most practical applications. Figure 4.12 shows the distribution of particles at the end of the oscillations shown in Fig. 4.11 when the rms width was a maximum. It is clear that the particles that stray far away from the core are completely eliminated. These figures may be compared with the corresponding ones in the previous section for the same mismatch with linear

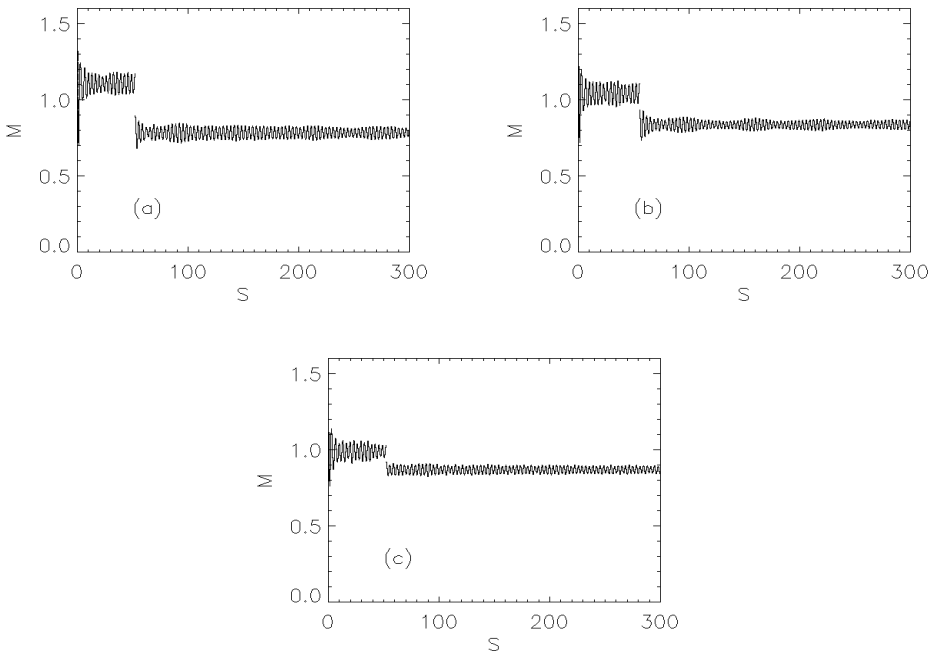

Figure 4.11: Oscillation of the dimensionless rms width of the beam with nonlinear focusing showing collimation for μ =(a)1.5,(b)1.35, (c) 1.2

focusing. Although the distributions were taken when the rms width was a maximum, this would not make a significant difference from another phase of the rms oscillation since their amplitudes are already well damped. The extent of the beam remains the same after this process regardless of the initial mismatch, while, the number of particles lost in the collimation increases with increased mismatch. The large spread in velocity space, which is a result of the nonlinear damping implies that more particles need to be collimated away if a small velocity distribution is desired. Despite this drawback, the absence of a halo would enable one to have a broader beam that would more than compensate for the additional loss in particles. For example, assume that particles cannot be allowed beyond a distance of $X = 3$. The particle distributions shown in Fig. 4.12 clearly satisfy the restrictions, while the ones shown in Fig 4.4 and Fig 4.5 do not because of the extended halo produced due to linear focusing. In addition to this, the core itself stretches to $X = 3$ for linear focusing as seen in Fig. 4.5 while in the nonlinear

Table 4.2: Table specifying the collimation of beam with nonlinear focusing

μ=1.5	c=2.75	d=2.5	particle loss = 15.15 %
μ=1.3	c=2.75	d=2.5	particle loss = 10.1 %
μ=1.2	c=2.5	d=2.5	particle loss = 6.4 %

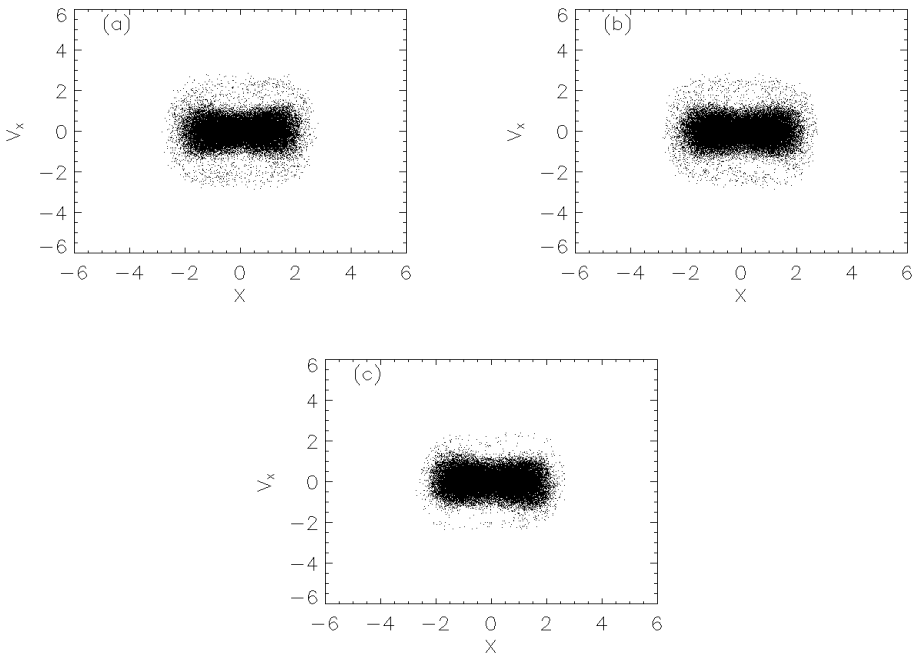

Figure 4.12: Phase space distribution with nonlinear oscillations and collimation at maximum rms width for μ = (a)1.5, (b)1.35, (c)1.2

case, even the at maximum rms width, the beam is restricted to well within a distance of $X = 3$. All this implies that the initial beam will have to be considerably narrower in the case of linear focusing in order to restrict the halo to within a distance of $X = 3$ and thus allowing less particles in the channel. Another point to be noted is that the nonlinear focusing requires only a localized collimation system, while collimation with linear focusing will require repeated collimation resulting in further loss of particles.

4.6 Summary

In this paper, we have proposed a new method that combines nonlinear damping and beam collimation to control beam halos. Our results showed that particles oscillating with large amplitudes compared with the width of the core can be completely eliminated with this mechanism making the need for repeated collimation unnecessary.

Particle-core and PIC simulations showed that nonlinear focusing leads to damping, thus reducing the beam mismatch. However, the damping was accompanied by the particle distribution spreading in the velocity space. This is a result of transfer of energy stored in the mismatch to the velocity distribution of the particles. The high velocity particles are prevented from straying far away from the beam due to the strong focusing force exerted by the nonlinear component at large radial distances. The beam was collimated soon after this nonlinear damping was achieved, and the damped oscillations prevented further halo formation. Results showed that the particles with large amplitude oscillations were completely eliminated. The apparent drawbacks of this process is the spread of particles in velocity space because of which the collimation process results in loss of particles. However, we argue that the knowledge that beam halos are controlled would enable one to extend the beam closer to the walls, thus increasing the beam overall current that would more than compensate for the loss in collimation.

It must be mentioned that the model used here was idealized in many respects because it had constant focusing and was purely radial. While this system is nearly integrable in the absence of space charge, this would not be true in real systems with nonlinear focusing components. This is because the Courant-Syder invariants [15] are broken when nonlinear focusing components like sextupoles or octupoles are used. This will cause the orbits to be chaotic leading to poor confinement even in the absence of space charges. However, it has been shown that [57] it is possible to reduce the nonlinear system to an equivalent, continuous and radially focusing one upon averaging

over the lattice period given that the nonlinear components are arranged in a specific manner along with an alternate gradient quadrupole focusing system. It has also been shown that this symmetry can be retained in the presence of space charge forces [55]. We propose the use of such a lattice for further study involving a two dimensional simulation.

Since the method proposed in this paper is not specific to a particular application, different applications will demand conditions that may be different to the ones used in this paper. For example, collimation of the halo is being studied for the SNS accumulator ring [10]. The collimators use scrapers and absorbers to clean the transverse halo. The accumulator ring already has a straight section dedicated to the collimation system. Applying the proposed method to such a system will require more extensive study. This is because the tune depression in this ring is close to unity, in contrast to the ones chosen in this paper. In addition to this, including nonlinear components in a ring will not be straight forward due to the effect of resonances and beam instabilities. However, one of the advantages of the proposed method is the fact that the nonlinear damping is only a transient process. Once the collimation is achieved, the system may be adiabatically matched to a linear focusing system. The possibility of such a matching has been analyzed by Batygin [4] and could be considered in such a study.

Less effort has been spent in devising methods to eliminate beam halos when compared to the extensive study of the properties of halo production itself. This paper could be an important step toward this direction. The results are encouraging enough to perform simulations in higher dimensions using nonlinear focusing components such as sextupoles or octupoles along with realistic designs for collimators.

Chapter 5

Lie Transform Perturbation Methods for Hamiltonian Systems

In this chapter, we outline the Hamiltonian perturbation method described in detail in Ref. [9] and more briefly in Ref. [42]. This method is based on previous work [34, 28, 19, 20, 21] that introduced Lie transform theory as a convenient method to perform Hamilton perturbation analysis. The Lie transformation is defined with respect to a phase space function w such that it satisfies the following Poisson bracket relationship,

$$\frac{d\mathbf{Z}}{d\epsilon} = \{\mathbf{Z},\ w(\mathbf{Z}(\mathbf{z}, t, \epsilon), t, \epsilon)\}, \tag{5.1}$$

where $\mathbf{Z} = (\mathbf{P}, \mathbf{Q})$ is a phase space vector representing the generalized positions and momenta of the system, w is the Lie generating function and ϵ is a continuously varying parameter such that $\mathbf{Z}(\epsilon = 0) = \mathbf{z}$, the original phase space vector. The above relationship resembles Hamilton's equation with respect to a "Hamiltonian", w and "time", ϵ. This guarantees that the transformation is canonical for all values of ϵ.

The Lie operator L is defined such that it performs a Poisson bracket operation with respect to w. Symbolically,

$$L = \{w,\ \}. \tag{5.2}$$

A transformation operator T is defined such that its role is to replace the variables of a function by the new canonical variables. For the identity function this is simply,

$$T\mathbf{z} = \mathbf{Z}(\mathbf{z}, \epsilon, t). \tag{5.3}$$

The operator T is analogous to the "evolution" operator with respect to ϵ. Using Eq. (5.1) it can be verified that T satisfies

$$\frac{dT}{d\epsilon} = -TL. \tag{5.4}$$

For a similar relationship involving the inverse transformation operator T^{-1}, we differentiate the equation $TT^{-1} = 1$ and use the above equation to obtain

$$\frac{dT^{-1}}{d\epsilon} = T^{-1}L. \tag{5.5}$$

The transformed Hamiltonian K can be expressed in terms of the original Hamiltonian $\mathcal{H}$ as

$$K(\epsilon) = T^{-1}(\epsilon)(\mathcal{H}) + T^{-1}(\epsilon)\int_0^\epsilon d\epsilon' T(\epsilon')\frac{\partial w}{\partial t}(\epsilon'). \tag{5.6}$$

This expression was obtained by Dewar [20].

To obtain explicit equations for each perturbation term, every physical quantity and operator is expressed as a power series in ϵ known as the Deprit power series [19]. The original and transformed Hamiltonians are given by

$$H(\mathbf{z}, \epsilon, t) = \sum_{n=0}^{\infty} \epsilon^n H_n(\mathbf{z}, t), \tag{5.7}$$

$$K(\mathbf{z}, \epsilon, t) = \sum_{n=0}^{\infty} \epsilon^n K_n(\mathbf{z}, t) \tag{5.8}$$

The Lie generating function is represented a little differently because it appears as a derivative in Eq. (5.6). This is,

$$w(\mathbf{z}, t, \epsilon) = \sum_{n=0}^{\infty} \epsilon^n w_{n+1}(\mathbf{z}, t) \tag{5.9}$$

The operators T and L are represented in a similar way as,

$$T(t, \epsilon) = \sum_{n=0}^{\infty} \epsilon^n T_n(t), \tag{5.10}$$

$$L(w) = \sum_{n=0}^{\infty} \epsilon^n L_n \tag{5.11}$$

where $L_n = \{w_n, \ \}$, the Poisson bracket with respect to w_n. The parameter ϵ is used to keep track of the terms representing different orders in the expansion and is usually set to one in the end.

Using Eq. (5.4), and the Deprit series expression for the operators L and T, gives us the following recursion relationship

$$T_n = -\frac{1}{n}\sum_{m=0}^{n-1} T_m L_{n-m}. \tag{5.12}$$

Up to third order, this may be expressed as

$$T_0 = I, \tag{5.13}$$

$$T_1 = -L_1, \tag{5.14}$$

$$T_2 = -\frac{1}{2}L_2 + \frac{1}{2}L_1^2, \tag{5.15}$$

$$T_3 = -\frac{1}{3}L_3 + \frac{1}{6}L_1L_2 + \frac{1}{3}L_2L_1 - \frac{1}{6}L_1^3. \tag{5.16}$$

Similarly, using Eq. (5.5), and the Deprit series expression for the operators L and T^{-1}, the inverse transformation operator may be expressed recursively as

$$T_n^{-1} = \frac{1}{n}\sum_{m=0}^{n-1} L_{n-m} T_m^{-1} \tag{5.17}$$

and up to third order it may be expressed as

$$T_0^{-1} = I, \tag{5.18}$$

$$T_1^{-1} = L_1, \tag{5.19}$$

$$T_2^{-1} = \frac{1}{2}L_2 + \frac{1}{2}L_1^2, \tag{5.20}$$

$$T_3^{-1} = \frac{1}{3}L_3 + \frac{1}{6}L_1L_2 + \frac{1}{3}L_2L_1 + \frac{1}{6}L_1^3. \tag{5.21}$$

It may be noted that when L, T and T^{-1} act upon any phase space function, they are expressed in the form of Poisson brackets, which are independent of the canonical variables used. This makes the whole formulation canonically invariant.

To obtain the nth order perturbation equation, we premultiply Eq. (5.6) by T and diffrentiate with respect to ϵ to obtain

$$\frac{\partial T}{\partial \epsilon} K + T \frac{\partial K}{\partial \epsilon} = \frac{\partial H}{\partial \epsilon} + T \frac{\partial w}{\partial t} \tag{5.22}$$

Using Eq. (5.4) to eliminate $\partial T/\partial \epsilon$ (with $dT/d\epsilon \to \partial T/\partial \epsilon$, since here T also depends explicitly on t) and premultiplying by T^{-1},

$$\frac{\partial w}{\partial t} = \frac{\partial K}{\partial \epsilon} - LK - T^{-1} \frac{\partial H}{\partial \epsilon} \tag{5.23}$$

Inserting the series expansions and equating like powers of ϵ, we obtain in nth order,

$$\frac{\partial w_n}{\partial t} = nK_n - \sum_{m=0}^{n-1} L_{n-m} K_m - \sum_{m=1}^{n} m T^{-1}_{n-m} H_m. \tag{5.24}$$

By writing out the first term in the first sum,

$$L_n K_0 = L_n H_0 = \{w_n, H_0\}, \tag{5.25}$$

and the last term in the last sum, we get for $n > 0$ the final result

$$\frac{\partial w_1}{\partial t} + \{w_1, H_0\} = n(K_n - H_n) - \sum_{m=1}^{n-1} (L_{n-m} K_m + m T^{-1}_{n-m} H_m) \tag{5.26}$$

To third order, this equation yields,

$$K_0 = H_0, \tag{5.27}$$

$$\frac{\partial w_1}{\partial t} + \{w_1, H_0\} = K_1 - H_1, \tag{5.28}$$

$$\frac{\partial w_2}{\partial t} + \{w_2, H_0\} = 2(K_2 - H_2) - L_1(K_1 + H_1), \tag{5.29}$$

$$\begin{aligned} \frac{\partial w_3}{\partial t} + \{w_3, H_0\} &= 3(K_3 - H_3) - L_1(K_2 + 2H_2) \\ &\quad - L_2(K_1 + \frac{1}{2} H_1) - \frac{1}{2} L_1^2 H_1. \end{aligned} \tag{5.30}$$

The expression $\frac{\partial w_n}{\partial t} + \{w_n, H_0\}$ is the variation of w_n along the unperturbed trajectory described by H_0. In the following chapter we use this perturbation scheme to perform

time averaging. To do this, we set $H_0 = 0$ which reduces the variation of w_n along a trajectory to a partial derivative with respect to t. Thus, instead of integrating along the unperturbed trajectory, we simply perform an integration over time to determine w_n. At each order, K_n is chosen such that it cancels the terms that average to a nonzero value over fast oscillations. As a result, the corresponding value of w_n will have a zero average. This is necessary to prevent w_n from being secular (unbounded) in time [9]. For a systematic derivation of all these relationships one may refer to Ref. [9] where they are given up to fourth order in ϵ.

Chapter 6

Finding a Nonlinear Lattice with Improved Integrability using Lie Transform Perturbation Theory

6.1 Introduction

A condition for improved dynamic aperture for nonlinear, alternating gradient transport systems is derived using Lie transform perturbation theory. The Lie transform perturbation method is used here to perform averaging over fast oscillations by canonically transforming to slowly oscillating variables. This is first demonstrated for a linear sinusoidal focusing system. This method is then employed to average the dynamics over a lattice period for a nonlinear focusing system, provided by the use of higher order poles such as sextupoles and octupoles along with alternate gradient quadrupoles. Unlike the traditional approach, the higher order focusing is not treated as a perturbation. The Lie transform method is particularly advantageous for such a system where the form of the Hamiltonian is complex. This is because the method exploits the property of canonical invariance of Poisson brackets so that the change of variables is accomplished by just replacing the old ones with the new. The analysis shows the existence of a condition in which the system is azimuthally symmetric in the transformed, slowly oscillating frame. Such a symmetry in the time averaged frame renders the system nearly integrable in the laboratory frame. This condition leads to reduced chaos and improved confinement when compared to a system that is not close to integrability. Numerical calculations of single particle trajectories and phase space projections of the dynamic

aperture performed for a lattice with quadrupoles and sextupoles confirm that this is indeed the case.

Linear focusing systems such as the alternate gradient quadrupole systems are relatively easy to analyze because of the existence of the Courant-Snyder invariants [15], which reduce the system to an uncoupled set of systems of one degree of freedom. In the presence of higher order components such as sextupoles or octupoles, these invariants are destroyed. Such a system is nonintegrable and has trajectories that are chaotic and poorly confined. Despite this shortcoming in the use of nonlinear components, their use has been proposed in a variety of applications. They include, for example, achieving uniform particle distributions [61], control of beam emittance growth and beam halo formation [5, 6], providing strong sextupole focusing in planar undulators in free electron lasers [60], folding of beam phase space distributions as an alternate to beam collimation [49], introducing Landau damping by providing octupole or sextupole induced tune spread [43, 59], photoelectron trapping in quadrupole and sextupole magnetic fields [64], etc. In addition to this sextupoles, are widely used in storage rings for cromaticity corrections. Nonlinear forces also arise as a result of beam-beam interactions at an interaction point of a storage ring collider which limit the dynamic aperture of the system [27]. Thus, a general analysis of the nonlinear focusing problem is important. It is well known that a near integrable Hamiltonian system will typically possess regular trajectories intermingled with regions of chaos. The aim of this work is to find a condition that optimizes the integrability of the system thereby minimizing the chaotic region in the presence of certain nonlinear focusing components.

To perform the analysis we use the Lie transform perturbation method, which exploits the invariance of the Poisson brackets under canonical transformations. In this analysis all dynamical variables appear within Poisson brackets, so the whole formulation is canonically invariant. If this were not true, one would need to express the Hamiltonian in terms of the new variables up to the desired order before performing

the perturbation analysis. This could make the problem more tedious when the form of the Hamiltonian is not simple, and when it is required to carry the expansion up to third order, both of which are true in this case. References [11, 17, 62] contain other procedures for averaging applied to beam physics. We follow the Lie transform method described in Ref. [9] and show that rearranging the different order terms of the Hamiltonian in this method enables one to perform a time averaging rather than average the motion over the trajectory described by the integrable component of the Hamiltonian.

To start with, Chapter 5. provided a brief description of the Lie transform method used in this chapter. Section 6.2 presents an illustration of the method applied to a linear sinusoidal focusing system, an example also used by Channell [11]. In Sec. 6.3, we introduce a nonlinear focusing system which has a higher order multipoles in addition to quadrupoles. The resulting Hamiltonian describing the motion transverse to the beam propagation is nonautonomous (independent of time) and has two degrees of freedom. By averaging the motion over the lattice period up to third order, we derive a condition for the new time-independent Hamiltonian to also be independent of the transformed azimuthal variable. Under such a condition, the transformed angular momentum will be an adiabatic invariant. It will be shown that this condition is satisfied when the functions describing the forces due to the respective multipole are orthogonal to each other in a certain manner.

In order to show that the condition of azimuthal invariance is a desirable one, various numerical calculations are performed. Section 6.4 includes results which show that as one deviates from the desired condition, the particle oscillations acquire additional frequency components and also have larger oscillation amplitudes. Section 6.5 illustrates the projection of the dynamic aperture on to different planes in phase space. The dynamic aperture is the region that allows what may be defined as confined particles. Estimating the dynamic aperture for different cases shows that maximum confinement can be achieved when the associated time averaged Hamiltonian is integrable in the

transformed coordinates and hence the system is nearly integrable in the laboratory frame. The dynamic aperture is shown to gradually diminish in size as one deviates from this condition.

6.2 A linear Sinusoidal Focusing System

As an illustration and a test for the validity of the method, we perform the analysis for a linear periodic focusing system. The same example was used in Ref. [11] for the method developed in that paper. The single particle Hamiltonian associated with such a system is given by

$$H = \frac{p^2}{2} + \frac{kq^2}{2}\sin(\omega t). \tag{6.1}$$

This Hamiltonian also describes the motion of a particle in systems such as the Paul trap and the ponderomotive potential. We apply Eqs. (5.27 - 5.30) to perform the averaging. As explained in the previous section, we set $H_0 = 0$ and $H_1 = H$. From Eq (5.27) we get,

$$K_0 = H_0 = 0, \tag{6.2}$$

Applying the first order relationship, Eq (5.28), we get

$$\frac{\partial w_1}{\partial t} = K_1 - \frac{p^2}{2} - \frac{kq^2}{2}\sin(\omega t). \tag{6.3}$$

The third term on the right averages to zero with respect to time. In order that the net result average to zero, we require

$$K_1 = \frac{p^2}{2}. \tag{6.4}$$

Since w_1 is relevant only up to an additive constant, it is sufficient to evaluate the indefinite integral to determine w_1, hence

$$w_1 = \frac{kq^2}{2\omega}\cos(\omega t). \tag{6.5}$$

The second order equation Eq.(5.29) gives

$$\frac{\partial w_2}{\partial t} = 2K_2 - \frac{2kpq}{\omega}\cos(\omega t). \tag{6.6}$$

Since the second term on the right side averages to zero, we choose

$$K_2 = 0, \tag{6.7}$$

and so,

$$w_2 = -\frac{2kqp}{\omega^2}\sin(\omega t). \tag{6.8}$$

Applying the third order relationship, Eq. (5.30) then gives

$$\begin{aligned}\frac{\partial w_3}{\partial t} &= 3K_3 + \frac{3p^2k}{\omega^2}\sin(\omega t) \\ -\frac{k^2q^2}{\omega^2}\sin^2(\omega t) &- \frac{k^2q^2}{2\omega^2}\cos^2(\omega t).\end{aligned} \tag{6.9}$$

Note that the third and fourth terms on the right side do not average to zero. In order that they cancel, we set

$$K_3 = \frac{1}{4}\frac{k^2q^2}{\omega^2} \tag{6.10}$$

and as a result,

$$w_3 = -\frac{3p^2k}{\omega^3}\cos(\omega t). \tag{6.11}$$

Collecting the nonzero terms, the transformed Hamiltonian is now given as a function of the new variables by

$$K = \frac{P^2}{2} + \frac{\Omega^2 Q^2}{2} \tag{6.12}$$

where $\Omega = k/\sqrt{2}\omega$. This is the Hamiltonian for a harmonic oscillator with solution

$$Q(t) = Q(0)\cos(\Omega t) + \frac{P(0)}{\Omega}\sin(\Omega t), \tag{6.13}$$

$$P(t) = P(0)\cos(\Omega t) - \Omega Q(0)\sin(\Omega t). \tag{6.14}$$

To transform back to the original coordinate system, we use the operator T^{-1} for which we need to know L up to the desired order. The operators L_n can be expressed in terms of the values of w_n as

$$L_1 = \{\frac{kQ^2}{2\omega}\cos(\omega t),\ \}, \tag{6.15}$$

$$L_2 = \{-\frac{2kQP}{\omega^2}\sin(\omega t),\ \}, \tag{6.16}$$

$$L_3 = \{-\frac{3kP^2}{\omega^3}\cos(\omega t),\ \}. \tag{6.17}$$

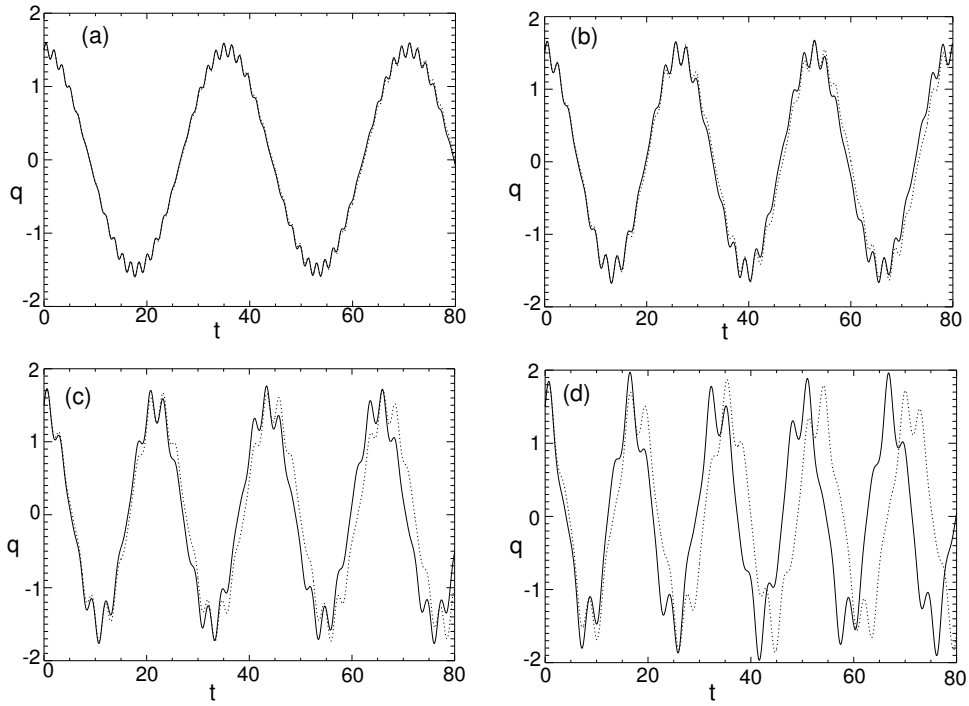

Figure 6.1: q vs t with $k = 1$, $\omega =$ (a) 4, (b) 3, (c) 2.5 and (d) 2. The solid line represents the numerical solution

Using these to perform the inverse transformation as described by Eqs. (5.18-5.21), we get, up to third order,

$$q = Q + \frac{kQ}{\omega^2}\sin(\omega t) + \frac{2kP}{\omega^3}\cos(\omega t), \tag{6.18}$$

$$p = P + \frac{kQ}{\omega}\cos(\omega t) - \frac{kP}{\omega^2}\sin(\omega t) + \frac{1}{3}\frac{k^2}{\omega^3}Q\sin(\omega t)\cos(\omega t). \tag{6.19}$$

The above solution is compared with calculations from a fourth order symplectic integrator [24, 8] and is shown in Figs. (6.1) and (6.2). The parameters used were the same as those used in Ref. [11]. The accuracy of the approximate solution compares well

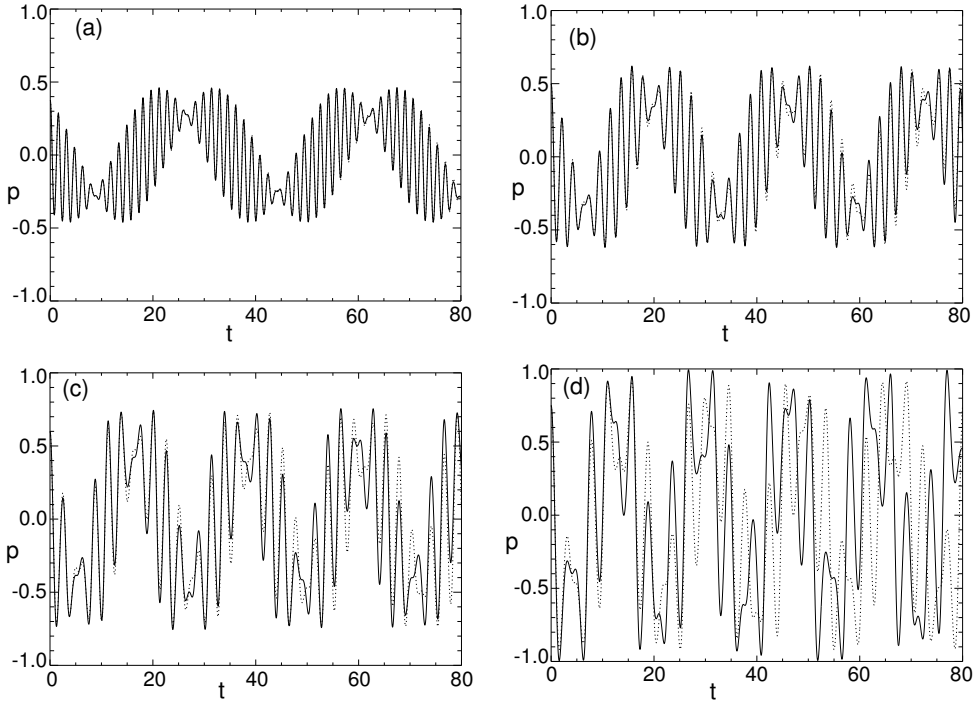

Figure 6.2: p vs t with $k = 1$, $\omega =$ (a) 4, (b) 3, (c) 2.5, (d) 2. The solid line represents the numerical solution

with that obtained by Channell [11] using a different method. That is, the solution given by Eqs. (6.18) and (6.19) overlaps well with the numerical solution for $k/\omega^2 = 1/16$ and the accuracy gradually decreases with decreasing ω.

6.3 Single Particle Averaging for a Nonlinear Lattice

6.3.1 Alternate Gradient Sextupoles and Quadrupoles

The external magnetic fields in the beam channel are expected to satisfy Maxwell's equations in vacuum which are given by, $\nabla \times \vec{B} = 0$, $\nabla \cdot \vec{B} = 0$. The two dimensional multipole expansion expression for such a magnetic field is

$$B_y + iB_x = B_0 \sum_{n=0}^{\infty} (b_n + ia_n)(x + iy)^n. \tag{6.20}$$

Ideally, b_n and a_n, must be constants for the above to be valid. However, when analyzing alternate gradient focusing systems, they are regarded as step functions of the axial

distance. This is still valid if fringe effects are disregarded.

The orientation of the reference frame can be chosen such that $a_1 = 0$. Assuming the presence of only quadrupole ($n = 1$) terms and sextupole ($n = 2$) terms, b_1, a_2 and b_2 will generally be nonzero. The velocity of the particle in the z direction is assumed to be constant. The resulting Hamiltonian can be obtained from the Lorentz force. In cylindrical coordinates it is,

$$\begin{aligned} H &= \frac{1}{2}(p_r^2 + \frac{l^2}{r^2}) + \frac{1}{2}\kappa_2(s) r^2 \cos(2\theta) \\ &\quad \frac{1}{3}\kappa_3(s) r^3 \cos(3\theta + \alpha). \end{aligned} \tag{6.21}$$

The variable s is the distance along the axis, which is equivalent to time for constant axial velocity. The momentum in the radial direction is p_r and l is the angular momentum. The values of $\kappa_2(s)$ and $\kappa_3(s)$ depend upon the strength of the quadrupole and sextupole magnets respectively and also the velocity of the particle in the axial direction. The angle α depends upon the relative values of a_2 and b_2 which is determined by the orientation of the sextupoles with respect to the quadrupoles. We use normalized units in which the charge and mass of the particle are unity. It is assumed that the Hamiltonian is periodic in s with periodicity S, **ie**, $\kappa_2(s + S) = \kappa_2(s)$ and $\kappa_3(s + S) = \kappa_3(s)$. It is further assumed that the average of $\kappa_2(s)$ and $\kappa_3(s)$ over a period S is zero. That is,

$$\langle \kappa_2 \rangle = \frac{1}{S} \int_s^{s+S} \kappa_2(s) ds = 0 \tag{6.22}$$

and the same for κ_3. The angle brackets $\langle \cdots \rangle$ denote an average over one period in the rest of this section. With these conditions, κ_2 and κ_3 can in general be represented in the form of Fourier series as

$$\kappa_2(s) = \sum_{n=1}^{\infty} f_n \sin(\frac{2n\pi s}{S}) + \sum_{n=1}^{\infty} g_n \cos(\frac{2n\pi s}{S}), \tag{6.23}$$

and

$$\kappa_3(s) = \sum_{n=1}^{\infty} k_n \sin(\frac{2n\pi s}{S}) + \sum_{n=1}^{\infty} l_n \cos(\frac{2n\pi s}{S}). \tag{6.24}$$

However, the analysis in this section will show that it would be desirable for the above series to satisfy certain restrictions.

The averaging procedure to follow is valid when the averaged orbits are slowly varying over one lattice period S. The procedure is identical to the one used in the previous section except that the algebra is more tedious since the Hamiltonian is more complex. Once again, we set $H_0 = 0$ and $H_1 = H$. From Eq. (5.28) we get $K_0 = H_0 = 0$. Equation (5.29) yields

$$\frac{\partial w_1}{\partial s} = K_1 - \frac{1}{2}(p_r^2 + \frac{l^2}{r^2}) - \frac{1}{2}\kappa_2(s) r^2 \cos(2\theta) - \frac{1}{3}\kappa_3(s) r^3 \cos(3\theta + \alpha). \tag{6.25}$$

From Eqs. (6.23) and (6.24) it follows that $\langle \kappa_2^{\mathrm{I}} \rangle = \langle \kappa_3^{\mathrm{I}} \rangle = 0$. The Roman numerical superscript indicates an integral over s with a constant of integration chosen so that the integral has a zero average over one lattice period S. Similarly, a superscript 'II' will indicate a double integration over s with the same conditions and so on.

Choosing K_1 to cancel the terms with a nonzero average value then gives

$$K_1 = \frac{1}{2}(p_r^2 + \frac{l^2}{r^2}). \tag{6.26}$$

Integrating Eq.(6.25) yields

$$w_1 = -[\frac{1}{2}\kappa_2^{\mathrm{I}}(s) r^2 \cos(2\theta) + \frac{1}{3}\kappa_3^{\mathrm{I}}(s) r^3 \cos(3\theta + \alpha)]. \tag{6.27}$$

Proceeding to evaluate the second order term w_2 from Eq. (5.29) and noting that $L_1 = \{w_1, \ \}$, we get

$$\begin{aligned} \frac{\partial w_2}{\partial s} &= 2K_2 + 2p_r[\kappa_2^{\mathrm{I}}(s) r \cos(2\theta) + \kappa_3^{\mathrm{I}}(s) r^2 \cos(3\theta + \alpha)] \\ &\quad -2l[\kappa_2^{\mathrm{I}}(s) \sin(2\theta) + \kappa_3^{\mathrm{I}}(s) r \sin(3\theta + \alpha)]. \end{aligned} \tag{6.28}$$

Given that $\langle \kappa_2^{\mathrm{I}} \rangle = \langle \kappa_3^{\mathrm{I}} \rangle = 0$, we must choose $K_2 = 0$ since there are no nonzero average terms. On integrating the above equation, we find

$$w_2 = 2p_r[\kappa_2^{\mathrm{II}} r \cos(2\theta) + \kappa_3^{\mathrm{II}}(s) r^2 \cos(3\theta + \alpha)]$$

$$-2l[\kappa_2^{\mathrm{II}}(s)\sin(2\theta)+\kappa_3^{\mathrm{II}}(s)r\sin(3\theta+\alpha)]. \tag{6.29}$$

Knowing w_2, we can proceed to the next order to calculate w_3 and K_3. Applying Eq. (5.30) we get

$$\begin{aligned}
\frac{\partial w_3}{\partial s} &= 3K_3 - 3p_r^2[\kappa_2^{\mathrm{II}}(s)\cos(2\theta) \\
&\quad +2\kappa_3^{\mathrm{II}}(s)r\cos(3\theta+\alpha)] + 3lp_r[\kappa_3^{\mathrm{II}}(s)\sin(3\theta+\alpha)] \\
&\quad +3\frac{p_r l}{r}[2\kappa_2^{\mathrm{II}}(s)\sin(2\theta)+3\kappa_3^{\mathrm{II}}(s)r\sin(3\theta+\alpha)] \\
&\quad +3\frac{l^2}{r^2}[2\kappa_2^{\mathrm{II}}(s)\cos(2\theta)+3\kappa_3^{\mathrm{II}}(s)r\cos(3\theta+\alpha)] \\
&\quad +[\kappa_2^{\mathrm{II}}(s)r\cos(2\theta)+\kappa_3^{\mathrm{II}}r^2\cos(3\theta+\alpha)][\kappa_2(s)r\cos(2\theta)+\kappa_3 r^2\cos(3\theta+\alpha)] \\
&\quad +[\kappa_2^{\mathrm{II}}(s)\sin(2\theta)+\kappa_3^{\mathrm{II}}(s)r\sin(3\theta+\alpha)][\kappa_2(s)r^2\sin(2\theta)+\kappa_3(s)r^3\sin(3\theta+\alpha)] \\
&\quad -\frac{1}{2}[\kappa_2^{\mathrm{I}}(s)r\cos(2\theta)+\kappa_3^{\mathrm{I}}(s)r^2\cos(3\theta+\alpha)]^2 \\
&\quad -\frac{1}{2}[\kappa_2^{\mathrm{I}}(s)r\sin(2\theta)+\kappa_3^{\mathrm{I}}(s)r^2\sin(3\theta+\alpha)]^2.
\end{aligned} \tag{6.30}$$

From Eqs. (6.23) and (6.24) one can easily identify the terms that average to zero over fast oscillations and those that do not. Once again K_3 is chosen such that it cancels the terms that average to a nonzero value. On simplifying certain averaged terms from integration by parts, the third order transformed Hamiltonian may be expressed as

$$K_3 = \frac{1}{2}\langle(\kappa_2^{\mathrm{I}})^2\rangle r^2 - \frac{1}{3}\langle\kappa_2^{\mathrm{I}}\kappa_3^{\mathrm{I}}\rangle r^3\cos(\theta+\alpha) + \frac{1}{2}\langle(\kappa_3^{\mathrm{I}})^2\rangle r^4. \tag{6.31}$$

Since the Hamiltonian K is defined in the transformed coordinate system, the variables must be replaced by the corresponding transformed variables in the above equation as well as in Eq. (6.26).

In order for K_3 to be independent of Θ, the transformed azimuthal variable, $\langle\kappa_2^{\mathrm{I}}\kappa_3^{\mathrm{I}}\rangle$ must vanish. It is clear from Eqs. (6.23) and (6.24) that one way this can be accomplished is if $\kappa_2(s)$ can be expressed as a pure cosine series and $\kappa_3(s)$ as a pure sine series. Figure (6.3) represents a practical design for $\kappa_2(s)$ and $\kappa_3(s)$ which satisfies this condition. This is a specific case where the two lattices have equal periodicity.

In this case, $\kappa_2(s)$ and $\kappa_3(s)$ are periodic step functions alternating in sign and with opposite parity, which is equivalent to a phase lag of a quarter lattice period with respect to each other. It may be noted that once the Θ dependence is eliminated, the nonlinear force is purely focusing and leads to a positive tune shift. This design is

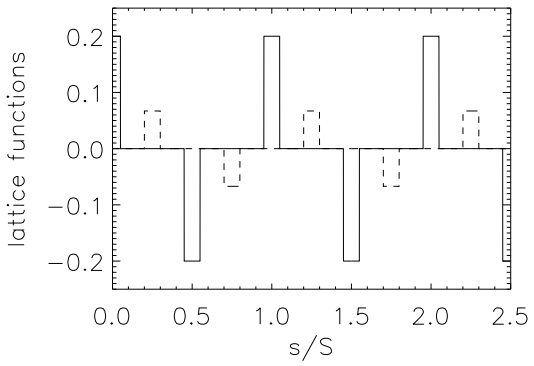

Figure 6.3: A step function lattice that will lead to a near integrable condition. The shorter steps represent the sextupole function $\kappa_3(s)$ while the higher ones the quadrupole function $\kappa_2(s)$.

only the simplest method of realizing optimum integrability and need not necessarily be the most practical one for real machines. However, the formulation of this condition is general enough to accommodate other designs that are possibly easier to implement. The general procedure to apply this is to first express $\kappa_2(s)$ and $\kappa_3(s)$ of an existing design in the form of Eqs. (6.23) and (6.24). Then the coefficient $\langle \kappa_2^{\mathrm{I}} \kappa_3^{\mathrm{I}} \rangle$ will need to be evaluated. This would then tell us how to reposition the magnets in order to minimize this. Numerical results in section VI. will show that considerable improvement in the dynamic aperture can be accomplished even if $\langle \kappa_2^{\mathrm{I}} \kappa_3^{\mathrm{I}} \rangle$ does not completely vanish but is small enough.

The purpose of choosing K_3 to be independent of Θ is to look for a system with improved integrability and thereby improve confinement by reducing chaos. According to the Kolmogorov-Arnold-Moser (KAM) theorem, a system perturbed from integrability will consist of regions of regular motion and regions of chaos with the lat-

ter approaching zero exponentially as the system approaches integrability. This system would be perfectly integrable if the Θ dependence could be completely eliminated. However, the fourth order perturbation term will retain the Θ dependence. Despite this, the numerical results in the following sections will show that restricting the integrability up to third order makes a significant improvement in confinement in accordance with the KAM theorem. It is likely that a few mutipoles or other components such as undulators in synchrotron radiation sources cannot be incorporated in the averaging procedure. Another such example would be beam-beam interactions at interaction point of a storage ring collider where there might be many multipoles located at the same place. Superposing these additional effects randomly to the existing lattice would invariably make the system less integrable. In such a situation, it becomes even more important to obtain a system with optimum integrability since the KAM theorem would still guarantee that there exists a region in phase space with particles having regular trajectories. One could also consider using the method in Ref. [63] to implement the additional nonlinear components to a lattice that has already been designed to be nearly integrable using the method suggested here.

6.3.2 Alternate Gradient Quadrupoles, Sextupoles and Octupoles

Although the analysis in the previous subsection used only sextupoles, this can be extended to include higher multipoles. For example, if octupoles are used in addition to the sextupoles, the Hamiltonian would be

$$\begin{aligned} H = & \frac{1}{2}(p_r^2 + \frac{l^2}{r^2}) + \frac{1}{2}\kappa_2(s) r^2 \cos(2\theta) \\ & \frac{1}{3}\kappa_3(s) r^3 \cos(3\theta + \alpha) + \frac{1}{4}\kappa_4(s) r^4 \cos(4\theta + \gamma) \end{aligned} \tag{6.32}$$

where γ represents the orientation of the octupoles. The third order transformed Hamiltonian will then be

$$K_3 = \frac{1}{2}\langle(\kappa_2^{\mathrm{I}})^2\rangle r^2 + \frac{1}{2}\langle(\kappa_3^{\mathrm{I}})^2\rangle r^4 + \frac{1}{2}\langle(\kappa_4^{\mathrm{I}})^2\rangle r^6$$

$$-\frac{1}{3}\langle\kappa_2^{\rm I}\kappa_3^{\rm I}\rangle r^3\cos(\theta+\alpha)-\frac{1}{3}\langle\kappa_2^{\rm I}\kappa_4^{\rm I}\rangle r^4\cos(2\theta+\gamma)$$
$$-\frac{1}{3}\langle\kappa_3^{\rm I}\kappa_4^{\rm I}\rangle r^5\cos(\theta+\alpha+\gamma). \tag{6.33}$$

The condition $\langle\kappa_2^{\rm I}\kappa_3^{\rm I}\rangle = 0$, $\langle\kappa_2^{\rm I}\kappa_4^{\rm I}\rangle = 0$ and $\langle\kappa_3^{\rm I}\kappa_4^{\rm I}\rangle = 0$ would optimize the integrability of such a system. A practical but idealized design for this to be satisfied is given in Fig. (6.4).

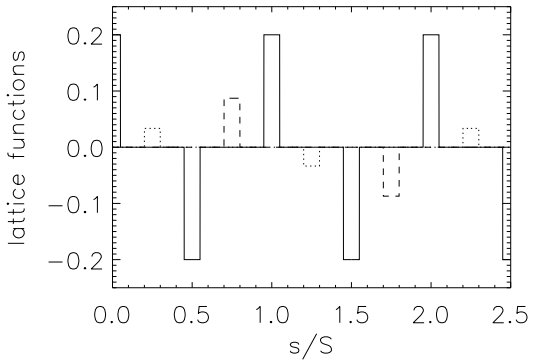

Figure 6.4: A step function lattice leading to a near integrable condition. The shortest steps represent the octupole function $\kappa_4(s)$ while the higher ones the sextupole functions function $\kappa_3(s)$, and the highest ones the quadrupole functions $\kappa_2(s)$.

6.4 Single Particle Trajectories with Nonzero Angular Momentum

To show that particles are better confined when the 90^o phase difference condition is satisfied, numerical calculations were performed using the original Hamiltonian. The results are discussed in this and the next sections. Calculations were performed using a fourth order symplectic integrator [24, 8] in cartesian coordinates. Cartesian coordinates are more convenient for numerical calculations as they enable one to avoid the singularity at the origin arising in the cylindrical coordinate system. The focusing channel consisted of alternating gradient quadrupoles and sextupoles with various phase differences between $\kappa_2(s)$ and $\kappa_3(s)$. The sextupoles were oriented such that $\alpha = -45^o$.

In cartesian coordinates, the force due to quadrupoles is given by

$$\vec{F} = \kappa_2(s)(x\hat{x} - y\hat{y}) \tag{6.34}$$

and that due to the sextupoles (with $\alpha = -45^o$) is given by

$$\vec{F} = \kappa_3(s)[(x^2 - y^2 + 2xy)\hat{x} + (x^2 - y^2 - 2xy)\hat{y})]. \tag{6.35}$$

We define a radial distance $R = \frac{1}{3}|\kappa_2|/|\kappa_3|$ where $|--|$ corresponds to the positive nonzero values of the respective step function. The ratio $|\kappa_2|/|\kappa_3|$ represents a measure of the position where the forces due to the linear and nonlinear components become comparable. The tune shift due to the nonlinear force was close to 15% for a particle initially at $r = R$ and $\theta = 45^o$. The fill factor η is defined as the ratio between the length of the magnets and the length of one lattice period. This was set to 0.2 for both, the quadrupoles and sextupoles. This is typical for most applications. For example, the storage ring of the advanced photon source (APS) has a fill factor of about 0.21 for quadrupoles. When expressed in units of S, η is the smallest time scale to be resolved and so the time step in the computation needs to be much smaller than η. In all the computations, this time step was set to 0.01η. The parameter $\kappa_2(s)$ has units of frequency squared so we can define another dimensionless quantity as $|\kappa_2|S^2$ to which the value of 8.0 was assigned for all calculations. This corresponds to about 7 lattice periods per betatron radial oscillation about the origin. The separation between the quadrupoles and sextupoles is represented by a term,

$$\psi = \frac{2\pi\Delta s}{S} \tag{6.36}$$

where Δs is the spatial distance between the two of them. The averaged Hamiltonian K is independent of Θ when $\psi = 90^o$, *ie*, when the sextupoles are placed halfway between two quadrupoles of opposite sign. The values of R, η, $|\kappa_2|S^2$ and ψ completely specify the focusing system.

When a system is azimuthally symmetric, angular momentum is conserved. In this system, when $\psi = 90^o$, the angular momentum is nearly conserved because the averaged angular momentum is azimuthally symmetric. As one deviates from $\psi = 90^o$, the dependence on θ becomes stronger and the variation of angular momentum becomes more significant. This would lead to increased chaotic motion. In order to verify this, as an example, we examined the trajectory of a particle at $r = 0.15R$. The particle had an initial velocity of $0.05R/S$ in a direction perpendicular to its initial displacement.

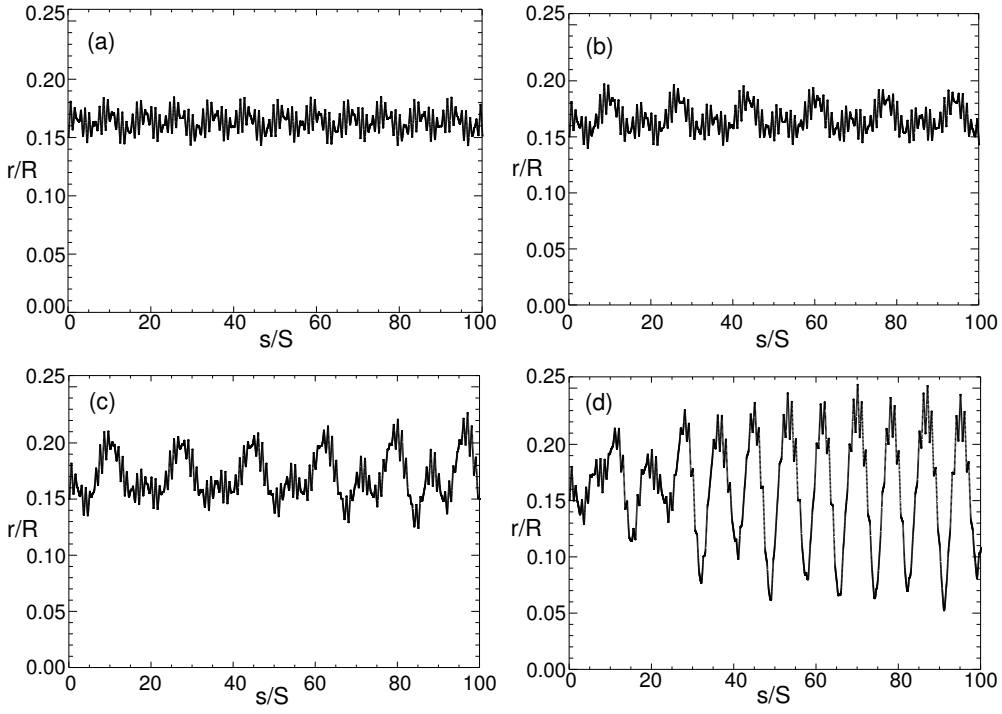

Figure 6.5: Radial oscillation of particles for (a) $\psi = 90^o$, (b) $\psi = 60^o$ (c) $\psi = 30^o$, (d) $\psi = 0^o$

The results of these calculations with respect to different values of ψ are shown in Fig (6.5). The rapid variation in amplitude represents the lattice oscillations. The values of ψ used were 90^o, 60^o, 30^o and 0^o respectively. It is clear that there is a transition to chaotic motion as ψ deviates from 90^o. For $\psi = 90^o$, the maximum amplitude of oscillation is relatively small. When ψ changes to 60^o, the maximum amplitude

increases. At $\psi = 60^o$, we see that additional frequency components are added to the oscillation. When $\psi = 0$, the sextupoles and quadrupoles overlap. In this situation the motion is chaotic. There is no observable repetition in the motion of the particle and it travels well beyond the maximum radial distance attained in the $\psi = 90^o$ case. This transition would have been more rapid if the initial position of the particle was further away from the center. It is sufficient to examine cases where the phase lag between the quadrupoles and sextupoles, ψ, varies from 0^o to 90^o. Phase differences outside this range can be mapped back to a corresponding point between 0^o - 90^o by making an appropriate linear transformation in θ.

The requirement of reduced chaos becomes important when sextupoles or other higher multipoles are present in certain segments of a storage ring where this segment is periodically encountered by the particles. With reduced integrability, the motion becomes sensitive to the initial conditions of the particle at the entrance of the segment. This would eventually lead to increase in oscillation amplitude in the rest of the channel and consequently limit the dynamic aperture of the storage ring.

6.5 Estimation of Dynamic Aperture for Different Cases

The dynamic aperture is defined as the volume in phase space in which all particles remain confined throughout their trajectories in the accelerator. The calculations in this section estimate the projection of the dynamic aperture onto various phase space planes for different values of ψ. In order to perform these calculations, we used 5000 particles that were initially distributed uniformly over the respective plane in phase space, and these were then evolved for 500 lattice periods. It was assumed that particles that travel beyond $r = R$ at any time during this period are not confined. After identifying the particles that remain confined and those that do not, the initial distribution was separated and the positions of these two sets of particles were plotted. In Figs. (6.6,6.7,6.8) the left side represents the initial phase space positions of confined

particles and the ones on the right represent the unconfined particles from the same

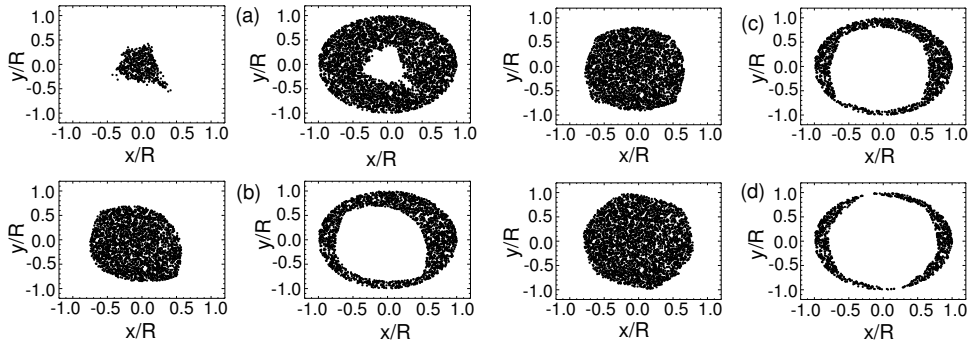

Figure 6.6: Initial distribution of confined and unconfined particles lying on the x-y plane for $\psi =$ (a) 0^o, (b) 30^o (c) 60^o, (d) 90^o

initial distribution. It is important to plot the confined and unconfined particles separately in order to ensure that there is no overlap between the two regions, which is true in these simulations. This is expected because all the phase space variables other than those shown in the respective plot were set to zero. Given that the dynamic aperture allows only confined particles and not a mixture of the two, the left side plots represent the projection of the dynamic aperture onto the respective plane.

Figure (6.6) shows particles lying in the x-y plane that were all initially at rest and distributed uniformly within a circle of radius $r = R$. It may be noticed that when ψ is 0^o, a very small number of these particles are confined. This is the case when the quadrupoles and sextupoles completely overlap. The confinement increases very rapidly as one deviates from $\psi = 0^o$. The area containing the confined particles then gradually increases, reaching a maximum when $\psi = 90^o$ as predicted by the analytic result of the previous section. Another interesting feature revealed by these plots is that the area of confinement acquires sharper corners with increasing ψ.

Figure (6.7) shows confined and unconfined particles from the initial distribution spread out in momentum space. These particles are all located initially at $x = y = 0$ and distributed uniformly within a circle of radius $P = 0.44R/S$. Once again, a rapid

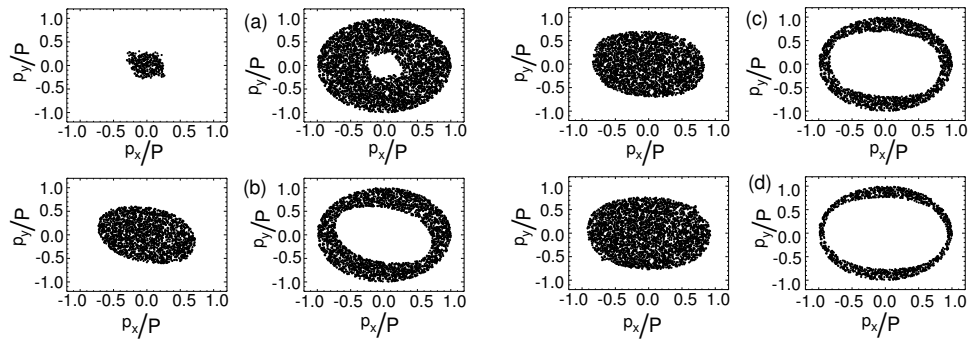

Figure 6.7: Initial distribution of confined and unconfined particles lying on the $p_x - p_y$ plane for $\psi =$ (a) 0^o, (b) 30^o (c) 60^o, (d) 90^o

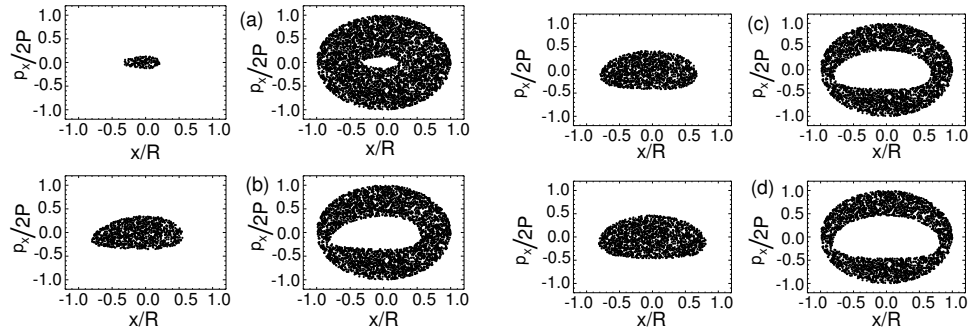

Figure 6.8: Initial distribution of confined and unconfined particles lying on the $x - p_x$ plane for $\psi =$ (a) 0^o, (b) 30^o (c) 60^o, (d) 90^o

improvement in confinement is seen as one deviates from $\psi = 0^o$ and there is then a gradual improvement as ψ approaches 90^o. Unlike the previous case, the boundary of the region of confinement is smooth for all values of ψ. We also see that the dynamic aperture attains a more circular shape for $\psi = 90^o$ which could be attributed to weaker dependence of the dynamics on θ.

Figure (6.8) shows particles distributed over an ellipse such that

$$\frac{x^2}{R^2} + \frac{p_x^2}{(2P)^2} < 1 \tag{6.37}$$

while all other phase space values are zero. Qualitatively, the same behavior is noticeable as in the previous cases. The figures also show that the shape of the dynamic aperture exhibits less symmetry about the origin along the x-axis as ψ decreases from 90^o. This

is also a reflection of increased symmetry in the dynamics along θ.

In contrast to the dramatic improvement in the dynamic aperture seen when ϕ was close to zero, there was only a small improvement when ψ changed from 60^o to 90^o, This phenomena is important in applications where it is not possible to achieve the idealized condition due to other practical limitations often demanding that such theoretically derived conditions be sufficiently robust to be useful. Improvement in the region of confinement, which is directly related to increased size of the dynamic aperture is an important aspect in improving the performance of particle accelerators. It has been shown how the presence of higher order poles can limit the size of the dynamic aperture in circular accelerators [26].

6.6 Summary

In this chapter, a condition for improved dynamic aperture is derived for nonlinear lattices in particle accelerators. To start with, the Lie transform perturbation method is presented for averaging over fast time scales. The validity of the method is first verified numerically for a linear periodic focusing system. This averaging procedure is then applied to nonlinear focusing systems with quadrupoles and sextupoles. The Hamiltonian of this system contains terms with mixed variables, a situation in which the Lie transform method greatly simplifies the analysis. This analysis yields a condition for the Hamiltonian to have increased symmetry thereby reducing chaos and increasing the dynamic aperture. The condition leads to a canonical transformation where the new Hamiltonian is independent of its azimuthal variable up to third order in the perturbation expansion. While the analysis was performed explicitly for a lattice with quadrupoles and sextupoles, it was straightforward to show that similar conditions exist when even higher order mutipoles or combinations of these are used. Unlike the traditional approach of analyzing a nonlinear lattice, no assumption was made that the nonlinear focusing was small compared to the linear focusing strength.

Hence this analysis is valid even when the nonlinearity is strong enough that the closed form Courant-Snyder solutions are not valid.

Numerical calculations were performed for a particular case in which the focusing components were quadrupoles and sextupoles represented by periodic step function lattices of equal periodicity. In this case, the condition of azimuthal symmetry in the transformed frame was satisfied by having a phase difference of $\psi = 90^o$, equivalent to a quarter of a lattice period between the quadupoles and sextupoles. Single particle trajectories of particles with angular momentum showed increased chaotic behavior as ψ decreased from 90^o to 0^o. The size of the dynamic aperture was estimated by allowing the particles to drift up to a maximum radial distance which allowed a maximum tune shift of about 15% when compared to arbitrarily small oscillations. Calculations showed that the size of the dynamic aperture increased rapidly as ψ increased from 0^o and gradually reached a maximum as ψ approached 90^o. Results showed that the condition was robust enough for possible practical applications

While the parameters used in the calculations were realistic, they were also simplified. This theory remains to be applied to parameters specific to real machines. For example, it would be interesting to apply it in the use of sextupoles for chromaticity corrections in storage rings with their lattice periods different from that of the quadrupoles and also having a different fill factor. This would still allow conditions for a near integrable system and so one should expect improved confinement by imposing the same.

The derivation of the symmetric transformed Hamiltonian in this chapter is expected to benefit various current and proposed applications of nonlinear lattices in particle accelerators. It would also add to previous work on increasing the dynamic aperture of accelerator lattices in the presence of nonlinear components [63]. The Lie transform perturbation method presented here is easily applicable to other areas of Hamiltonian dynamics as well where it is required to perform a time averaging over certain fast time scales.

Chapter 7

A Near Equilibrium Phase Space Distribution for High Intensity Beams with Nonlinear Focusing.

7.1 Introduction

A procedure to obtain a near equilibrium phase space distribution function has been derived for high intensity beams with space charge effects and nonlinear focusing. A method to average the single particle Hamiltonian over fast time scales in the presence of space charge forces is first derived, by using the Lie Transform method to canonically transform to slowly oscillating phase space coordinates. Such a formulation is useful in calculating physical effects that evolve over the slowly varying time scale and where fast oscillating phenomena may be ignored. The theory is then applied to a beam propagating through a nonlinear focusing channel. The lattice is arranged such that the resulting Hamiltonian for a single particle system is azimuthally symmetric when the dynamics is averaged over fast oscillations. The analysis first shows the existence of a phase space distribution that retains this symmetry, and then a near equilibrium solution is obtained that also retains this symmetry. The resulting equilibrium distribution will then have no oscillations in the slow time scales but will have only perturbed fast oscillations along with density perturbations in the azimuthal direction. The distribution functions may be numerically determined for a linear and nonlinear lattice.

There is a wide interest in the study of periodically focused beams with intensities high enough that self field effects become important [16]. Interest has also arisen in

the study and applications of nonlinear focusing, some of which involve intense beams [61, 5, 4, 60, 49, 43, 56]. Of particular value in the study of intense beams is obtaining an equilibrium or near equilibrium distribution. This is useful in various stability analysis, in preparing beams that are well matched or to perform numerical simulations of beams that are perturbed from this matched condition. The only known exact beam equilibrium is the Kapchinskij-Vladmirskij (KV) distribution [38]. This distribution applies only to a linear focusing system and is also unphysical with the density having a discontinuity at the edge and being exactly uniform in the interior of the beam. Recently, perturbation methods have been developed to perform Hamiltonian averaging to study high intensity beams including obtaining more realistic near equilibrium distributions. These studies have been applied primarily to linear focusing systems [17, 62].

In this paper, we first extend the Lie Transform method to average the dynamics of a single particle over fast oscillations. This is done by canonically transforming to slowly varying phase space coordinates. The resulting phase space distribution derived from the analysis satisfies the Vlasov-Poisson equation up to the desired order. This kind of averaging is useful in problems where only the slow evolution of a system is of interest, where the transformed or averaged Hamiltonian is often more convenient to use in numerical calculations. Moreover, in many cases the transformed Hamiltonian reduces a two dimensional problem to a one dimensional one, reducing the computation time by many orders of magnitude.

The method is then applied to a beam propagating through a nonlinear focusing channel consisting of alternating gradient quadrupoles and higher order poles like sextupoles or octupoles along with the quadrupoles. It has already been proved [57] that a condition exists wherein this nonlinear lattice can be designed in such a way that the resulting Hamiltonian is azimuthally symmetric in the slowly varying coordinate system for the motion of a single charged particle. The analysis in this chapter will prove the existence of a phase space distribution such that this condition of symmetry is retained

in the presence of space charge forces for the same nonlinear lattice. A symmetric Hamiltonian also implies improved integrability, a condition that is desirable because it leads to increased dynamic aperture which is generally difficult to achieve for nonlinear focusing channels especially in the presence of space charge forces. The combination of an equilibrium solution with improved integrability is favorable for a stable beam with respect to mismatches and minimizing initial emittance growth.

The equilibrium distribution may be determined by numerically solving the steady state Vlasov-Poisson equation in the averaged reference frame. Transforming back to the laboratory frame of reference yields a distribution function which has no envelope oscillations but has perturbations over the lattice period, leading to a near equilibrium distribution.

7.2 Obtaining Averaged Hamiltonians with Space Charge Terms

This section gives a brief introduction to the Lie Transform method as used for averaging over fast oscillations along with the additional terms arising due to a space charge component in the Hamiltonian. As discussed in previous chapters, using ϵ as an order parameter, it is possible to transform perturbatively to a new reference frame starting from a Hamiltonian expressed as

$$H = H_0 + \epsilon H_1 + \epsilon^2 H_2 + \epsilon^3 H_3 + \cdots \tag{7.1}$$

this Hamiltonian will then be transformed to

$$K = K_0 + \epsilon K_1 + \epsilon^2 K_2 + \epsilon^3 K_3 + \cdots \tag{7.2}$$

In the presence of space charge forces, the Hamiltonian may be expressed as

$$H = H^e + H^{sc} \tag{7.3}$$

where H^e is the term arising due to external forces and kinetic energy terms while H^{sc} arises due to space charge forces. We consider a thin, long beam with the space

charge potential satisfying Poisson's equation. It may be noted that the force due to the magnetic field arising from the motion of the charge has the same form as the electrostatic potential, so the units can be normalized to accommodate both the forces. The Hamiltonian of such a system may be expressed in cylindrical coordinates as

$$H = \frac{1}{2}(p_r^2 + \frac{l^2}{r^2}) + U(r,\theta,s) + \frac{q}{mv_s^2\gamma^3}\phi(r,\theta,s) \tag{7.4}$$

Where $H^e = \frac{1}{2}(p_r^2 + \frac{l^2}{r^2}) + U(r,\theta,s)$ and $H^{sc} = (q/mv_s^2\gamma^3)\phi(r,\theta,s)$, the space charge potential takes into account both the electric and magnetic self forces acting on the particles of the beam in which m is the mass, q the charge and v_s the axial velocity of the particle, and γ is the Lorentz relativistic factor. The external focusing potential U is periodic with a periodicity S. The axial distance, s is equivalent to time for a beam with constant axial velocity.

In the analysis to follow, we disregard the effects of a finite boundary. A Green's function approach to the same problem which can include the effect of finite boundaries can be found in Ref. [11]. Where ever convenient, we represent the phase space vectors by $\mathbf{q} = (r,\theta)$, $\mathbf{p} = (p_r, l)$ in the original reference frame, and by $\mathbf{Q} = (R,\Theta)$, $\mathbf{P} = (P_r, \mathcal{L})$ in the transformed reference frame. The space charge potential satisfying Poisson's equation is then given by,

$$\nabla^2\phi(\mathbf{q},t) = -\frac{q}{\epsilon_0}\int d\mathbf{q}'d\mathbf{p}'\delta(\mathbf{q}-\mathbf{q}')f(\mathbf{q}',\mathbf{p}',t) \tag{7.5}$$

where f is the phase space density that is given by the Vlasov equation.

$$\frac{df}{ds} = \frac{\partial f}{\partial s} + \{H, f\}. \tag{7.6}$$

If $F(\mathbf{Q},\mathbf{P},t) = f(\mathbf{q}(\mathbf{Q},\mathbf{P},t),\mathbf{p}(\mathbf{Q},\mathbf{P},t),t)$, then it can be easily verified that $f = TF$ where T is the transformation operator defined in chapter 5. From the property of canonical invariance of the Vlasov equation, we have

$$\frac{dF}{ds} = \frac{\partial F}{\partial s} + \{K, F\}, \tag{7.7}$$

where K is the transformed Hamiltonian. Using the perturbation expansion terms of the transformation operator T given by Eqs. (5.13 - 5.16), we can in principle expand f in terms of F. This would give,

$$\begin{aligned} f &= TF = T_0F + T_1F + T_2F + T_3F \ldots \\ &= f_0 + \epsilon f_1 + \epsilon^2 f_2 + \epsilon^3 f_3 + \ldots \end{aligned} \tag{7.8}$$

From this, the number density $n(\mathbf{q}, \mathbf{p}, t)$, which is the number of particles per unit area of cross section per unit length can be determined, where

$$n(\mathbf{q}, \mathbf{p}, t) = \int d\mathbf{p} f(\mathbf{q}, \mathbf{p}, t) \tag{7.9}$$

and n_0, n_1, n_2 etc can be got by integrating f_0, f_1, f_2 etc respectively in momentum space. This expansion can be used to determine the different order terms of ϕ from Eq. (7.5) giving

$$\phi = \phi_1 + \phi_2 + \phi_3 + \phi_4 + \cdots \tag{7.10}$$

The index for representing the expansion terms of ϕ has been deliberately shifted for reasons that will become clear later. Since T_0 is simply the identity operator, it is straight forward to verify that the first term of ϕ satisfies,

$$\nabla^2 \phi_1 = -\frac{q}{\epsilon_0} \int dp F \tag{7.11}$$

In this analysis, we carry out the transformation up to third order. It is assumed that the lowest nonzero term of the Hamiltonian is proportional to ϵ, a quantity that turns out to be the ratio between the fast and slow oscillation time periods respectively. This ordering scheme enables one to perform a canonical transformation to slowly varying coordinates and has been used before [11, 18, 57]. In this case, we have $H_0 = 0$, $H_1 = H^e + \phi_1$, $H_2 = \phi_2$ and $H_3 = \phi_3$. Applying these terms in the equations (5.27 - 5.30), the transformed Hamiltonian K and the Lie operator w may be determined. Up to third order, we get the following equations.

$$K_0 = 0, \tag{7.12}$$

$$\frac{\partial w_1}{\partial t} = K_1 - H^e - \frac{q}{mv_s^2\gamma^3}\phi_1, \tag{7.13}$$

$$\frac{\partial w_2}{\partial t} = 2(K_2 - \frac{q}{mv_s^2\gamma^3}\phi_2) - L_1(K_1 + H^e + \frac{q}{mv_s^2\gamma^3}\phi_1), \tag{7.14}$$

$$\begin{aligned}\frac{\partial w_3}{\partial t} &= 3(K_3 - \frac{q}{mv_s^2\gamma^3}\phi_3) - L_1(K_2 + 2\frac{q}{mv_s^2\gamma^3}\phi_2) - \\ &L_2(K_1 + \frac{1}{2}H^e + \frac{1}{2}\frac{q}{mv_s^2\gamma^3}\phi_1) - \frac{1}{2}L_1^2(H^e + \frac{q}{mv_s^2\gamma^3}\phi_1)\end{aligned} \tag{7.15}$$

It may be noted that, K is initially expressed as a function of $(\mathbf{q}, \mathbf{p})$, the original variables. However, based on the canonical invariance of the whole formulation, in the end, $(\mathbf{q}, \mathbf{p})$ may be simply replaced by $(\mathbf{Q}, \mathbf{P})$, the transformed variables.

We apply these equations to the Hamiltonian in Eq (7.4). The external potential is decomposed into a term averaged over a period S and an oscillating term. This is,

$$U(r, \theta, s) = \langle U(r, \theta, s)\rangle + \tilde{U}(r, \theta, s), \tag{7.16}$$

where the angle brackets represents the following,

$$\langle U(r, \theta, s)\rangle = \frac{1}{S}\int_s^{s+S} U(r, \theta, s)ds. \tag{7.17}$$

The zeroth order equation simply gives $K_0 = 0$. The first order equation gives,

$$\frac{\partial w_1}{\partial s} = K_1 - (\frac{1}{2}p_r^2 + \frac{l^2}{r^2}) - \langle U\rangle - \tilde{U} - \frac{q}{mv_s^2\gamma^3}\phi_1. \tag{7.18}$$

The term K_1 will be chosen such that it contains only terms with a nonzero average over the fast time scale. It is clear from Eq. (7.11) that the space charge term ϕ_1 does not average to zero, since F depends upon only the transformed coordinates. As a result, we obtain,

$$K_1 = \frac{1}{2}(p_r^2 + \frac{l^2}{r^2}) + \langle U\rangle + \frac{q}{mv_s^2\gamma^3}\phi_1. \tag{7.19}$$

Inserting this into Eq (7.18) and integrating with respect to s yields,

$$w_1 = -\tilde{U}^{\mathrm{I}}. \tag{7.20}$$

The Roman numerical superscript represents an integration over s where a constant is chosen such that $\langle w \rangle = 0$. This is equivalent to an indefinite integral of a Fourier expansion of $\tilde{U}$. This condition is necessary to prevent w_n from being secular (unbounded) in "time" s [9]. Similarly, a superscript "II" represents a double integral with the same condition and so on.

Knowing w_1 enables us to determine f_1 and ϕ_2 in terms of F. These are, from Eq (7.8)

$$f_1 = T_1 F = -\frac{\partial \tilde{U}^{\mathrm{I}}}{\partial \mathbf{q}} \cdot \frac{F(\mathbf{q}, \mathbf{p}, t)}{\partial \mathbf{p}} \tag{7.21}$$

and

$$\nabla^2 \phi_2 = -\frac{q}{\epsilon} \int d\mathbf{p} f_1 = \frac{q}{\epsilon_0} \frac{\partial \tilde{U}^{\mathrm{I}}}{\partial \mathbf{q}} \cdot \int d\mathbf{p} \frac{F(\mathbf{q}, \mathbf{p}, t}{\partial \mathbf{p}} = 0 \tag{7.22}$$

where it is assumed that $f_1 \to 0$ as $\mathbf{p} \to \infty$. Consequently, the first order term of the number density $n_1 = 0$.

Repeating the same procedure with the second order equation gives

$$K_2 = 0 \tag{7.23}$$

and this gives

$$w_2 = 2(\frac{\partial \tilde{U}^{\mathrm{II}}}{\partial r} p_r + \frac{\partial \tilde{U}^{\mathrm{II}}}{\partial \theta} \frac{l}{r^2}) \tag{7.24}$$

requiring that $\langle \tilde{U}^{\mathrm{II}} \rangle = 0$, leads to the condition $\langle w_2 \rangle = 0$. Knowing the expression for w_2 can now enable us to determine f_2 and ϕ_3 from T_2 given by Eq. (5.15). This gives

$$\begin{aligned} f_2 = T_2 F = &- \left[\frac{\partial^2 \tilde{U}^{\mathrm{II}}}{\partial r^2} p_r + \frac{\partial^2 \tilde{U}^{\mathrm{II}}}{\partial \theta \partial r} \frac{l}{r} - 2 \frac{\partial \tilde{U}^{\mathrm{II}}}{\partial \theta} \frac{l}{r^3} \right] \frac{\partial F}{\partial p_r} \\ &- \left[\frac{\partial^2 \tilde{U}^{\mathrm{II}}}{\partial \theta \partial r} + \frac{\partial^2 \tilde{U}^{\mathrm{II}}}{\partial \theta^2} \frac{l}{r^2} \right] \frac{\partial F}{\partial l} + \left[\frac{\partial \tilde{U}^{\mathrm{II}}}{\partial r} \frac{\partial F}{\partial r} + \frac{\partial \tilde{U}^{\mathrm{II}}}{\partial \theta} \frac{1}{r^2} \frac{\partial F}{\partial \theta} \right] \\ &+ \frac{1}{2} \left(\frac{\partial \tilde{U}^{\mathrm{I}}}{\partial r} \right)^2 \frac{\partial^2 F}{\partial p_r^2} + \frac{\partial \tilde{U}^{\mathrm{I}}}{\partial \theta} \frac{\partial \tilde{U}^{\mathrm{I}}}{\partial r} \frac{\partial^2 F}{\partial p_r \partial l} + \frac{1}{2} \left(\frac{\partial \tilde{U}^{\mathrm{I}}}{\partial \theta} \right)^2 \frac{\partial^2 F}{\partial l^2} \end{aligned} \tag{7.25}$$

Integrating by parts and using the assumption that $F \to 0$ as $\mathbf{p} \to \infty$ we get,

$$\begin{aligned} &\nabla^2 \phi_3 = -\frac{q}{\epsilon_0} \int d\mathbf{p} f_2 = \\ &-\frac{q}{\epsilon_0} \left[\frac{\partial^2 \tilde{U}^{\mathrm{II}}}{\partial r^2} + \frac{\partial^2 \tilde{U}^{\mathrm{II}}}{\partial \theta^2} \frac{1}{r^2} \right] n_0 - \frac{q}{\epsilon_0} \left[\frac{\partial \tilde{U}^{\mathrm{II}}}{\partial r} \frac{\partial n_0}{\partial r} + \frac{\partial \tilde{U}^{\mathrm{II}}}{\partial \theta} \frac{1}{r^2} \frac{\partial n_0}{\partial \theta} \right] \end{aligned} \tag{7.26}$$

Applying the third order equation is less straightforward. Simplifying Eq.(7.15), gives

$$\begin{aligned}\frac{\partial w_3}{\partial s} &= 3K_3 - 3\frac{q}{mv_s^2\gamma^3}\phi_3 - \frac{3}{2}(\frac{\partial w_2}{\partial r}p_r + \frac{\partial w_2}{\partial \theta}\frac{l}{r^2}) \\ &\quad -3\frac{l^3}{r^3}\frac{\partial \tilde{U}^{\mathrm{I}}}{\partial r} + D(3\langle U\rangle + \tilde{U} + 3\frac{q}{mv_s^2\gamma^3}\phi_1) \\ &\quad -\frac{1}{2}[(\frac{\partial \tilde{U}^{\mathrm{I}}}{\partial r})^2 + \frac{1}{r^2}(\frac{\partial \tilde{U}^{\mathrm{I}}}{\partial \theta})^2] \end{aligned} \tag{7.27}$$

where D is a differential operator given by

$$D = \frac{\partial \tilde{U}^{\mathrm{II}}}{\partial r}\frac{\partial}{\partial r} + \frac{1}{r^2}\frac{\partial \tilde{U}^{\mathrm{II}}}{\partial \theta}\frac{\partial}{\partial \theta} \tag{7.28}$$

While integrating Eq (7.27) with respect to s, we need to retain only the third order terms. Integrating $D\phi_1(r,\theta,s)$ by parts recurrently, we get

$$(D\phi_1)^{\mathrm{I}} = D^{\mathrm{I}}\phi_1 + D^{\mathrm{II}}\frac{\partial \phi_1}{\partial s} + D^{\mathrm{III}}\frac{\partial^2 \phi_1}{\partial s^2} + \ldots \tag{7.29}$$

The order parameter, ϵ is proportional to the ratio between the frequencies of the slow and fast oscillating components. The operator D is a fast oscillating term, so integrating it results in introducing a factor that is the inverse of the frequency of oscillation of D. On the other hand, $\phi_1(r,\theta,s)$ is a slowly oscillating term and so differentiating it with respect to s effectively introduces a factor equivalent to the frequency of oscillation of ϕ_1. Thus, the only term of relevance in the expansion is $D^{\mathrm{I}}\phi_1(r,\theta,s)$. As a result, up to the desired order in ϵ we have,

$$(D\phi_1)^{\mathrm{I}} \simeq \frac{\partial \tilde{U}^{\mathrm{III}}}{\partial r}\frac{\partial \phi_1}{\partial r} + \frac{1}{r^2}\frac{\partial \tilde{U}^{\mathrm{III}}}{\partial \theta}\frac{\partial \phi_1}{\partial \theta} \tag{7.30}$$

For the same reason, we have

$$\langle D(r,\theta,s)\phi_1(r,\theta,s)\rangle \simeq \langle D(r,\theta,s)\rangle\phi_1(r,\theta,s) = 0 \tag{7.31}$$

Equation (7.26) indicates that ϕ_3 is also a product of a slow and a fast oscillating term and the same rules may be applied while integrating with respect to s. As a result,

we have $\langle\phi_3\rangle \simeq 0$ and also,

$$\nabla^2\phi_3^{\mathrm{I}}(\mathbf{q},s) \simeq -\frac{q}{\epsilon_0}\left[\frac{\partial^2\tilde{U}^{\mathrm{III}}}{\partial r^2}+\frac{\partial^2\tilde{U}^{\mathrm{III}}}{\partial\theta^2}\frac{l}{r^3}\right]n_0-\frac{q}{\epsilon_0}\left[\frac{\partial\tilde{U}^{\mathrm{III}}}{\partial r}\frac{\partial n_0}{\partial r}+\frac{\partial\tilde{U}^{\mathrm{III}}}{\partial\theta}\frac{1}{r^3}\frac{\partial n_0}{\partial\theta}\right] \quad (7.32)$$

Once again, K_3 needs to be chosen so that it cancels terms with nonzero averages over the lattice periods. Using the result $\langle\phi_3\rangle \simeq 0$ and Eq.(7.31), and recognizing other terms that average to zero over the lattice period S, we get

$$K_3 = \frac{1}{3}[-\langle\frac{\partial\tilde{U}^{\mathrm{II}}}{\partial r}\frac{\partial\tilde{U}}{\partial r}+\frac{1}{r^2}\frac{\partial\tilde{U}^{\mathrm{II}}}{\partial\theta}\frac{\partial\tilde{U}}{\partial\theta}\rangle+\frac{1}{6}\langle(\frac{\partial\tilde{U}^{\mathrm{I}}}{\partial r})^2+\frac{1}{r^2}(\frac{\partial\tilde{U}^{\mathrm{I}}}{\partial\theta})^2\rangle] \quad (7.33)$$

The third order transformed Hamiltonian contains no space charge term and is identical to what would be obtained for a single particle in the absence of any space charge. However, it will be seen that the space charge terms appear in the third order transformation equations.

Evaluating w_3 explicitly will involve integrating all terms in the manner similar to previous cases and also applying the results from Eq.(7.30) and (7.32). Let us first define a term $\tilde{G}$ such that

$$\begin{aligned}\tilde{G} \quad &= 3K_3+(\frac{\partial\tilde{U}^{\mathrm{II}}}{\partial r}\frac{\partial U}{\partial r}+\frac{1}{r^2}\frac{\partial\tilde{U}^{\mathrm{II}}}{\partial\theta}\frac{\partial U}{\partial\theta})\\ &\quad -\frac{1}{2}[(\frac{\partial\tilde{U}^{\mathrm{I}}}{\partial r})^2+\frac{1}{r^2}(\frac{\partial\tilde{U}^{\mathrm{I}}}{\partial\theta})^2] \end{aligned} \quad (7.34)$$

Based on the choice of K_3, we know that $\tilde{G}$ is fast oscillating with a zero average. The function w_3 can now be expressed more compactly as

$$\begin{aligned} w_3 \;=\; &\tilde{G}^{\mathrm{I}}-3\frac{q}{mv_s^2\gamma^3}\phi_2^{\mathrm{I}}-\frac{3}{2}(\frac{\partial w_3}{\partial r}+\frac{\partial w_2}{\partial\theta}\frac{l}{r^2})^{\mathrm{I}}\\ &-3\frac{l^3}{r^3}\frac{\partial\tilde{U}^{\mathrm{III}}}{\partial r}+3D^{\mathrm{I}}(\langle U\rangle+\frac{q}{mv_s^2\gamma^3}\phi_1) \end{aligned} \quad (7.35)$$

This would enable one to determine expressions for f_3 and ϕ_4 which are, from Eq. 5.16

$$f_3 = T_3F = -\frac{1}{3}\{w_3,F\}+\frac{1}{6}\{w_1,\{w_2,F\}\}+\frac{1}{3}\{w_2,\{w_1,F\}\}-\frac{1}{6}\{w_1,\{w_1,\{w_1,F\}\}\} \quad (7.36)$$

and from this,

$$\nabla^2\phi_4 = -\frac{q}{\epsilon_0}\int d\mathbf{p} f_3 \tag{7.37}$$

These shall not be evaluated explicitly but enough has been done to show how it could be done in principle.

The transformed Hamiltonian is now given up to third order by

$$K = K_1 + K_2 + K_3 \tag{7.38}$$

where the parameter ϵ is now set to one. The variables of this function will need to be replaced by the transformed ones, and then this Hamiltonian will contain a constant focusing potential and in general a slowly varying space charge potential, which would also be time invariant in the case of an equilibrium distribution in the transformed reference frame. This completes the general derivation of an averaged Hamiltonian along with the procedure to transform the variables between the two coordinate systems.

7.3 A Near Equilibrium Solution for a Nonlinear Focusing System

We now apply the method developed in the previous section to a specific case of nonlinear focusing. The Hamilton for a system with quadrupoles and sextupoles and a space charge potential can be represented as [57].

$$\begin{aligned} H &= \frac{1}{2}(p_r^2 + \frac{l^2}{r^2}) + \frac{1}{2}\kappa_2(s)r^2\cos(2\theta) \\ &\quad \frac{1}{3}\kappa_3(s)r^3\cos(3\theta+\alpha) + \phi(r,\theta,s). \end{aligned} \tag{7.39}$$

The values of $\kappa_2(s)$ and $\kappa_3(s)$ depend upon the strength of the quadrupole and sextupole magnets respectively and also the velocity of the particle in the axial direction. The angle α is determined by the orientation of the sextupoles with respect to the quadrupoles. We use normalized units in which the charge and mass of the particle are unity. In this case, it is assumed that the Hamiltonian is periodic in s with periodicity S, *ie*, $\kappa_2(s+S) = \kappa_2(s)$ and $\kappa_3(S+s) = \kappa_3(s)$. It is further assumed that $\kappa_2(s)$ and

$\kappa_3(s)$ are periodic step functions with the same periodicity S, with a zero average over S. That is,

$$\langle \kappa_2 \rangle = \frac{1}{S}\int_s^{s+S} \kappa_2(s)ds = 0 \tag{7.40}$$

and the same for κ_3. Thus, for this case, we have $\langle U \rangle = 0$ and $\tilde{U} = \frac{1}{2}\kappa_2(s)r^2\cos(2\theta) + \frac{1}{3}\kappa_3(s)r^3\cos(3\theta+\alpha)$.

It has already been shown [57] that when the analysis of the previous section is applied to this system in the absence of space charges, the Hamiltonian can be transformed to an azimuthally symmetric if $\langle \kappa_2^{\mathrm{I}}\kappa_3^{\mathrm{I}} \rangle = 0$. Using the Hamiltonian derived in this reference and including the effects of space charge based on the analysis of Sec.7.2, we get up to third order,

$$K = \frac{1}{2}(P_r^2 + \frac{\mathcal{L}^2}{R^2}) + \frac{1}{2}\langle(\kappa_2^{\mathrm{I}})^2\rangle R^2 + \frac{1}{4}\langle(\kappa_3^{\mathrm{I}})^2\rangle R^4 + \frac{q}{mv_s^2\gamma^3}\phi_1 \tag{7.41}$$

This expression for the Hamiltonian can be obtained from a realistic focusing system such as a step function lattice, which brings about a connection with the idealized constant focusing model used in the study of beam halos in chapter 4.

Since this system has focusing components that are azimuthally symmetric, it should allow a self consistent phase space distribution F that is also independent of Θ. The transformed angular momentum would then be a conserved quantity. Since the focusing is constant, we can seek an equilibrium solution in the transformed coordinate frame. A practical choice would be a thermal equilibrium which is given by

$$\begin{aligned} F(P,R,\mathcal{L}) &= N_0\zeta\exp[K/\mathcal{K}_0] \\ &N_0\zeta\exp\{-[\frac{1}{2}(P_r^2+\frac{\mathcal{L}^2}{R^2}) + V(R) + \frac{q}{mv_s^2\gamma^3}\phi_1]/\mathcal{K}_0\} \end{aligned} \tag{7.42}$$

where, $\mathcal{K}_0$ is a constant, N_0 is the total number of particles, and ζ is chosen such that F is normalized to the total number of particles, *ie*,

$$\frac{1}{\zeta} = \int d\mathbf{Q}d\mathbf{P}\exp\{-[\frac{1}{2}(P_r^2+\frac{\mathcal{L}^2}{R^2}) + V(R) + \frac{q}{mv_s^2\gamma^3}\phi_1]/\mathcal{K}_0\} \tag{7.43}$$

and, from Eq (7.41) the external potential is given by,

$$V(R) = \frac{1}{2}\langle(\kappa_2^{\rm I})^2\rangle R^2 + \frac{1}{4}\langle(\kappa_3^{\rm I})^2\rangle R^4. \tag{7.44}$$

Substituting this into Eq(7.5) and recognizing that that there is only one independent variable, r, we obtain,

$$\frac{1}{r}\frac{d}{dr}r\frac{d}{r}\phi_1 = -\frac{q}{\epsilon_0}\zeta N_0 \mathcal{K}_0 \pi \exp\{-[V(r) + \frac{q}{mv_s^2\gamma^3}\phi_1(r)]/\mathcal{K}_0\} \tag{7.45}$$

On solving for ϕ_1, we can determine F from which f_1, f_2 and f_3, and their integrals over momentum space, n_1, n_2 and n_3 can calculated as described in the previous section. These are,

$$n_0(\mathbf{q}, s) = \int \mathbf{dp} F \tag{7.46}$$

$$n_1 = 0 \tag{7.47}$$

$$n_2 = \left[\frac{\partial^2 \tilde{U}^{\rm II}}{\partial r^2} + \frac{\partial^2 \tilde{U}^{\rm II}}{\partial \theta^2}\frac{1}{r^2}\right] n_0 + \left[\frac{\partial \tilde{U}^{\rm II}}{\partial r}\frac{\partial n_0}{\partial r} + \frac{\partial \tilde{U}^{\rm II}}{\partial \theta}\frac{1}{r^2}\frac{\partial n_0}{\partial \theta}\right] \tag{7.48}$$

since in this case, $\tilde{U} = \frac{1}{2}\kappa_2(s)r^2\cos(2\theta) + \frac{1}{3}\kappa_3(s)r^3\cos(3\theta+\alpha)$, and n_0 is independent of θ, we obtain

$$n_2 = -[\kappa_2^{\rm II}\cos(2\theta) + 2r\kappa_3^{\rm II}\cos(3\theta+\alpha)]n_0 + [\kappa_2^{\rm II} r\cos(2\theta) + \kappa_3^{\rm II} r^2\cos(3\theta+\alpha)]\frac{\partial n_0}{\partial r} \tag{7.49}$$

It is clear that with F being independent of θ and s, n_0 will be stationary and independent of θ too. The variation in θ and s comes about only in the second order perturbation in n, which is n_2. The coefficients $\kappa_2^{\rm II}$ and $\kappa_3^{\rm II}$ are plotted in Fig 7.1 for a step function lattice corresponding to the one used in the dynamic aperture analysis in chapter 6.

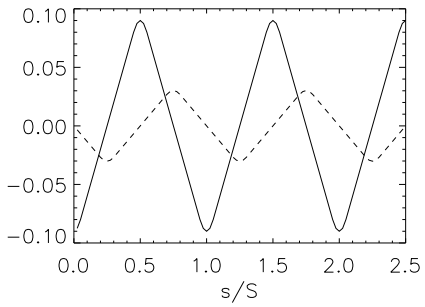

Figure 7.1: Plot of κ_2^{II} and κ_3^{II} for the step function lattice shown in Fig 6.3

7.4 Summary

In this chapter the Lie transformation perturbation method was presented for performing an averaging over fast oscillations for high intensity beams with a general external potential and a space charge potential. This method proves to be convenient under certain circumstances when compared to other methods. A procedure was then derived to transform the phase space distribution from the averaged phase space coordinates to the laboratory coordinates. When one is interested in observing physical phenomena occurring over long time scales, it is sufficient to solve the averaged Vlasov-Poisson equations. This reduces computation time especially when the averaging procedure reduces the number of degrees of freedom. The phase space distribution may be transformed back to the laboratory reference frame once the computation is completed if necessary.

The averaging procedure was then applied to a nonlinear focusing lattice with quadrupoles and sextupoles for a beam with space charge effects. The focusing components were arranged in such a way that the external component of the Hamiltonian was independent of the azimuthal variable after performing the averaging. This proved the existence of a phase space distribution that is also independent of the transformed azimuthal variable. A procedure to obtain an equilibrium phase space distribution for the

azimuthally symmetric Hamiltonian was described. On transforming this equilibrium back into the laboratory frame, it could be seen that only the higher order perturbations of the distribution were fast oscillating and had azimuthal variation. This procedure can have more general applications where a near equilibrium distribution is sought for a nonautonomous Hamiltonian in self consistent systems.

Chapter 8

Conclusion

This thesis addressed various aspects related to nonlinear focusing in particle accelerators. To begin with, a brief overview of some well established theories related to linear focusing was presented. The systems that were analyzed in this overview corresponded to the respective systems studied in subsequent chapters with nonlinear terms included in the focusing. These systems included the motion of a single charged particle, the dynamics of a beam with space charge effects with a mismatched, or oscillating envelope, and finally the derivation of a beam equilibrium.

A simple model using a cold beam with a circular cross-section and uniform density was used to show the existence of a parametric resonance between the oscillations of the envelope and a single particle. Calculations of trajectories of particles with different initial conditions showed that this resonance is a potential cause of beam halo formation. It was then proposed that a combination of nonlinear focusing and collimation can be used to control such a mechanism of halo production. Numerical results using a PIC code showed that this was true. The model used in this study was a continuous focusing channel. The PIC simulations also showed that the extent and intensity of the beam halo increased with mismatch ratio, and also that some halo particles were formed as a result of initial Vlasov mixing in an rms mismatched beam.

We then moved to the analysis of the motion a single particle in a nonlinear focusing channel. The Lie Transform perturbation theory was used to show that it is

possible to obtain a nonlinear lattice with improved integrability. The lattice composed of a combination of quadrupoles and higher order poles such as sextupoles and/or octupoles. In this analysis, it was shown that it is possible to obtain a focusing system that is continuous and azimuthally symmetric in a reference frame that was averaged over the lattice period. Such a focusing system corresponded with the model used in the study of control of beam halos. Numerical calculations showed that satisfying this condition of improved integrability, or equivalently, azimuthal symmetry in the averaged reference frame, led to reduced chaos and improved dynamic aperture. This study has the potential of being useful in various applications of nonlinear focusing besides the one studied here.

Finally, the Lie Transform analysis was extended to include space charge forces. In this, it was shown that it is possible to retain the above mentioned azimuthal symmetry in beams with space charge effects. In addition to this, a near equilibrium phase space distribution function was derived. This is particularly important in the context of a nonlinear lattice because a KV beam equilibrium does not exist in such a system.

There are many directions in which this work can be extended. One can explore the possibility of increasing the dynamic aperture of a lattice for a real machine design by improving the integrability of the system. This would involve tracking the motion of particles through a more complex arrangement of magnets and trying to vary the arrangement within practical limitations in order to improve integrability by employing the method prescribed in this thesis. Increased dynamic aperture is particularly important in synchrotron radiation sources for the quest for brighter beams. Another possible extension of this work would be to perform two and three dimensional PIC simulations for the study of beam halo mitigation. This would involve the use of a nonlinear lattice with an azimuthal symmetry in the averaged reference frame. In addition to that it would involve incorporating real collimation devices. Such a study could be useful in to the Spallation Neutron Source (SNS) accumulator ring and in heavy ion fusion

experiments. It is hoped that this thesis and the publications produced by this work will contribute toward improving the performance of various particle accelerators thus benefiting the scientific community at large. This work also has the potential of being of use to other areas of Hamiltonian dynamics and plasma physics.

Bibliography

[1] C. K. Allen and et al. Phys. Rev. Lett, 89:214802, 2002.

[2] C. K. Allen and T. P. Wangler. Phys. Rev. ST Accel and Beams, 5:124202, 2002.

[3] John Banard and Steve Lund. Notes from USPAS course in Boulder, CO, 2001.

[4] Y. K. Batygin. Phys. Rev. E, 54:5673, 1996.

[5] Y. K. Batygin. Phys. Rev. E, 57:6020, 1998.

[6] Y.K. Batygin. Phys. Rev. E, 53:5358, 1996.

[7] C. K. Birdsall and A. B. Langdon. Plasma Physics via Computer Simulation (The Adam Hilger Series on Plasma Physics), 1991.

[8] J. Candy and W. Rozmus. J. of Comp. Phys., 92:230, 1991.

[9] J. R. Cary. Physics Reports, 79:129, 1981.

[10] N. Catalan-Lasheras, Y. Y. Lee, H. Ludewig, N. Simons, and J. Wei. Phys Rev. ST Accel and Beams, 4:010101, 2001.

[11] P. Channel. Phys. Plasmas, 6:982, 1999.

[12] C. Chen and R. A. Jemeson. Phys Rev E, 52:3075, 1995.

[13] N. C. Christofilos. U.S. Patent, pages 2,736,799, 1950.

[14] E. D. Courant, M. S. Livingston, and H. Snyder. Phys. Rev., 88:1190, 1952.

[15] E. D. Courant and H. S. Snyder. Annals of Physics, 3:1, 1958.

[16] R. C. Davidson and H. Qin. Physics of Intense Charged Particle Beams in High Energy Accelerators. World Scientific, Singapore, 2001.

[17] R. C. Davidson and H. Qin. Phys. Rev. ST Accel. Beams, 4:104401, 2001.

[18] R. C. Davidson, H. Qin, and P.J. Channell. Phys. Rev. ST Accel. Beams, 2:074401, 1999.

[19] A. Deprit. Cel. Mech., 1:12, 1969.

[20] R. L. Dewar. J. Phys., A9:2043, 1976.

[21] A. J. Dragt and J. M. Finn. J. Math. Phys., 17:2215, 1976.

[22] D. A. Edwards and M. J. Syphers. An Introduction to the Physics of High Energy Accelerators. John Wiley and Sons, Inc,, New York, 1993.

[23] A. V. Fedotov, R. L. Gluckstern, S. S. Kurennoy, and R. D. Ryne. Phys Rev ST Accel. Beams, 2:014201, 1999.

[24] E. Forest and R.D. Ruth. Physica D, 43:105, 1990.

[25] A. Friedman and S. Lund. Private discussion.

[26] J. Gao. Nucl. Insrum. Methods Phys Res. A, 451:545, 2000.

[27] J. Gao. Nucl. Insrum. Methods Phys Res. A, 463:50, 2001.

[28] L. M. Garrido. J. Math. Phys., 10:1045, 1968.

[29] R. L. Gluckstern. Phys Rev. Lett., 73:1247, 1994.

[30] R. L. Gluckstern, W.-H. Cheng, S. S. Kurennoy, and H. Ye. Phys. Rev. E, 54:6788, 1996.

[31] R. L. Gluckstern, W.-H. Cheng, and H. Ye. Phys. Rev. Lett, 75:2835, 1995.

[32] R. L. Gluckstern, A. V. Fedotov, S. S. Kurennoy, and R. D. Ryne. Phys Rev E, 58:4, 1998.

[33] Steve Holmes. Notes from USPAS course in Nashville, TN, 1999.

[34] G. Hori. Astron. Soc. Japan, 18:287, 1966.

[35] M. Ikegami. Phys Rev E, 59:2330, 1999.

[36] M. Ikegami and H. Okamoto. Jpn. J. Appl. Phys., 36:7028, 1997.

[37] D. Jeon and et al. Phys. Rev. ST Accel and Beams, 5:094201, 2002.

[38] I. Kapchinskij and V. Vladimirskij. Proceedings of the International Conference on High Energy Accelerators and Instrumentation (CERN Scientific Information Services, Geneva 1959), page 274, 1959.

[39] J. Lagniel. Nucl. Instrum. Methods Phys. Res, Sect A, 345:405, 1994.

[40] J. Lagniel. Nucl. Instrum. Methods Phys. Res, Sect A, 345:46, 1994.

[41] P. M. Lapostolle. IEEE Trans. Nucl. Sci., 18:1101, 1971.

[42] A.J. Lichtenberg and M.A. Lieberman. Regular and chaotic dynamics (Springer-Verlag), 1992.

[43] C. Montag, J. Kewisch, D. Trbojevic, and F. Schmidt. Phys. Rev. ST Accel. Beams, 5:084401, 2002.

[44] J. S. O'Connell, T.P. Miller, R. S. Mills, and K. R. Crandall. Proceedings of the 1993 Particle Accelerator Conferemce, Washington, DC, edited by S. T. Corneliussen, page 3757, 1993.

[45] H. Okamoto and M. Ikegami. Phys Rev E, 55:4694, 1997.

[46] N. C. Petroni, S. D. Martino, S. D. Siena, and F. Illuminati. Phys. Rev. ST Accel and Beams, 6:034206, 2003.

[47] Q. Qian, R. C. Davidson, and C. Chen. Phys. Plasmas, 2:2674, 1995.

[48] J Qiang and R. Ryne. Phys. Rev. ST Accel and Beams, 3:064201, 2000.

[49] P. Raimondi and A. Seryi. Proceedings of the 2001 Particle Accelerator Conference, 2001 edited by P. Lucas and S. Webber (IEEE, New York, 2001) , page 3657, 2001.

[50] M. Reiser. Theory and Design od Charged Particle Beams. John Wiley and Sons, Inc,, New York, 1994.

[51] M. Reiser and et al. Phys Rev. Lett., 61:2933, 1998.

[52] R. D. Ruth. IEEE Trans. Nucl. Sci., 30:2669, 1983.

[53] R. D. Ryan and S. Habib. Part Accel, 55:365, 1996.

[54] F. J. Sacherer. IEEE Trans. Nucl. Sci., 18:1105, 1971.

[55] K. G. Sonnad and J. R. Cary. In Preparation.

[56] K. G. Sonnad and J. R. Cary. In review for Phys. Rev. ST Accel. and Beams.

[57] K. G. Sonnad and J. R. Cary. Phys. Rev. E, 69:056501, 2004.

[58] S. Strasburg and R. C. Davidson. Phys. Rev. E, 61:5753, 2000.

[59] L. Tosi, V. Samaluk, and E. Karantzoulis. Phys. Rev. ST Accel. Beams, 6:054401, 2003.

[60] G. Travish and J. Rosenweig. Nucl. Instrumn. and Methods in Phys. Res, Sect A., 345:585, 1994.

[61] N. Tsoupas, M.S. Zucker, T.E. Ward, and C.L. Snead. Nucl. Sci. and Engg., 126(1):71, 1997.

[62] S.I. Tzenov and R. C. Davidson. Phys. Rev. ST Accel. Beams, 5:021001, 2002.

[63] W. Wan and J. R. Cary. Phys. Rev. Lett., 81:3655, 1998.

[64] L. F. Wang, H. Fukuma, S. Kurokawa, and K. Oide. Phys. Rev. E., 66:036502–1, 2002.

[65] T.S. Wang. Phys. Rev. E, 61:855, 2000.

[66] Thomas. P. Wangler. RF Linear Accelerators. John Wiley and Sons, Inc,, New York, 1998.

[67] T.P. Wangler, K. R. Crandall, R. Ryne, and T. S. Wang. Phys. Rev. ST Accel and Beams, 1:084201, 1998.

Appendix A

Numerical scheme used for the PIC simulations

PIC simulations require an accurate method to weigh the charge on to the grid points, calculate the field at the grid points and also weigh the fields on to the particles. The particles then need to be moved at every time step in an accurate enough manner. The numerical scheme used in the PIC simulations in this thesis is based on methods proposed by Birdsall and Langdon [7].

The weighing of particles on to the grid points needs to be done in such a manner that the total charge is conserved. The method that has been used in this work is known as area weighing. Figure A.1 shows the radial positions of two adjacent grid points along a radial axis and a particle located between them. Since there is no θ dependence, these particles and grid points represent rings. The regions a and b represent areas between adjacent rings of radius r_i, r_{j+1} and r_j, r_i respectively. Let the particle be located at r_i, then the fraction of the charge q_i assigned to the point r_j is (area a)/(areas a + b) , leading to

$$Q_j = q_i \frac{r_{j+1}^2 - r_i^2}{r_{j+1} - r_j^2} \tag{A.1}$$

and for the point r_{j+1} it is (area b)/(areas a + b), leading to

$$Q_{j+1} = q_i \frac{r_i^2 - r_j^2}{r_{j+1} - r_j^2} \tag{A.2}$$

At the origin, we need to use, $r_j = 0$

The electric fields are first calculated on the points lying midway between the grids

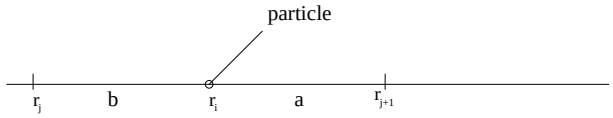

Figure A.1: Grid points and particle position for weighing on to grid

points containing the charge as shown in Fig A.2. The fields are computed using Gauss' law which guarantees flux conservation. For the particular case of the cylindrical surface $j = 1/2$, Gauss' law produces (in rationalized cgs units) the following radial electric field equation from the charge at the origin,

$$Q_0 = 2\pi r_{1/2} E_{1/2}. \tag{A.3}$$

For the case where $r_{j+1/2}$ is some radius equal to $1/2(r_{j+1} + r_j)$, the following equation is satisfied,

$$Q_j = 2\pi r_{j+1/2} E_{j+1/2} - 2\pi r_{j-1/2} E_{j-1/2} \tag{A.4}$$

The fields are calculated sequentially starting from the $j = 1/2$ surface, and Eq. A.4 is used to solve for $E_{3/2}, E_{5/2}$, and so on.

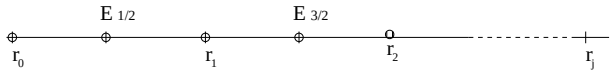

Figure A.2: Location of grid points with mid-points where electric field is calculated

These fields are then weighed on to the grid points, by a flux wighted average scheme. In this, the electric field at r_j satisfies

$$r_j E_j = \frac{r_{j+1/2} E_{j+1/2} + r_{j-1/2} E_{j-1/2}}{2} \tag{A.5}$$

At the origin, the electric field is set to zero.

The electric fields are then assigned to the particles using area weights where referring to fig.A.1

$$E_i = E_j \frac{r_{j+1}^2 - r_i^2}{r_{j+1}^2 - r_j^2} + E_{j+1} \frac{r_i^2 - r_j^2}{r_{j+1}^2 - r_j^2} \tag{A.6}$$

Once the field on the particle is known, the force on the particle may be calculated from $F_i = q_i E_i$, which is used to move the particle. In this case, the particles are moved using a the leap-frog scheme which is a second order syplectic map. The leap from scheme will be analyzed in Appendix B.

Appendix B

Symplectic Integrators

There exist several standard numerical methods for integrating ordinary differential equations. However, if one is interested in integrating Hamiltonian systems, these methods may lead to wrong results. This is due to the fact that these methods do not explicitly preserve the symplectic condition. One manifestation of this is that the Jacobian of the transformation for one time step differs slightly by unity and as a result, the system will be damped or excited artificially. This can lead to misleading results after the system has been evolved for a sufficiently long time. This chapter will discuss integrators that are symplectic to varying orders in time step for a special class of functions.

B.1 The General Method

The method described here is based on the work by R. D. Ruth [52] in 1983. This work involved derivation of an integration scheme that was symplectic up to third order in the time step. The work was extended to fourth order by E. Forest and R. D. Ruth [24], and independently by J. Candy and W. Rozmus [8]. The approach of the problem is as follows: Consider a Hamiltonian of the form

$$H(q,p) = A(p) + V(q) \tag{B.1}$$

where q and p are the phase space vectors. The aim is to make a canonical transformation such that the new Hamiltonian K in the new variables is zero. Since this may

not be practical, we attempt to make K zero up to a given order t^k where t is the time step. The new Hamiltonian will then be

$$K(q', p', t) = O(t^{k+1}) \tag{B.2}$$

and using Hamilton's equations, we get

$$q'(t) = q_0 + O(t^{k+1}) \tag{B.3}$$

$$p'(t) = p_0 + O(t^{k+1}) \tag{B.4}$$

Once this is accomplished, the motion in the original variables can be obtained (accurate to order k) by inverting the canonical transformation. Therefore, we get a map from $q(0), p(0)$ to $q(t), p(t)$. The process can be repeated to go from $q(t), p(t)$ to $q(2t), p(2t)$ and so on.

B.2 The First Order Map

For the sake of illustration, we start from a low order map. We use a generating function of the new coordinates and old momenta which will have the form,

$$F_3(q', p, t) = -q'p + G(q', p, t) \tag{B.5}$$

The function G will take on the form

$$G = -[A(q) + V(q')]t \tag{B.6}$$

The transformed Hamiltonian is

$$K = H + \frac{\partial F_3}{\partial t} = V(q) - V(q') \tag{B.7}$$

Using the canonical transformation equations appropriate for this we get

$$q = -\frac{\partial F_3}{\partial p} = q' + A_p(p)t \tag{B.8}$$

$$p' = -\frac{\partial F_3}{\partial q'} = p + V_{q'}(q') \tag{B.9}$$

Substituting this into the Hamiltonian yields

$$K = tV_{q'}(q')A_{p'}(p') + O(t^2) \tag{B.10}$$

Consequently, we get

$$q' = q_0 + O(t^2) \tag{B.11}$$

$$p' = p_0 + O(t^2) \tag{B.12}$$

So, if q', p' are used as initial conditions, the error introduced is $O(t^2)$. This approach has yielded a first order symplectic map.

B.3 Second Order Map, the Leap Frog Scheme

Deriving a second order map consists of modifying the previous method to two canonical transformations instead of one. These are given by $(q, p) \rightarrow (q', p')$ and then $(q', p') \rightarrow (q'', p'')$. The generating function of the first step is

$$F_3 = -q'p - aA(p)t - tV(q', bt) \tag{B.13}$$

Note that we are assuming a time dependent potential here. This yields the transformation

$$q = q' + aA_p(p)t \tag{B.14}$$

$$p' = p - tV_{q'}(q', bt) \tag{B.15}$$

The second map is performed through the generating function

$$F_3' = q''p' - (1-a)A(p')t \tag{B.16}$$

which yields the transformation

$$q' = q'' + (1-a)A_{p'}(p')t \tag{B.17}$$

$$p'' = p'. \tag{B.18}$$

The transformed Hamiltonian is

$$K = t(1-2a)A_{p''}(p'')V_{q''}(q'',0) + t(1-2b)V_t(q'',0) + O(t^2) \tag{B.19}$$

The purpose of the expansion of K in t is to identify the coefficients of various powers in K. Setting $a = b = 1/2$ gives $K = O(t^2)$.

We can now specify the integration procedure. We shift the notation $q \to q'', p \to p''$ since in the real problem one needs to perform an inverse canonical transformation from the initial condition. Letting $q'' = q_0$, $p'' = p_0$ and time step $t = h$, the map may then be defined by

$$p_1 = p_0 \tag{B.20}$$

$$q_1 = q_0 + \frac{h}{2}A_{p_1}(p_1) \tag{B.21}$$

$$p = p_1 + hV_{q_1}(q_1, t_0 + h/2) \tag{B.22}$$

$$q = q_1 + \frac{h}{2}A_p(p) \tag{B.23}$$

This method is the well known leap-frog scheme and used frequently in circumstances where anomalous damping and excitation is a problem. It may be noted that it is written a little differently than the typical implementations in a computer code since it is expressed for one full time step.

B.4 The Third and Fourth Order Maps

The third and fourth order maps can be derived in a similar manner, *ie*, by constructing a sequence of maps. Using the general form

$$p_{i+1} = p_i - c_i t V_q(q_i) \tag{B.24}$$

$$q_{i+1} = q_i + d_i t A_p(p_{i+1}). \tag{B.25}$$

Because the new Hamiltonian is in terms of the initial conditions, the transformations are applied in the reverse order. That is, $(q,p) \to (q_{n-1}, p_{n-1}) \to (q_{n-2}, p_{n-2}) \to \ldots \to$

(q_0, p_0). For $n = 2$ it has already been shown that $c_1 = 0$, $d_1 = 1/2$, $c_2 = 1$, $d_2 = 1/2$. For $n = 3$, it can be found that [52]

$$\begin{aligned} c_1 &= 7/24, \quad c_2 = 3/4, \quad c_3 = -1/24 \\ d_1 &= 2/3, \quad d_2 = -2/3 \quad d_3 = 1 \end{aligned} \tag{B.26}$$

Solving for the $n = 4$ case is rather tedious and has been done [24, 8] The coefficients are

$$\begin{aligned} c_1 &= 0, & d_1 &= x + 1/2 \\ c_2 &= 2x + 1, & d_2 &= -x \\ c_3 &= -4x - 1, & d_3 &= -x \\ c_4 &= 2x + 1, & d_4 &= x + 1/2 \end{aligned} \tag{B.27}$$

or alternately,

$$\begin{aligned} c_1 &= x + 1/2, & d_1 &= 2x + 1 \\ c_2 &= -x, & d_2 &= -4x - 1 \\ c_3 &= -x, & d_3 &= 2x + 1 \\ c_4 &= x + 1/2, & d_4 &= 0 \end{aligned} \tag{B.28}$$

where the value of x is given by

$$x = 1/6(2^{1/3} + 2^{-1/3} - 1) = 0.1756\ldots \tag{B.29}$$

This algorithm can be extended to case where the potential V is an explicit function of time. In this case, the Hamiltonian will be given as

$$H(q, p, t) = A(p) + V(q, t) \tag{B.30}$$

If we define the type 1 generating function $F_1 = P_\tau t$, then time can be eliminated by introducing the canonically conjugate pair (τ, p_τ). The equations of transformation are

$$\tau = \frac{\partial F_1}{\partial p_\tau} = t \tag{B.31}$$

$$H_{new} = H + \frac{\partial F_1}{\partial t} = H + p_\tau \tag{B.32}$$

It may be noted that τ is numerically equal to t and that $p_\tau = -H(q,p,t) + \text{constant}$. Upon substitution, we find

$$H_{new}(q,\tau,p,p_\tau) = [A(p) + p_\tau] + V(q,\tau) \tag{B.33}$$

In this chapter, the syplectic map has been explained for a specific class of functions, where the Hamiltonian can be separated into functions depending purely on momentum and position respectively. All the systems used in this thesis fell under this category. More sophisticated methods will be required if the Hamiltonian does not fall under this category.

Finding a nonlinear lattice with improved integrability using Lie transform perturbation theory

Kiran G. Sonnad and John. R. Cary
Center for Integrated Plasma Studies and Department of Physics, University of Colorado, Boulder, Colorado 80309, USA
(Received 12 October 2003; published 12 May 2004)

A condition for improved dynamic aperture for nonlinear, alternating gradient transport systems is derived using Lie transform perturbation theory. The Lie transform perturbation method is used here to perform averaging over fast oscillations by canonically transforming to slowly oscillating variables. This is first demonstrated for a linear sinusoidal focusing system. This method is then employed to average the dynamics over a lattice period for a nonlinear focusing system, provided by the use of higher order poles such as sextupoles and octupoles along with alternate gradient quadrupoles. Unlike the traditional approach, the higher order focusing is not treated as a perturbation. The Lie transform method is particularly advantageous for such a system where the form of the Hamiltonian is complex. This is because the method exploits the property of canonical invariance of Poisson brackets so that the change of variables is accomplished by just replacing the old ones with the new. The analysis shows the existence of a condition in which the system is azimuthally symmetric in the transformed, slowly oscillating frame. Such a symmetry in the time averaged frame renders the system nearly integrable in the laboratory frame. This condition leads to reduced chaos and improved confinement when compared to a system that is not close to integrability. Numerical calculations of single-particle trajectories and phase space projections of the dynamic aperture performed for a lattice with quadrupoles and sextupoles confirm that this is indeed the case.

DOI: 10.1103/PhysRevE.69.056501 PACS number(s): 29.27.−a, 45.10.Hj, 05.45.Gg

I. INTRODUCTION

Linear focusing systems such as the alternate gradient quadrupole systems are relatively easy to analyze because of the existence of the Courant-Snyder invariants [1], which reduce the system to an uncoupled set of systems of one degree of freedom. In the presence of higher order components such as sextupoles or octupoles, these invariants are destroyed. Such a system is nonintegrable and has trajectories that are chaotic and poorly confined. Despite this shortcoming in the use of nonlinear components, their use has been proposed in a variety of applications. They include, for example, achieving uniform particle distributions [2], control of beam emittance growth and beam halo formation [3,4], providing strong sextupole focusing in planar undulators in free electron lasers [3], folding of beam phase space distributions as an alternate to beam collimation [4], introducing Landau damping by providing octupole or sextupole induced tune spread [5,6], photoelectron trapping in quadrupole and sextupole magnetic fields [7], etc. In addition to this sextupoles are widely used in storage rings for cromaticity corrections. Nonlinear forces also arise as a result of beam-beam interactions at interaction point of a storage ring collider which limit the dynamic aperture of the system [8]. Thus, a general analysis of the nonlinear focusing problem is important. It is well known that a near integrable Hamiltonian system will typically possess regular trajectories intermingled with regions of chaos. The aim of this paper is to find a condition that optimizes the integrability of the system thereby minimizing the chaotic region in the presence of certain nonlinear focusing components.

To perform the analysis we use the Lie transform perturbation method, which exploits the invariance of the Poisson brackets under canonical transformations. In this analysis all dynamical variables appear within Poisson brackets, so the whole formulation is canonically invariant. If this were not true, one would need to express the Hamiltonian in terms of the new variables up to the desired order before performing the perturbation analysis. This could make the problem more tedious when the form of the Hamiltonian is not simple, and when it is required to carry the expansion up to third order, both of which are true in this case. References [9–11] contain other procedures for averaging applied to beam physics. We follow the Lie transform method described in Ref. [12] and show that rearranging the different order terms of the Hamiltonian in this method enables one to perform a time averaging rather than average the motion over the trajectory described by the integrable component of the Hamiltonian.

To start with, Sec. II provides a brief description of the Lie transform method used in this paper. Section III presents an illustration of the method applied to a continuous periodic focusing system, an example also used by Channel [9]. In Sec. IV, we introduce a nonlinear focusing system which has a higher order multipoles in addition to quadrupoles. The resulting Hamiltonian describing the motion transverse to the beam propagation is nonautonomous and has two degrees of freedom. By averaging the motion over the lattice period up to third order, we derive a condition for the new time-independent Hamiltonian to also be independent of the transformed azimuthal variable. Under such a condition, the transformed angular momentum will be an adiabatic invariant. It will be shown that this condition is satisfied when the functions describing the forces due to the respective multipole are orthogonal to each other in a certain manner.

In order to show that the condition of azimuthal invariance is a desirable one, various numerical calculations are performed. Section V includes results which show that as one deviates from the desired condition, the particle oscillations acquire additional frequency components and also have larger oscillation amplitudes. Section VI illustrates the pro-

jection of the dynamic aperture on to different planes in phase space. The dynamic aperture is the region that allows what may be defined as confined particles. Estimating the dynamic aperture for different cases shows that maximum confinement can be achieved when the associated time averaged Hamiltonian is integrable in the transformed coordinates and hence the system is nearly integrable in the laboratory frame. The dynamic aperture is shown to gradually diminish in size as one deviates from this condition.

II. THE LIE TRANSFORM METHOD FOR AVERAGING OVER FAST OSCILLATIONS

In this section we outline the Hamilton perturbation method described in Ref. [12]. This method is based on previous work [13–17] that introduced Lie transform theory as a convenient method to perform Hamilton perturbation analysis. The Lie transformation is defined with respect to a phase space function w such that it satisfies the following Poisson bracket relationship:

$$\frac{d\mathbf{Z}}{d\epsilon} = \{\mathbf{Z}, w(\mathbf{Z}(\mathbf{z},t,\epsilon),t,\epsilon)\}, \tag{1}$$

where $\mathbf{Z}=(\mathbf{P},\mathbf{Q})$ is a phase space vector representing the generalized positions and momenta of the system, w is the Lie generating function, and ϵ is a continuously varying parameter such that $\mathbf{Z}(\epsilon=0)=\mathbf{z}$, the original phase space vector. The above relationship resembles Hamilton's equation with respect to a "Hamiltonian," w and "time," ϵ. This guarantees that the transformation is canonical for all values of ϵ.

The Lie operator L is defined such that it performs a Poisson bracket operation with respect to w. Symbolically,

$$L = \{w,\}. \tag{2}$$

A transformation operator T is defined such that its role is to replace the variables of a function by the new canonical variables. For the identity function this is simply,

$$T\mathbf{z} = \mathbf{Z}(\mathbf{z},\epsilon,t). \tag{3}$$

The operator T is analogous to the "evolution" operator with respect to ϵ. Using Eq. (1) it can be verified that T satisfies

$$\frac{dT}{d\epsilon} = -TL. \tag{4}$$

For a similar relationship involving the inverse transformation operator T^{-1}, we differentiate the equation $TT^{-1}=1$ and use the above equation to obtain

$$\frac{dT^{-1}}{d\epsilon} = T^{-1}L. \tag{5}$$

The transformed Hamiltonian K can be expressed in terms of the original Hamiltonian $\mathcal{H}$ as

$$K(\epsilon) = T^{-1}(\epsilon)(\mathcal{H}) + T^{-1}(\epsilon)\int_0^\epsilon d\epsilon' T(\epsilon')\frac{\partial w}{\partial t}(\epsilon'). \tag{6}$$

This expression was obtained by Dewar [16].

To obtain explicit equations for each perturbation term, every physical quantity and operator is expressed as a power series in ϵ known as the Deprit power series [15]. The original and transformed Hamiltonians are given by $H(\mathbf{z},\epsilon,t)=\sum_{n=0}^{\infty}\epsilon^n H_n(\mathbf{z},t)$, $K(\mathbf{z},\epsilon,t)=\sum_{n=0}^{\infty}\epsilon^n K_n(\mathbf{z},t)$. The Lie generating function is represented a little differently because it appears as a derivative in Eq. (6). This is, $w(\mathbf{z},t,\epsilon)=\sum_{n=0}^{\infty}\epsilon^n w_{n+1}(\mathbf{z},t)$. The operators T and L are represented in a similar way as $T(t,\epsilon)=\sum_{n=0}^{\infty}\epsilon^n T_n(t)$, $L(w)=\sum_{n=0}^{\infty}\epsilon^n L_n$, where $L_n=\{w_n,\}$, the Poisson bracket with respect to w_n. The parameter ϵ is used to keep track of the terms representing different orders in the expansion and is usually set to one in the end.

By substituting the Deprit expansions into Eqs. (4), (5), and (6), one can obtain relationships between the corresponding terms for each order of ϵ. Doing this for Eq. (6), we get, up to third order,

$$K_0 = H_0, \tag{7a}$$

$$\frac{\partial w_1}{\partial t} + \{w_1,H_0\} = K_1 - H_1, \tag{7b}$$

$$\frac{\partial w_2}{\partial t} + \{w_2,H_0\} = 2(K_2 - H_2) - L_1(K_1 + H_1), \tag{7c}$$

$$\frac{\partial w_3}{\partial t} + \{w_3,H_0\} = 3(K_3 - H_3) - L_1(K_2 + 2H_2) - L_2\left(K_1 + \frac{1}{2}H_1\right) - \frac{1}{2}L_1^2 H_1. \tag{7d}$$

The expression $\partial w_n/\partial t + \{w_n,H_0\}$ is the variation of w_n along the unperturbed trajectory described by H_0. Setting $H_0=0$ reduces this to a partial derivative with respect to t. Thus, instead of integrating along the unperturbed trajectory, we simply perform an integration over time to determine w_n. At each order, K_n is chosen such that it cancels the terms that average to a nonzero value over fast oscillations. As a result, the corresponding value of w_n will have a zero average. This is necessary to prevent w_n from being secular (unbounded) in time [12].

Using Eq. (5), and the Deprit series expression for the operators L and T, the inverse transformation operator to third order may be expressed as

$$T_0^{-1} = I, \tag{8a}$$

$$T_1^{-1} = L_1, \tag{8b}$$

$$T_2^{-1} = \tfrac{1}{2}L_2 + \tfrac{1}{2}L_1^2, \tag{8c}$$

$$T_3^{-1} = \tfrac{1}{3}L_3 + \tfrac{1}{6}L_1L_2 + \tfrac{1}{3}L_2L_1 + \tfrac{1}{6}L_1^3. \tag{8d}$$

It may be noted that when L, T, and T^{-1} act upon any phase space function, they are expressed in the form of Poisson brackets, which are independent of the canonical variables used. This makes the whole formulation canonically invariant. For a systematic derivation of all these relation-

ships one may refer to Ref. [12] where they are given up to fourth order. A shorter description of the same may be found in Ref. [18].

III. APPLICATION TO A LINEAR SINUSOIDAL FOCUSING SYSTEM

As an illustration and a test for the validity of the method, we perform the analysis for a linear periodic focusing system. The same example was used in Ref. [9] for the method developed in that paper. The single-particle Hamiltonian associated with such a system is given by

$$H = \frac{p^2}{2} + \frac{kq^2}{2}\sin(\omega t). \tag{9}$$

This Hamiltonian also describes the motion of a particle in systems such as the Paul trap and the ponderomotive potential. We apply Eqs. (7) to perform the averaging. As explained in the preceding section, we set $H_0=0$ and $H_1=H$. From Eq. (7a) we get

$$K_0 = H_0 = 0. \tag{10}$$

Applying the first-order relationship, Eq. (7b), we get

$$\frac{\partial w_1}{\partial t} = K_1 - \frac{p^2}{2} - \frac{kq^2}{2}\sin(\omega t). \tag{11}$$

The third term on the right averages to zero with respect to time. In order that the net result average to zero, we require

$$K_1 = \frac{p^2}{2}. \tag{12}$$

Since w_1 is relevant only up to an additive constant, it is sufficient to evaluate the indefinite integral to determine w_1, hence

$$w_1 = \frac{kq^2}{2\omega}\cos(\omega t). \tag{13}$$

The second-order equation, Eq. (7c), gives

$$\frac{\partial w_2}{\partial t} = 2K_2 - \frac{2kpq}{\omega}\cos(\omega t). \tag{14}$$

Since the second term on the right side averages to zero, we choose

$$K_2 = 0, \tag{15}$$

and so,

$$w_2 = -\frac{2kqp}{\omega^2}\sin(\omega t). \tag{16}$$

Applying the third-order relationship, Eq. (10) then gives

$$\frac{\partial w_3}{\partial t} = 3K_3 + \frac{3p^2k}{\omega^2}\sin(\omega t) - \frac{k^2q^2}{\omega^2}\sin^2(\omega t) - \frac{k^2q^2}{2\omega^2}\cos^2(\omega t). \tag{17}$$

Note that the third and fourth terms on the right side do not average to zero. In order that they cancel, we set

$$K_3 = \frac{1}{4}\frac{k^2q^2}{\omega^2} \tag{18}$$

and as a result,

$$w_3 = -\frac{3p^2k}{\omega^3}\cos(\omega t). \tag{19}$$

Collecting the nonzero terms, the transformed Hamiltonian is now given as a function of the new variables by

$$K = \frac{P^2}{2} + \frac{\Omega^2 Q^2}{2}, \tag{20}$$

where $\Omega = k/\sqrt{2}\omega$. This is the Hamiltonian for a harmonic oscillator with solution

$$Q(t) = Q(0)\cos(\Omega t) + \frac{P(0)}{\Omega}\sin(\Omega t), \tag{21}$$

$$P(t) = P(0)\cos(\Omega t) - \Omega Q(0)\sin(\Omega t). \tag{22}$$

To transform back to the original coordinate system, we use the operator T^{-1} for which we need to know L up to the desired order. The operators L_n can be expressed in terms of the values of w_n as

$$L_1 = \left\{ \frac{kQ^2}{2\omega}\cos(\omega t), \right\}, \tag{23}$$

$$L_2 = \left\{ -\frac{2kQP}{\omega^2}\sin(\omega t), \right\}, \tag{24}$$

$$L_3 = \left\{ -\frac{3kP^2}{\omega^3}\cos(\omega t), \right\}. \tag{25}$$

Using these to perform the inverse transformation as described by Eqs. (8), we get, up to third order,

$$q = Q + \frac{kQ}{\omega^2}\sin(\omega t) + \frac{2kP}{\omega^3}\cos(\omega t), \tag{26}$$

$$p = P + \frac{kQ}{\omega}\cos(\omega t) - \frac{kP}{\omega^2}\sin(\omega t) + \frac{1}{3}\frac{k^2}{\omega^3}Q\,\sin(\omega t)\cos(\omega t). \tag{27}$$

The above solution is compared with calculations from a fourth-order symplectic integrator [19,20] and is shown in Figs. 1 and 2. The parameters used were the same as those used in Ref. [9]. The accuracy of the approximate solution compares well with that obtained by Channel [9] using a different method. That is, the solution given by Eqs. (26) and (27) overlaps well with the numerical solution for $k/\omega^2 = 1/16$ and the accuracy gradually decreases with decreasing ω.

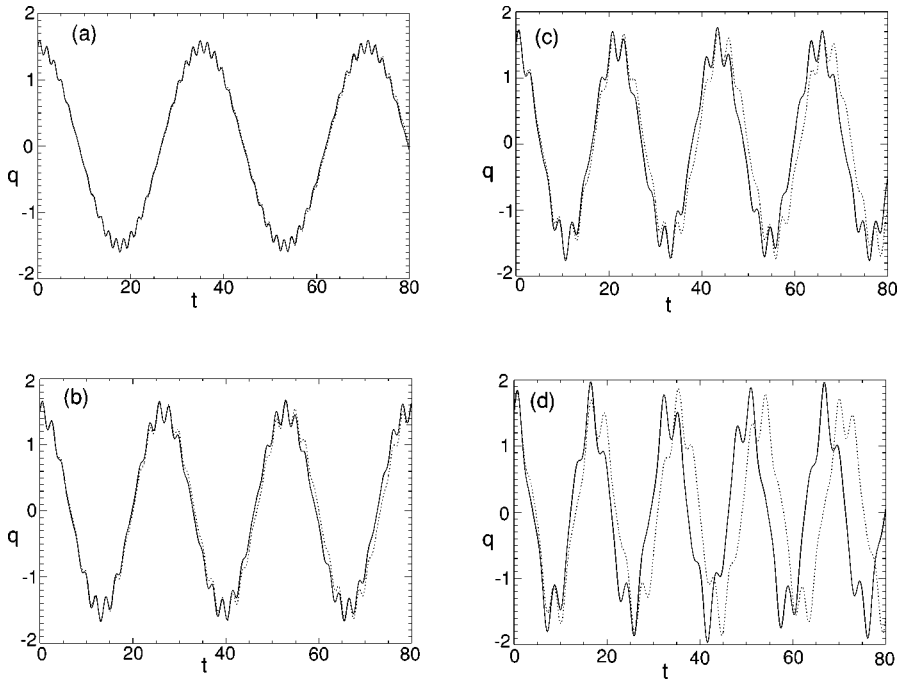

FIG. 1. q vs t with $k=1$, $\omega=$(a)4 , (b) 3, (c) 2.5, and (d) 2. The solid line represents the numerical solution.

IV. SINGLE PARTICLE AVERAGING FOR A NONLINEAR LATTICE

A. Alternate gradient sextupoles and quadrupoles

The external magnetic fields in the beam channel are expected to satisfy Maxwell's equations in vacuum which are given by $\vec{\nabla}\times\vec{B}=0$, $\vec{\nabla}\cdot\vec{B}=0$. The two-dimensional multipole expansion expression for such a magnetic field is

$$B_y + iB_x = B_0 \sum_{n=0}^{\infty} (b_n + ia_n)(x+iy)^n. \tag{28}$$

Ideally, b_n and a_n must be constants for the above to be valid. However, when analyzing alternate gradient focusing systems, they are regarded as step functions of the axial distance. This is still valid if fringe effects are disregarded.

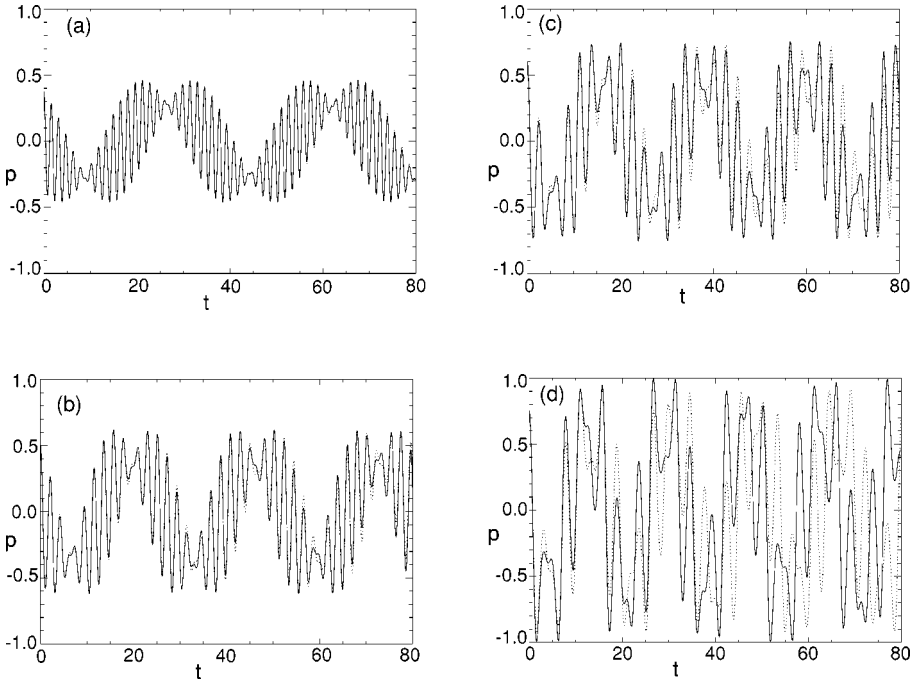

FIG. 2. p vs t with $k=1$, $\omega=$(a)4, (b) 3, (c) 2.5, and (d) 2. The solid line represents the numerical solution.

The orientation of the reference frame can be chosen such that $a_1=0$. Assuming the presence of only quadrupole ($n=1$) terms and sextupole ($n=2$) terms, b_1, a_2 and b_3 will generally be nonzero. The velocity of the particle in the z direction is assumed to be constant. The resulting Hamiltonian can be obtained from the Lorentz force. In cylindrical coordinates it is,

$$H=\frac{1}{2}\left(p_r^2+\frac{l^2}{r^2}\right)+\frac{1}{2}\kappa_2(s)r^2\cos(2\theta)+\frac{1}{3}\kappa_3(s)r^3\cos(3\theta+\alpha). \tag{29}$$

The variable s is the distance along the axis, which is equivalent to time for constant axial velocity. The momentum in the radial direction is p_r and l is the angular momentum. The values of $\kappa_2(s)$ and $\kappa_3(s)$ depend upon the strength of the quadrupole and sextupole magnets, respectively, and also the velocity of the particle in the axial direction. The angle α depends upon the relative values of a_2 and b_2, which is determined by the orientation of the sextupoles with respect to the quadrupoles. We use normalized units in which the charge and mass of the particle are unity. It is assumed that the Hamiltonian is periodic in s with periodicity S, i.e., $\kappa_2(s+S)=\kappa_2(s)$ and $\kappa_3(s+S)=\kappa_3(s)$. It is further assumed that the average of $\kappa_2(s)$ and $\kappa_3(s)$ over a period S is zero. That is,

$$\langle\kappa_2\rangle=\frac{1}{S}\int_s^{s+S}\kappa_2(s)ds=0 \tag{30}$$

and the same for κ_3. The angular brackets $\langle\cdots\rangle$ denote an average over one period in the rest of this section. With these conditions, κ_2 and κ_3 can in general be represented in the form of Fourier series as

$$\kappa_2(s)=\sum_{n=1}^{n=\infty}f_n\sin\left(\frac{2n\pi s}{S}\right)+\sum_{n=1}^{n=\infty}g_n\cos\left(\frac{2n\pi s}{S}\right) \tag{31}$$

and

$$\kappa_3(s)=\sum_{n=1}^{n=\infty}k_n\sin\left(\frac{2n\pi s}{S}\right)+\sum_{n=1}^{n=\infty}l_n\cos\left(\frac{2n\pi s}{S}\right). \tag{32}$$

However, the analysis in this section will show that it would be desirable for the above series to satisfy certain restrictions.

The averaging procedure to follow is valid when the averaged orbits are slowly varying over one lattice period S. The procedure is identical to the one used in the preceding section except that the algebra is more tedious since the Hamiltonian is more complex. Once again, we set $H_0=0$ and $H_1=H$. From Eq. (7b) we get $K_0=H_0=0$. Equation (7c) yields

$$\frac{\partial w_1}{\partial s}=K_1-\frac{1}{2}\left(p_r^2+\frac{l^2}{r^2}\right)-\frac{1}{2}\kappa_2(s)r^2\cos(2\theta)-\frac{1}{3}\kappa_3(s)r^3\cos(3\theta+\alpha). \tag{33}$$

From Eqs. (31) and (32) it follows that $\langle\kappa_2^{\mathrm{I}}\rangle=\langle\kappa_3^{\mathrm{I}}\rangle=0$. The roman numerical superscript indicates an integral over s with a constant of integration chosen so that the integral has a zero average over one lattice period S. Similarly, a superscript "II" will indicate a double integration over s with the same conditions, and so on. Choosing K_1 to cancel the terms with a nonzero average value then gives

$$K_1=\frac{1}{2}\left(p_r^2+\frac{l^2}{r^2}\right). \tag{34}$$

Integrating Eq. (39) yields

$$w_1=-\left[\tfrac{1}{2}\kappa_2^{\mathrm{I}}(s)r^2\cos(2\theta)+\tfrac{1}{3}\kappa_3^{\mathrm{I}}(s)r^3\cos(3\theta+\alpha)\right]. \tag{35}$$

Proceeding to evaluate the second-order term w_2 from Eq. (7c) and noting that $L_1=\{w_1,\}$, we get

$$\frac{\partial w_2}{\partial s}=2K_2+2p_r[\kappa_2^{\mathrm{I}}(s)r\cos(2\theta)+\kappa_3^{\mathrm{I}}(s)r^2\cos(3\theta+\alpha)]-2l[\kappa_2^{\mathrm{I}}(s)\sin(2\theta)+\kappa_3^{\mathrm{I}}(s)r\sin(3\theta+\alpha)]. \tag{36}$$

Given that $\langle\kappa_2^{\mathrm{I}}\rangle=\langle\kappa_3^{\mathrm{I}}\rangle=0$, we must choose $K_2=0$ since there are no nonzero average terms. On integrating the above equation, we find

$$w_2=2p_r[\kappa_2^{\mathrm{II}}r\cos(2\theta)+\kappa_3^{\mathrm{II}}(s)r^2\cos(3\theta+\alpha)]-2l[\kappa_2^{\mathrm{II}}(s)\sin(2\theta)+\kappa_3^{\mathrm{II}}(s)r\sin(3\theta+\alpha)]. \tag{37}$$

Knowing w_2, we can proceed to the next order to calculate w_3 and K_3. Applying Eq. (7d) we get

$$\begin{aligned}\frac{\partial w_3}{\partial s}=&3K_3-3p_r^2[\kappa_2^{\mathrm{II}}(s)\cos(2\theta)+2\kappa_3^{\mathrm{II}}(s)r\cos(3\theta+\alpha)]+3lp_r[\kappa_3^{\mathrm{II}}(s)\sin(3\theta+\alpha)]\\&+3\frac{p_rl}{r}[2\kappa_2^{\mathrm{II}}(s)\sin(2\theta)+3\kappa_3^{\mathrm{II}}(s)r\sin(3\theta+\alpha)]+3\frac{l^2}{r^2}[2\kappa_2^{\mathrm{II}}(s)\cos(2\theta)+3\kappa_3^{\mathrm{II}}(s)r\cos(3\theta+\alpha)]\\&+[\kappa_2^{\mathrm{II}}(s)r\cos(2\theta)+\kappa_3^{\mathrm{II}}r^2\cos(3\theta+\alpha)][\kappa_2(s)r\cos(2\theta)+\kappa_3r^2\cos(3\theta+\alpha)]\\&+[\kappa_2^{\mathrm{II}}(s)\sin(2\theta)+\kappa_3^{\mathrm{II}}(s)r\sin(3\theta+\alpha)][\kappa_2(s)r^2\sin(2\theta)+\kappa_3(s)r^3\sin(3\theta+\alpha)]\end{aligned}$$

$$-\frac{1}{2}[\kappa_2^{\mathrm{I}}(s)r\cos(2\theta)+\kappa_3^{\mathrm{I}}(s)r^2\cos(3\theta+\alpha)]^2-\frac{1}{2}[\kappa_2^{\mathrm{I}}(s)r\sin(2\theta)+\kappa_3^{\mathrm{I}}(s)r^2\sin(3\theta+\alpha)]^2. \tag{38}$$

From Eqs. (31) and (32) one can easily identify the terms that average to zero over fast oscillations and those that do not. Once again K_3 is chosen such that it cancels the terms that average to a nonzero value. On simplifying certain averaged terms from integration by parts, the third-order transformed Hamiltonian may be expressed as

$$K_3=\tfrac{1}{2}\langle(\kappa_2^{\mathrm{I}})^2\rangle r^2-\tfrac{1}{3}\langle\kappa_2^{\mathrm{I}}\kappa_3^{\mathrm{I}}\rangle r^3\cos(\theta+\alpha)+\tfrac{1}{2}\langle(\kappa_3^{\mathrm{I}})^2\rangle r^4. \tag{39}$$

Since the Hamiltonian K is defined in the transformed coordinate system, the variables must be replaced by the corresponding transformed variables, R and Θ, in the above equation as well as in Eq. (34).

In order for K_3 to be independent of Θ, $\langle\kappa_2^{\mathrm{I}}\kappa_3^{\mathrm{I}}\rangle$ must vanish. It is clear from Eqs. (31) and (32) that one way this can be accomplished is if $\kappa_2(s)$ can be expressed as a pure cosine series and $\kappa_3(s)$ as a pure sine series. Figure 3 represents a practical design for $\kappa_2(s)$ and $\kappa_3(s)$ which satisfies this condition. This is a specific case where the two lattices have equal periodicity. In this case, $\kappa_2(s)$ and $\kappa_3(s)$ are periodic step functions alternating in sign and with opposite parity, which is equivalent to a phase lag of a quarter lattice period with respect to each other. It may be noted that once the Θ dependence is eliminated, the nonlinear force is purely focusing and leads to a positive tune shift. This design is only the simplest method of realizing optimum integrability and need not necessarily be the most practical one for real machines. However, the formulation of this condition is general enough to accommodate other designs that are possibly easier to implement. The general procedure to apply this is to first express $\kappa_2(s)$ and $\kappa_3(s)$ of an existing design in the form of Eqs. (31) and (32). Then the coefficient $\langle\kappa_2^{\mathrm{I}}\kappa_3^{\mathrm{I}}\rangle$ will need to be evaluated. This would then tell us how to reposition the magnets in order to minimize this. Numerical results in Sec. IV will show that considerable improvement in the dynamic aperture can be accomplished even if $\langle\kappa_2^{\mathrm{I}}\kappa_3^{\mathrm{I}}\rangle$ does not completely vanish but is small enough.

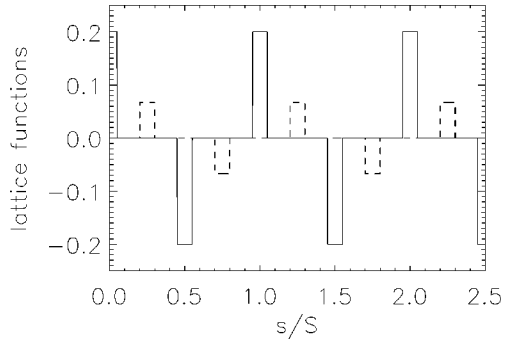

FIG. 3. A step function lattice that will lead to a near integrable condition. The shorter steps represent the sextupole function $\kappa_3(s)$ while the higher ones the quadrupole function $\kappa_2(s)$.

The purpose of choosing K_3 to be independent of Θ is to look for a system with improved integrability and thereby improve confinement by reducing chaos. According to the Kolmogorov-Arnold-Moser (KAM) theorem, a system perturbed from integrability will consist of regions of regular motion and regions of chaos with the latter approaching zero exponentially as the system approaches integrability. This system would be perfectly integrable if the Θ dependence could be completely eliminated. However, the fourth-order perturbation term will retain the Θ dependence. Despite this, the numerical results in the following sections will show that restricting the integrability up to third order makes a significant improvement in confinement in accordance with the KAM theorem. It is likely that a few mutipoles or other components such as undulators in synchrotron radiation sources cannot be incorporated in the averaging procedure. Another such example would be beam-beam interactions at interaction point of a storage ring collider where there might be many multipoles located at the same place. Superposing these additional effects randomly to the existing lattice would invariably make the system less integrable. In such a situation, it becomes even more important to obtain a system with optimum integrability since the KAM theorem would still guarantee that there exists a region in phase space with particles having regular trajectories. One could also consider using the method in Ref. [21] to implement the additional nonlinear components to a lattice that has already been designed to be nearly integrable using the method suggested here.

B. Alternate gradient quadrupoles, sextupoles, and octupoles

Although the analysis in the preceding section used only sextupoles, this can be extended to include higher multipoles. For example, if octupoles are used in addition to the sextupoles, the Hamiltonian would be

$$H=\frac{1}{2}\left(p_r^2+\frac{l^2}{r^2}\right)+\frac{1}{2}\kappa_2(s)r^2\cos(2\theta)+\frac{1}{3}\kappa_3(s)r^3\cos(3\theta+\alpha)+\frac{1}{4}\kappa_3(s)r^4\cos(4\theta+\gamma), \tag{40}$$

where γ represents the orientation of the octupoles. The third-order transformed Hamiltonian will then be

$$K_3=\tfrac{1}{2}\langle(\kappa_2^{\mathrm{I}})^2\rangle r^2+\tfrac{1}{2}\langle(\kappa_3^{\mathrm{I}})^2\rangle r^4+\tfrac{1}{2}\langle(\kappa_4^{\mathrm{I}})^2\rangle r^6-\tfrac{1}{3}\langle\kappa_2^{\mathrm{I}}\kappa_3^{\mathrm{I}}\rangle r^3\cos(\theta+\alpha)-\tfrac{1}{3}\langle\kappa_2^{\mathrm{I}}\kappa_4^{\mathrm{I}}\rangle r^4\cos(2\theta+\gamma)-\tfrac{1}{3}\langle\kappa_3^{\mathrm{I}}\kappa_4^{\mathrm{I}}\rangle r^5\cos(\theta+\alpha+\gamma). \tag{41}$$

The conditions $\langle\kappa_2^{\mathrm{I}}\kappa_3^{\mathrm{I}}\rangle=0$, $\langle\kappa_2^{\mathrm{I}}\kappa_4^{\mathrm{I}}\rangle=0$, and $\langle\kappa_3^{\mathrm{I}}\kappa_4^{\mathrm{I}}\rangle=0$ would

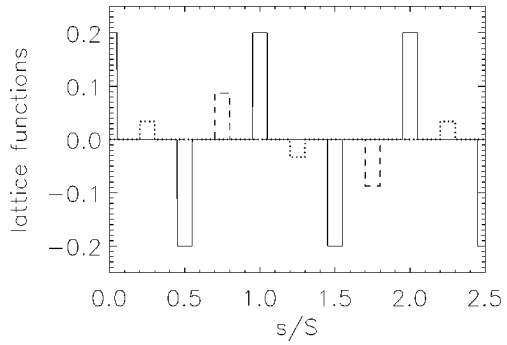

FIG. 4. A step function lattice leading to a near integrable condition. The shortest steps represent the octupole function $\kappa_4(s)$, while the higher ones the sextupole function $\kappa_3(s)$, and the highest ones the quadrupole function $\kappa_2(s)$.

optimize the integrability of such a system. A practical but idealized design for this to be satisfied is given in Fig. 4.

V. SINGLE-PARTICLE TRAJECTORIES WITH NONZERO ANGULAR MOMENTUM

To show that particles are better confined when the 90° phase difference condition is satisfied, numerical calculations were performed using the original Hamiltonian. The results are discussed in this and the following sections. Calculations were performed using a fourth-order symplectic integrator [19,20] in Cartesian coordinates. Cartesian coordinates are more convenient for numerical calculations as they enable one to avoid the singularity at the origin arising in the cylindrical coordinate system. The focusing channel consisted of alternating gradient quadrupoles and sextupoles with various phase differences between $\kappa_2(s)$ and $\kappa_3(s)$. The sextupoles were oriented such that $\alpha=-45°$. In Cartesian coordinates, the force due to quadrupoles is given by

$$\vec{F} = \kappa_2(s)(x\hat{x} - y\hat{y}). \tag{42}$$

and that due to the sextupoles (with $\alpha=-45°$) is given by

$$\vec{F} = \kappa_3(s)[(x^2 - y^2 + 2xy)\hat{x} + (x^2 - y^2 - 2xy)\hat{y}]. \tag{43}$$

We define a radial distance $R=\frac{1}{3}|\kappa_2|/|\kappa_3|$, where $|--|$ corresponds to the positive nonzero values of the respective step function. The ratio $|\kappa_2|/|\kappa_3|$ represents a measure of the position where the forces due to the linear and nonlinear components become comparable. The tune shift due to the nonlinear force was close to 15% for a particle initially at $r=R$ and $\theta=45°$. The fill factor η is defined as the ratio between the length of the magnets and the length of one lattice period. This was set to 0.2 for both, the quadrupoles and sextupoles. This is typical for most applications. For example, the storage ring of the advanced photon source has a fill factor of about 0.21 for quadrupoles. When expressed in units of S, η is the smallest time scale to be resolved and so the time step in the computation needs to be much smaller than η. In all the computations, this time step was set to 0.01η. The parameter $\kappa_2(s)$ has units of frequency squared so we can define another dimensionless quantity as $|\kappa_2|S^2$ to which the value of 8.0 was assigned for all calculations. This corresponds to about seven lattice periods per betatron radial oscillation about the origin. The separation between the quadrupoles and sextupoles is represented by a term

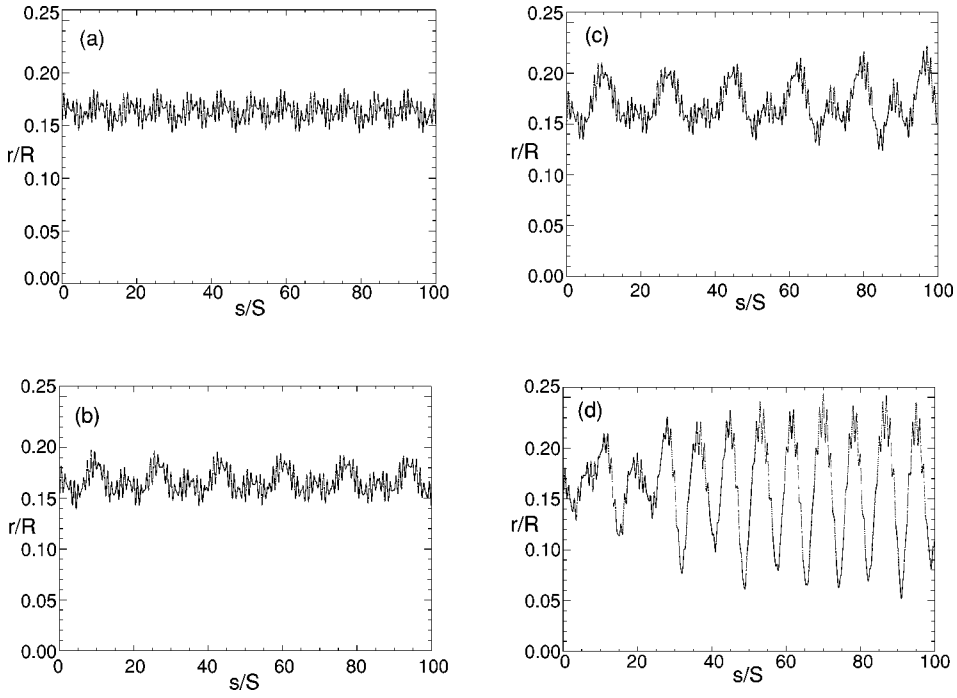

FIG. 5. Radial oscillation of particles for (a) $\psi=90°$, (b) $\psi=60°$, (c) $\psi=30°$, (d) $\psi=0°$.

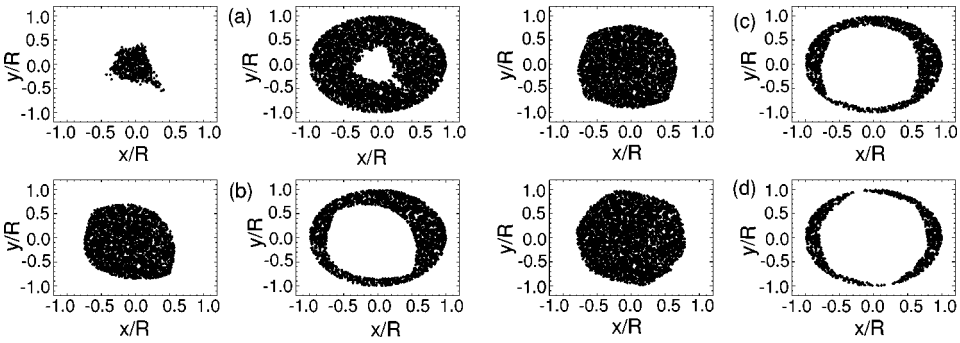

FIG. 6. Initial distribution of confined and unconfined particles lying on the x-y plane for ψ= (a) 0°, (b) 30°, (c) 60°, (d) 90°.

$$\psi = \frac{2\pi\Delta s}{S}, \tag{44}$$

where Δs is the spatial distance between the two of them. The averaged Hamiltonian K is independent of Θ when $\psi = 90°$, i.e., when the sextupoles are placed halfway between two quadrupoles of opposite sign. The values of R, η, $|\kappa_2|S^2$, and ψ completely specify the focusing system.

When a system is azimuthally symmetric, angular momentum is conserved. In this system, when $\psi = 90°$, the angular momentum is nearly conserved because the averaged angular momentum is azimuthally symmetric. As one deviates from $\psi = 90°$, the dependence on θ becomes stronger and the variation of angular momentum becomes more significant. This would lead to increased chaotic motion. In order to verify this, as an example, we examined the trajectory of a particle at $r = 0.15R$. The particle had an initial velocity of $0.05R/S$ in a direction perpendicular to its initial displacement.

The results of these calculations with respect to different values of ψ are shown in Fig. 5. The rapid variation in amplitude represents the lattice oscillations. The values of ψ used were 90°, 60°, 30°, and 0°, respectively. It is clear that there is a transition to chaotic motion as ψ deviates from 90°. For $\psi = 90°$, the maximum amplitude of oscillation is relatively small. When ψ changes to 60°, the maximum amplitude increases. At $\psi = 60°$, we see that additional frequency components are added to the oscillation. When $\psi = 0$, the sextupoles and quadrupoles overlap. In this situation the motion is chaotic. There is no observable repetition in the motion of the particle and it travels well beyond the maximum radial distance attained in the $\psi = 90°$ case. This transition would have been more rapid if the initial position of the particle was further away from the center. It is sufficient to examine cases where the phase lag between the quadrupoles and sextupoles, ψ, varies from 0° to 90°. Phase differences outside this range can be mapped back to a corresponding point between 0° and 90° by making an appropriate linear transformation in θ.

The requirement of reduced chaos becomes important when sextupoles or other higher multipoles are present in certain segments of a storage ring where this segment is periodically encountered by the particles. With reduced integrability, the motion becomes sensitive to the initial conditions of the particle at the entrance of the segment. This would eventually lead to increase in oscillation amplitude in the rest of the channel and consequently limit the dynamic aperture of the storage ring.

VI. ESTIMATION OF DYNAMIC APERTURE FOR DIFFERENT CASES

The dynamic aperture is defined as the volume in phase space in which all particles remain confined throughout their trajectories in the accelerator. The calculations in this section estimate the projection of the dynamic aperture onto various phase space planes for different values of ψ. In order to perform these calculations, we used 5000 particles that were initially distributed uniformly over the respective plane in phase space, and these were then evolved for 500 lattice periods. It was assumed that particles that travel beyond $r = R$ at any time during this period are not confined. After

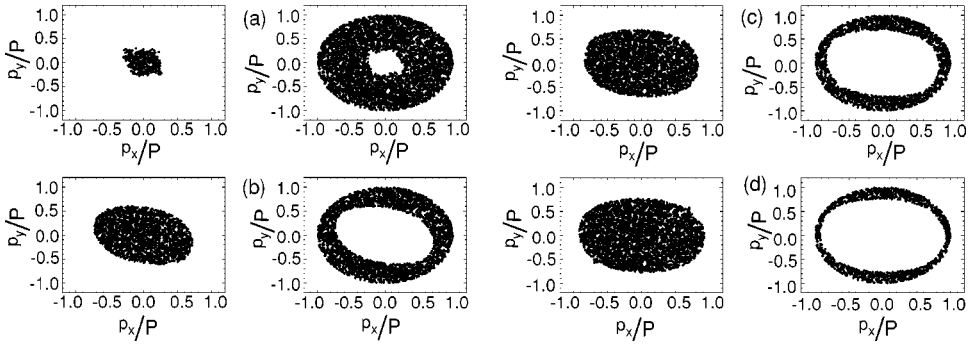

FIG. 7. Initial distribution of confined and unconfined particles lying on the p_x-p_y plane for ψ= (a) 0°, (b) 30°, (c) 60°, (d) 90°.

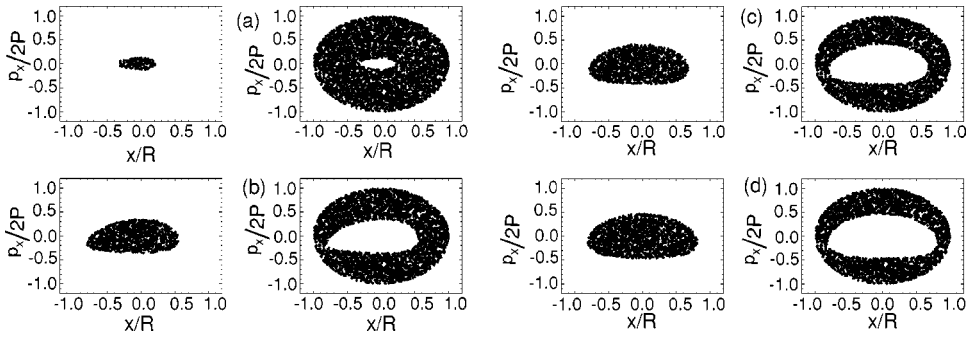

FIG. 8. Initial distribution of confined and unconfined particles lying on the x-p_x plane for ψ= (a) 0°, (b) 30°, (c) 60°, (d) 90°.

identifying the particles that remain confined and those that do not, the initial distribution was separated and the positions of these two sets of particles were plotted. In Figs. 6–8 the left side represents the initial phase space positions of confined particles and the ones on the right represent the unconfined particles from the same initial distribution. It is important to plot the confined and unconfined particles separately in order to ensure that there is no overlap between the two regions, which is true in these simulations. This is expected because all the phase space variables other than those shown in the respective plot were set to zero. Given that the dynamic aperture allows only confined particles and not a mixture of the two, the left side plots represent the projection of the dynamic aperture onto the respective plane.

Figure 6 shows particles lying in the x-y plane that were all initially at rest and distributed uniformly within a circle of radius $r=R$. It may be noticed that when ψ is 0°, a very small number of these particles are confined. This is the case when the quadrupoles and sextupoles completely overlap. The confinement increases very rapidly as one deviates from $\psi=0°$. The area containing the confined particles then gradually increases, reaching a maximum when $\psi=90°$ as predicted by the analytic result of the preceding section. Another interesting feature revealed by these plots is that the area of confinement acquires sharper corners with increasing ψ.

Figure 7 shows confined and unconfined particles from the initial distribution spread out in momentum space. These particles are all located initially at $x=y=0$ and distributed uniformly within a circle of radius $P=0.44R/S$. Once again, a rapid improvement in confinement is seen as one deviates from $\psi=0°$ and there is then a gradual improvement as ψ approaches 90°. Unlike the previous case, the boundary of the region of confinement is smooth for all values of ψ. We also see that the dynamic aperture attains a more circular shape for $\psi=90°$ which could be attributed to weaker dependence of the dynamics on θ.

Figure 8 shows particles distributed over an ellipse such that

$$\frac{x^2}{R^2}+\frac{p_x^2}{(2P)^2}<1, \tag{45}$$

while all other phase space values are zero. Qualitatively, the same behavior is noticeable as in the previous cases. The figures also show that the shape of the dynamic aperture exhibits less symmetry about the origin along the x axis as ψ decreases from 90°. This is also a reflection of increased symmetry in the dynamics along θ.

In contrast to the dramatic improvement in the dynamic aperture seen when ϕ was close to zero, there was only a small improvement when ψ changed from 60° to 90°. This phenomena is important in applications where it is not possible to achieve the idealized condition due to other practical limitations often demanding that such theoretically derived conditions be sufficiently robust to be useful. Improvement in the region of confinement, which is directly related to increased size of the dynamic aperture is an important aspect in improving the performance of particle accelerators. It has been shown how the presence of higher order poles can limit the size of the dynamic aperture in circular accelerators [22].

VII. SUMMARY

In this paper, a condition for improved dynamic aperture is derived for nonlinear lattices in particle accelerators. To start with, the Lie transform perturbation method is presented for averaging over fast time scales. The validity of the method is first verified numerically for a linear periodic focusing system. This averaging procedure is then applied to nonlinear focusing systems with quadrupoles and sextupoles. The Hamiltonian of this system contains terms with mixed variables, a situation in which the Lie transform method greatly simplifies the analysis. This analysis yields a condition for the Hamiltonian to have increased symmetry thereby reducing chaos and increasing the dynamic aperture. The condition leads to a canonical transformation where the new Hamiltonian is independent of its azimuthal variable up to third order in the perturbation expansion. While the analysis was performed explicitly for a lattice with quadrupoles and sextupoles, it was straightforward to show that similar conditions exist when even higher order mutipoles or combinations of these are used. Unlike the traditional approach of analyzing a nonlinear lattice, no assumption was made that the nonlinear focusing was small compared to the linear focusing strength. Hence this analysis is valid even when the nonlinearity is strong enough that the closed form Courant-Snyder solutions are not valid.

Numerical calculations were performed for a particular case in which the focusing components were quadrupoles and sextupoles represented by periodic step function lattices

of equal periodicity. In this case, the condition of azimuthal symmetry in the transformed frame was satisfied by having a phase difference of $\psi=90°$, equivalent to a quarter of a lattice period between the quadrupoles and sextupoles. Single-particle trajectories of particles with angular momentum showed increased chaotic behavior as ψ decreased from 90° to 0°. The size of the dynamic aperture was estimated by allowing the particles to drift up to a maximum radial distance which allowed a maximum tune shift of about 15% when compared to arbitrarily small oscillations. Calculations showed that the size of the dynamic aperture increased rapidly as ψ increased from 0° and gradually reached a maximum as ψ approached 90°. Results showed that the condition was robust enough for possible practical applications.

While the parameters used in the calculations were realistic, they were also simplified. This theory remains to be applied to parameters specific to real machines. For example, it would be interesting to apply it in the use of sextupoles for chromaticity corrections in storage rings with their lattice periods different from that of the quadrupoles and also having a different fill factor. This would still allow conditions for a near integrable system and so one should expect improved confinement by imposing the same.

The derivation of the symmetric transformed Hamiltonian in this paper is expected to benefit various current and proposed applications of nonlinear lattices in particle accelerators. It would also add to previous work on increasing the dynamic aperture of accelerator lattices in the presence of nonlinear components [21]. The Lie transform perturbation method presented here is easily applicable to other areas of Hamiltonian dynamics as well where it is required to perform a time averaging over certain fast time scales.

ACKNOWLEDGMENTS

One of us (K.S.G.) wishes to acknowledge Jim Howard for many useful suggestions. This work was supported by the U.S. Department of Energy under Grant No. DE-FG03-95ER40926.

[1] E. D. Courant and H. S. Snyder, Ann. Phys. (N.Y.) **3**, 1 (1958).
[2] N. Tsoupas, M. Zucker, T. Ward, and C. Snead, Nucl. Sci. Eng. **126**, 71 (1997).
[3] Y. K. Batygin, Phys. Rev. E **57**, 6029 (1998).
[4] Y. K. Batygin, Phys. Rev. E **53**, 5358 (1996).
[5] C. Montag, J. Kewisch, D. Trbojevic, and F. Schmidt, Phys. Rev. ST Accel. Beams **5**, 084401 (2002).
[6] L. Tosi, V. Samaluk, and E. Karantzoulis, Phys. Rev. ST Accel. Beams **6**, 054401 (2003).
[7] L. F. Wang, H. Fukuma, S. Kurokawa, and K. Oide, Phys. Rev. E **66**, 036502 (2002).
[8] J. Gao, Nucl. Instrum. Methods Phys. Res. A **463**, 50 (2001).
[9] P. Channel, Phys. Plasmas **6**, 982 (1999).
[10] R. C. Davidson and H. Qin, Phys. Rev. ST Accel. Beams **4**, 104401 (2001).
[11] S. Tzenov and R. C. Davidson, Phys. Rev. ST Accel. Beams **5**, 021001 (2002).
[12] J. R. Cary, Phys. Rep. **79**, 129 (1981).
[13] G. Hori, Publ. Astron. Soc. Jpn. **18**, 287 (1966).
[14] L. M. Garrido, J. Math. Phys. **10**, 1045 (1968).
[15] A. Deprit, Celest. Mech. **1**, 12 (1969).
[16] R. L. Dewar, J. Phys. A **9**, 2043 (1976).
[17] A. J. Dragt and J. M. Finn, J. Math. Phys. **17**, 2215 (1976).
[18] A. Lichtenberg and M. Lieberman, *Regular and Chaotic Dynamics* (Springer-Verlag, Berlin, 1992).
[19] E. Forest and R. Ruth, Physica D **43**, 105 (1990).
[20] J. Candy and W. Rozmus, J. Comp. Physiol. **92**, 230 (1991).
[21] W. Wan and J. R. Cary, Phys. Rev. Lett. **81**, 3655 (1998).
[22] J. Gao, Nucl. Instrum. Methods Phys. Res. A **451**, 545 (2000).

Control of beam halo formation through nonlinear damping and collimation

Kiran G. Sonnad and John R. Cary
Center for Integrated Plasma Studies and Department of Physics,
University of Colorado, Boulder, Colorado 80309, USA
(Dated: August 1, 2004)

This paper demonstrates that transverse beam halos can be controlled by combining nonlinear focusing and collimation. The study relies on one dimensional, constant focusing particle-in-cell (PIC) simulations and a particle-core model. Beams with linear and nonlinear focusing are studied. Calculations with linear focusing confirm previous findings that the extent and density of the halo depend strongly upon the initial mismatch of the beam. Calculations with nonlinear focusing are used to study damping in the beam oscillations caused by the mismatch. Although the nonlinear force damps the beam oscillations, it is accompanied by emittance growth. This process is very rapid and happens within the first 2-3 envelope oscillations. After this, when the halo is collimated, further evolution of the beam shows that the halo is not regenerated. The elimination of the beam halo could allow either a smaller physical aperture for the transport system or it could allow a beam of higher current in a system with the same physical aperture. This compensates for the loss of particles due to collimation.

PACS numbers: 29.17.+w,29.27.Bd,41.75.-i

I. INTRODUCTION

A major issue facing the functioning of high current accelerators is beam halo formation. High current accelerators find applications in heavy ion fusion, nuclear waste treatment, production of tritium, production of radio isotopes for medical use and spallation neutron sources [1]. The halo is formed by a small intensity distribution of particles surrounding the core of the beam. When such particles drift far away from the characteristic width of the beam, their loss will lead to the production of residual radioactivity of the accelerating system. Many of the above applications require that the number of particles lost to the system must be less that one part in 10^5 - 10^6. With such a stringent requirement, methods to control the beam halo can prove very useful. However there has been relatively less effort spent on devising such methods when compared to the extensive study that has already been done to understand the physics of beam halo formation. The methods employed to study beam halos include analytic models, multiparticle simulations using mainly the particle-core model and PIC simulations [2–20] and also experimental studies [21, 22].

The dependence of the extent of beam halos and the initial beam mismatch has been studied by Wangler *et al*, [15], where it been shown that the maximum dimensionless particle amplitude X_{max}, which is the distance with respect to the matched beam width, can be described by an approximate empirical formula, which is,

$$X_{max} = A + B|ln(\mu)|. \quad (1)$$

Here, A and B are weak functions of the tune depression ratio approximately given by $A = B = 4$ [15], and μ is the initial beam mismatch ratio. This result is not a good estimation for maximum amplitude for μ close to 1. It has also been shown [23] that in addition to increased halo extent, the number of halo particles grows with increased initial mismatch ratio. Batygin [24] showed that one can obtain a better match through nonlinear focusing for a a prescribed charge distribution leading to reduced halo. Thus, it is already well established that reducing the beam mismatch can be an important factor in halo mitigation.

O'Connell *et al* [3] traced the trajectories of various test particles with different initial conditions for beam in a constant, linear focusing channel. This led to the discovery of hybrid trajectories, which undergo a resonant interaction with the core which was later analysed by Gluckstern [2]. The discovery of these hybrid trajectories reveals the limitations on the effectiveness of a one time beam collimation, an issue that will be addressed in this paper. The removal of a halo using a multicollimator system has been studied previously [23] for a periodic linear focusing system.

In the present paper, we propose reducing mismatch by damping the transverse oscillations of the beam through nonlinear focusing before collimation to avoid the need for repeated collimation. Collimation still becomes essential in this process due the emmitance growth accompanying the nonlinear damping. Our studies are based on a radial particle-in-cell (PIC) code along with some preliminary studies using a modified particle-core model. This paper is organized as follows. Section II describes a modified particle-core model for nonlinear focusing and examines the effect of nonlinear focusing on beams through this model. In Sec III, the PIC algorithim and the physical model used to represent the beam has been described and simulation results of beam halo formation with different initial mismatches has been presented. In addition, results showing damping and emittance growth due to nonlinear focusing are also presented. The PIC simulation results are then compared with the particle-core model results. Finally, Sec. IV shows results of a combination of nonlinear focusing and collimation.

II. RESULTS FROM A PARTICLE-CORE MODEL

The particle-core model in this paper serves the purpose of obtaining a qualitatively similar result with a simpler model, thus exhibiting the general nature of the phenomena of damping and emittance growth due to nonlinear focusing. For a linear focusing system, the core is generally represented by the envelope equation, which is not valid for a nonlinear focusing system. Since nonlinear focusing is used in this study, the core is simulated using a different method.

The envelope equation will still be used as a reference to determine parameters such as mismatch ratio and tune depression ratio. Consider a uniform, round, thin beam moving in the axial direction and with a constant axial velocity in a linear and constant focusing channel. Under these conditions, the envelope equation describes the oscillation of R, the radius of the beam with respect to the axial distance s which is a time like variable for a beam with constant axial velocity. This can be expressed as (see for example [25, 26]).

$$\frac{d^2R}{ds^2} + k_0 R - \frac{\epsilon^2}{R^3} - \frac{K}{R} = 0. \tag{2}$$

The focusing force is represented by k_0, K is the space charge perveance which depends upon the intensity, axial velocity and charge to mass ratio of the particles [25, 26]. The rms emittance of the beam ϵ is given by

$$\epsilon = 4\sqrt{\langle x\rangle^2\langle v_x\rangle^2 - \langle x v_x\rangle^2} \tag{3}$$

where the angle bracket represents an average over the particle distribution in position space, x is dispacement along the horizontal axis and $v_x = dx/ds$. For a matched beam, the radius remains constant at $R = R_0$ satisfying the condition, $d^2R/ds^2 = 0$. It was shown by Sacherer [27] that the envelope equation can be generalized to even nonuniform distributions having elliptic symmetry (in this case, azimuthal symmetry). In such a case, the radius may be generalized to $R = 2a$ and $R_0 = 2a_0$, where a is the rms width of the beam, and a_0 is the matched rms width. We define a dimensionless displacement by $X = x/a_0$, a dimensionless velocity by $V_x = v_x/\sqrt{k_o}a_0$, a dimensionless axial distance given by $S = \sqrt{k_0}s$ and a dimensionless rms width given by $M = a/a_0$. The initial mismatch ratio, which is the initial value of M is represented as μ. All calculations will be made with respect to these dimensionless quantities.

The tune depression ratio, $\eta = \epsilon/\sqrt{k_0}R_0^2$ is a dimensionless quantity which gives a measure of the ratio between the wave numbers (or equivalently, frequencies) of a particle oscillating with and without the effect of space charge respectively. While this ratio is exact for any in-core particle in a uniform distribution core, the definition may be extended to provide information on a general beam, especially to determine if a beam is space charge dominated or emittance dominated. A tune depression ratio close to unity represents an emittance dominated beam while if η is much less than unity, it is a space charge dominated beam.

In this paper, the core was simulated through a series of infinitely long charged cylindrical "sheets" which could move radially inward or outward. The field on test particles and the sheets of the core were calculated from Gauss' law using a flux weighted averaging scheme [28]. The test particles did not contribute to the field. The sheets representing the core were advanced in the radial direction while the test particles were moved along the "x" and "y" coordinates. In both the cases, a leap frog scheme was used.

The sheets that represent the core and the test particles satisfy the following equation,

$$\frac{d^2r}{ds^2} = F + F_{sc}, \tag{4}$$

where r is the radial distance and s is the distance along the axis. F is the focusing force and F_{sc} is the space charge force. The purely linear focusing force had the form

$$F = -k_o r, \tag{5}$$

while the focusing force with the nonlinearity included had the form

$$F = -k_1 r - k_2 r^3. \tag{6}$$

The corresponding space charge densities that balance the focusing force will be equal to

$$\rho = \frac{\epsilon_0}{e} 2k_0 \tag{7}$$

and

$$\rho = \frac{\epsilon_0}{e}(2k_1 + 4k_2 r^2) \tag{8}$$

respectively for $r < R_0$, and equal to zero for $r > R_0$, where R_0 is the radius of the matched beam. Here, e is the charge on the particle and ϵ_0 is the permitivity in free space. A mismatch is introduced by expanding or contracting the core and uniformly scaling the charge density to ensure conservation of charge. In performing the calculations in this section, we used a core which was expanded to 1.35 times its matched width. All the sheets comprising the core were initially at rest. In the absence of a nonlinearity, the density of the core is uniform, corresponding to a Kapchinskij-Vladmirskij (KV) distribution [29].

Based on the parameter a_0, the matched rms width according to the envelope equation, we set the linear and nonlinear focusing parameters such that they satified the conditions,

$$k_0 a_0 = k_1 a_0 + k_2 a_0^2, \tag{9}$$

and

$$\frac{k_1}{k_2 a_0^2} = 4. \tag{10}$$

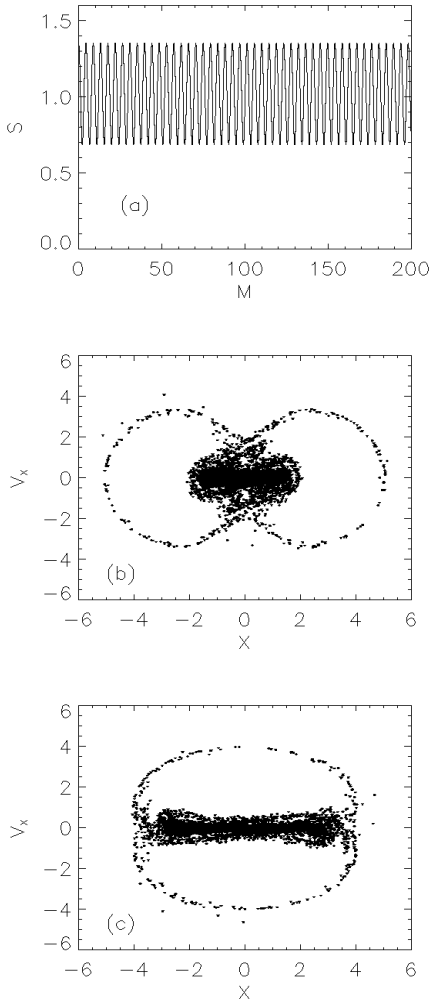

FIG. 1: Linear oscillations. (a) Oscillation of the rms width of the core with $\mu = 1.35$, (b) particle distribution at minimum beam width, (c) distribution at maximum beam width.

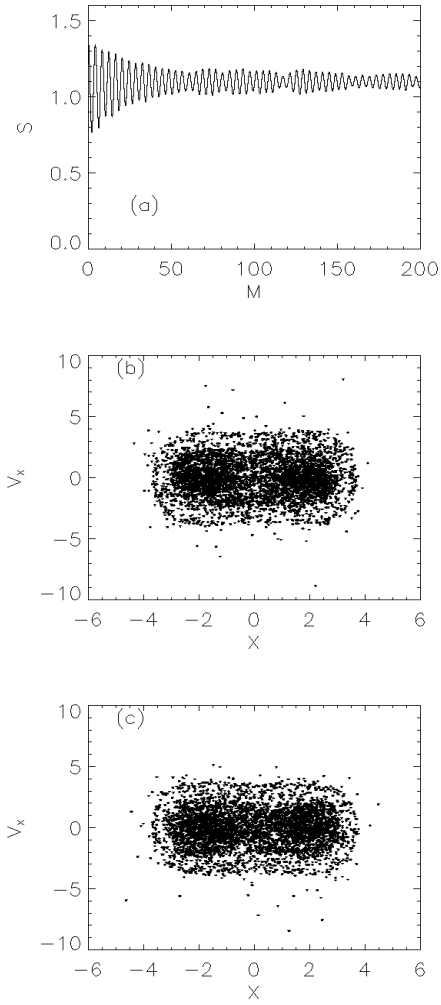

FIG. 2: Nonlinear oscillations. (a) Oscillation of the rms width of the core with $\mu = 1.35$, (b) particle distribution at minimum beam width, (c) distribution at maximum beam width.

Equation 9 indicates that the linear and nonlinear focusing forces were equal at the characteristic distace a_0, and these equations together give a measure of how much the linear force was reduced before introducing the nonlinear component. To study the distribution of the particles, 5000 test particles were used which had an initial Gaussian distribution with an rms width equal to half the initial radius of the core. In the linear case, this makes the core and particle distribution equivalent according to the envelope equation. The initial distribution was identical for the linear and nonlinear case corresponding to a tune depression of 0.1 in the linear focusing channel.

Figure 1(a) shows that the oscillations of the rms width of the core are sustained in the linear focusing case. This is because all the sheets in the core are oscillating in phase and at the same frequency. Figure 1(b) shows the corresponding phase space distribution of test particles moving under the influence of this core at the end of these oscillations when the core was at a minimum rms width, and in Fig 1(c), the core had a minimum rms width.

When nonlinearity is introduced, not only does the density become nonuniform, but the frequency distribution of the oscillations of the charged sheets for a mismatched beam also becomes nonuniform. This is expected to lead to damping of the oscillation in the rms width of the core as shown in Fig. 2(a). The mechanism is well known in many branches of physics as Landau damping. In the damping process, the velocity spread of the beam increases (the beam is heated). Figure 2(b) shows the corresponding phase space distribution of test particles moving under the influence of this core at the end of the oscillations when the core was at a minimum rms width, and in Fig 2(c), the core had a maximum rms width.

It is easily noticed that the width of the core does not

change significantly due to the damping of the oscillations. This would simplify the task of collimating the halo. Since the collimator radius has to be larger than the radius of the core, the phase of the core osillation becomes an important factor in the linear focusing case, where the core is seen to expand to almost twice its minimum size. The figures 2(b) and (c) also show that the beam spreads out in velocity space, while the spread in position space is comparable to the linear focusing case. The spread in velocity is due to a transfer of energy from the mismatched core to the velocity distribution of the particles. However, the particles having a higher kinetic energy must also overcome a stronger potential gradient as they drift away from the core. This restricts the spread in position space which helps restrict the radius of the collimator in position space.

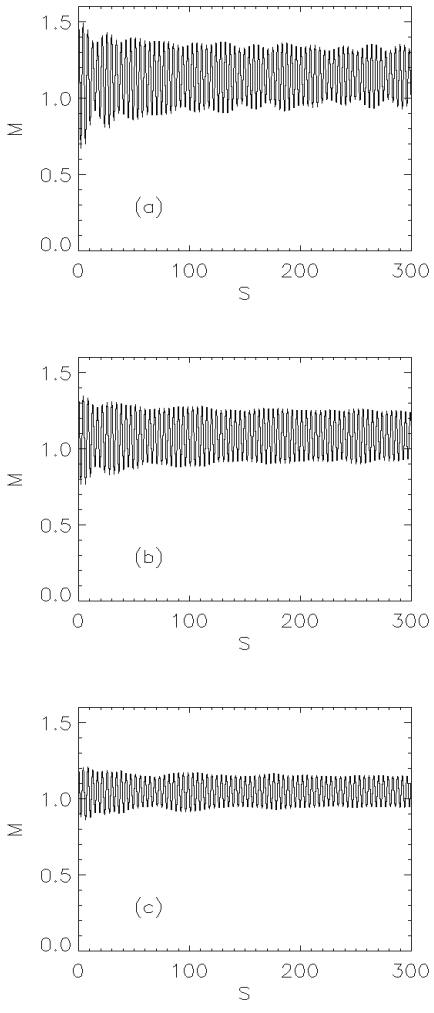

FIG. 3: Oscillation of the rms width of the beam for μ = (a) 1.5, (b) 1.35, (c) 1.2

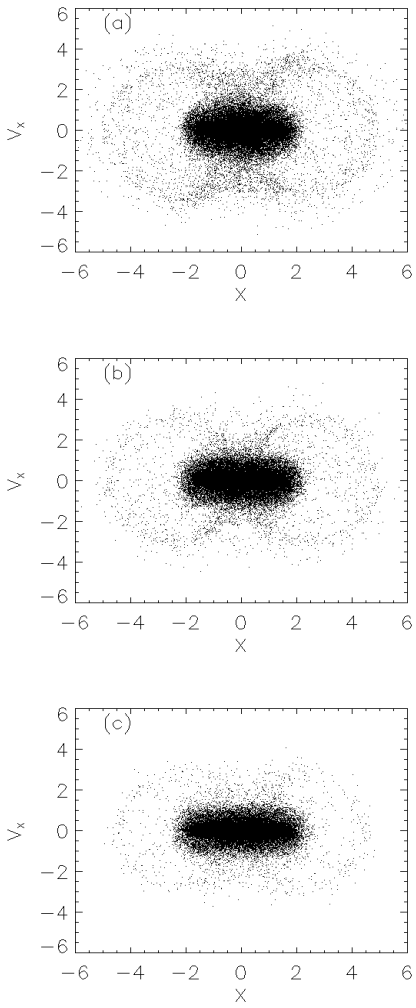

FIG. 4: Phase space distribution after about 40 oscillations at minimum beam width for μ = (a) 1.5, (b) 1.35, (c) 1.2

III. RESULTS FROM PIC SIMULATIONS

The evolution of the beam is now simulated using a radial PIC code. In these calculations, the charge distributions and forces used were azimuthally symmetric, a simplified model for which a one-dimensional field solver is sufficient. Since the fields vary along the radial direction, they are solved using Gauss's law over a radial grid. The particles however, are advanced using the leap frog scheme in cartesian coordinates along the 'x' and 'y' axis. This helps avoid problems arising due to singularities at the origin if radial and azimuthal motion was used [30]. The particles are distributed over the grid using area weighted averaging while the fields were assigned to the particles using flux weighted averaging [28].

We examine the halo generated for beams with different initial mismatch ratios. The beam had an initial Gaussian distribution in position and velocity space. The tune depression calculated from the corresponding enve-

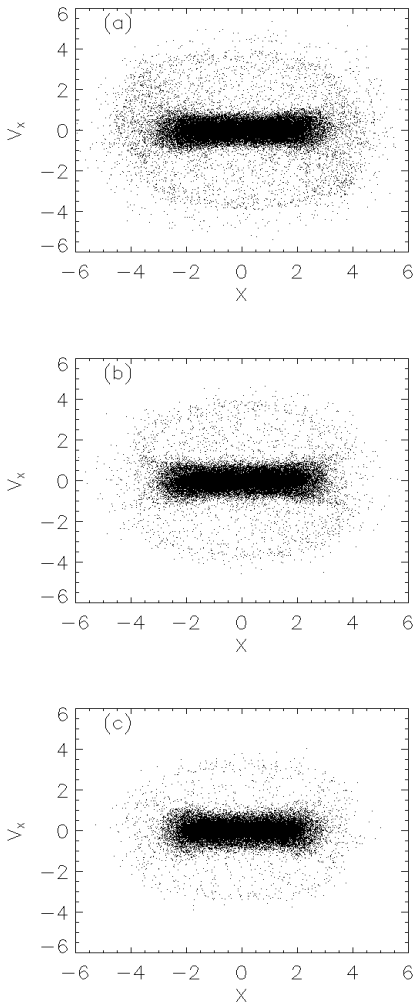

FIG. 5: Phase space distribution after about 40 oscillations at maximum beam width for μ = (a) 1.5, (b) 1.35, (c) 1.2

lope equation was chosen to be 0.1 for all the cases, which implies that the beam is space charge dominated. We used 100,000 particles in all the PIC simulations, which was large enough for the particle distributions to retain the desired azimuthal symmetry.

Figure 3 shows the oscillation of the normalized rms width of the beam with an rms mismatch ratio μ of (a) 1.5, (b) 1.35, (c) 1.2. It may be noticed that there is some initial damping of the oscillations after which a steady pattern emerges. The small initial damping could be attributed to the fact that a Gaussian distribution does not correspond to a Vlasov-Poisson equilibrium, so in the initial stage of the beam oscillation, one could expect some remixing of the distribution in phase space.

To examine the halo formation in these beams, the phase space distribution of the particles is then taken toward the end of the oscillations for two cases, which are (1) when the rms width of the distribution is a minimum, shown in Fig.4 and (2) when it is a maximum shown in Fig. 5. The relative change in the width of the core agrees very well with that obtained using the particle-core for the corresponding initial mismatch of 1.35. It can also be seen that the extent and intensity of the halo increases with increased mismatch, which confirms the need to obtain a reduced mismatch in order to control halo formation.

Figure 6 shows the damping of the oscilation of the rms width of beams with nonlinear focusing. The nonlinear focusing is of the same form as Eq. (6) with $k_0 a_0 = k_1 a_0 + k_2 a_0^3$ and $k_1/(k_2 a_0^2) = 4$, where a_0 is the matched rms width of the beam as predicted by the envelope equation. The initial distributions were indentical to the ones used in the linear focusing case. The parameter μ when defined for a nonlinear focusing case corresponds to the mismatch ratio in the linear focusing channel for the same initial distribution. It may be noticed that the damping takes place in the first $1-2$ rms oscillations while it takes about $5-6$ oscillations in the particle core

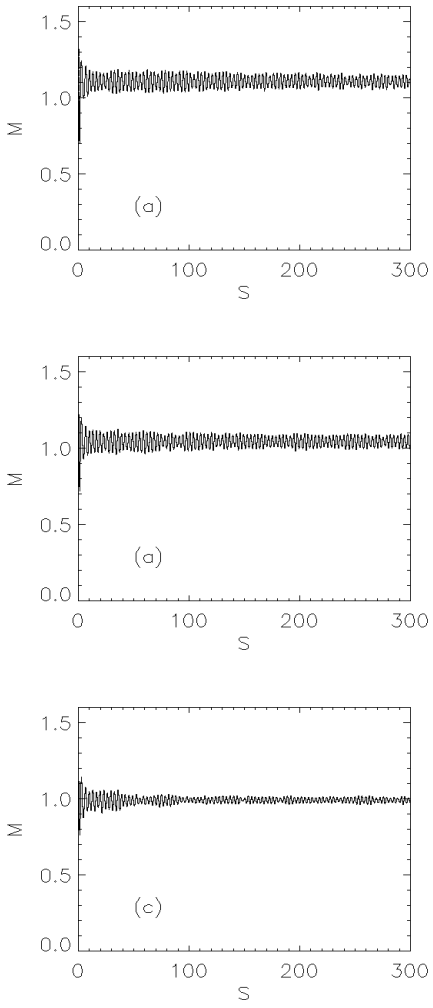

FIG. 6: Oscillation of the rms width of the beam with nonlinear focusing for μ = (a)1.5, (b) 1.35, (c)1.2

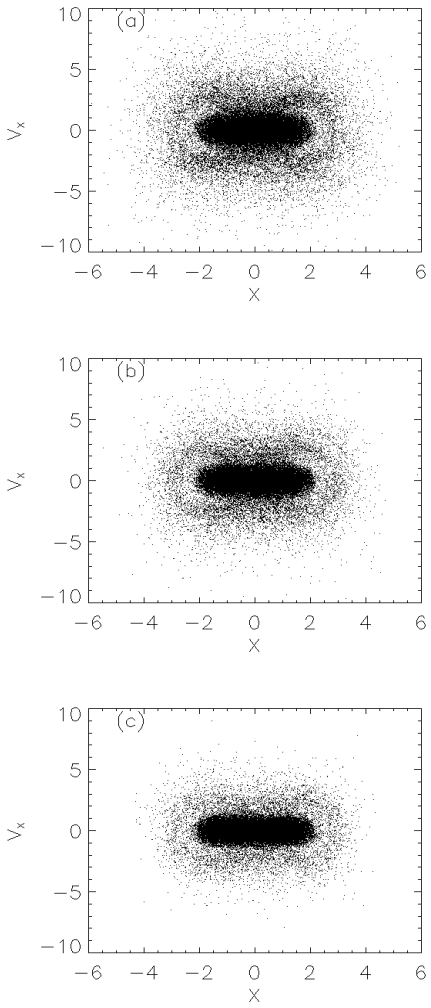

FIG. 7: Oscillation of the rms width of the beam with nonlinear focusing at minimum beam width for μ = (a)1.5, (b) 1.35, (c)1.2

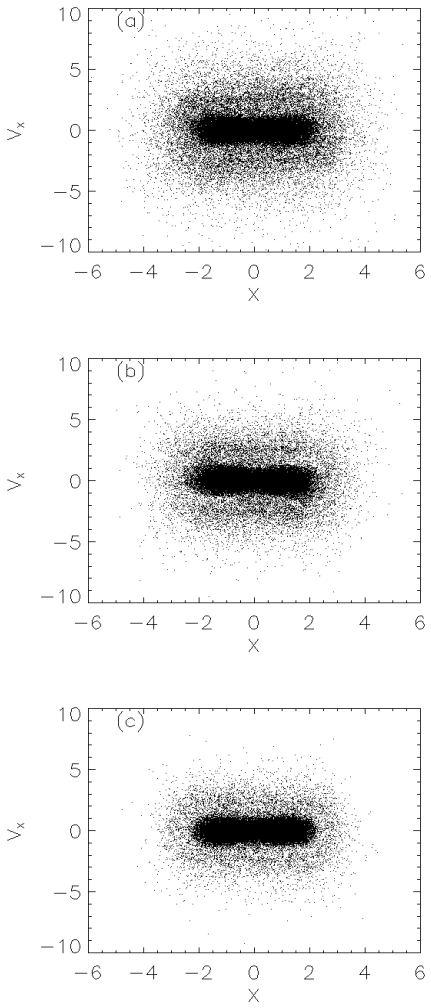

FIG. 8: Oscillation of the rms width of the beam with nonlinear focusing at maximum beam width for μ = (a) 1.5, (b) 1.35, (c) 1.2

model. Also, the final amplitude of the oscillation after the damping is seen to decrease with decrease in μ, the initial "mismatch".

Figures 7 and 8 show the corresponding phase space distribution of the particles when the beam width was a minimum and a maximum respectively. Similar to the particle core model results, the rms width of the beam does not change significantly while oscillating as a consequence of the damping. Also, these figures show that the particles spread far in velocity space while their spread in position space is comparable to the linear focusing case.

The PIC simulation results in general show a similar response to nonlinear focusing when compared to the particle-core model, which is damping accompanied by emittance growth. However, we see in Fig. 6 that the damping is more rapid in the PIC simulations. In the particle core model, we see a gap between the halo particles and the core for linear focusing which is not seen in the PIC simulation. This could be attributed to the fact that the particles in the particle-core model do not contribute to the field due to which they are influenced only by the perfectly linear oscillations of the core. For the same initial conditions used in both the models, which is $\mu = 1.35$, the size of the core and the extent of the halo was the same for both linear and nonlinear focusing.

IV. COLLIMATION WITH NONLINEAR FOCUSING

This section will show that the combination of nonlinear focusing and collimation eliminates the beam halos permanently. There is no established quantitative definition as yet of a beam halo although recent efforts are being made to quantify such a halo [31]. The halo was

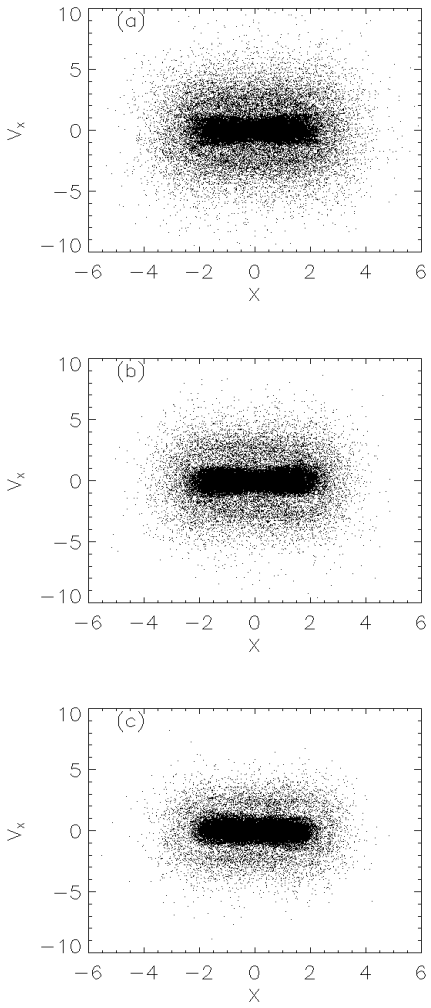

FIG. 9: Phase space distribution of particles just before collimation for a beam with nonlinear focusing for μ = (a) 1.5, (b) 1.35, (c) 1.2

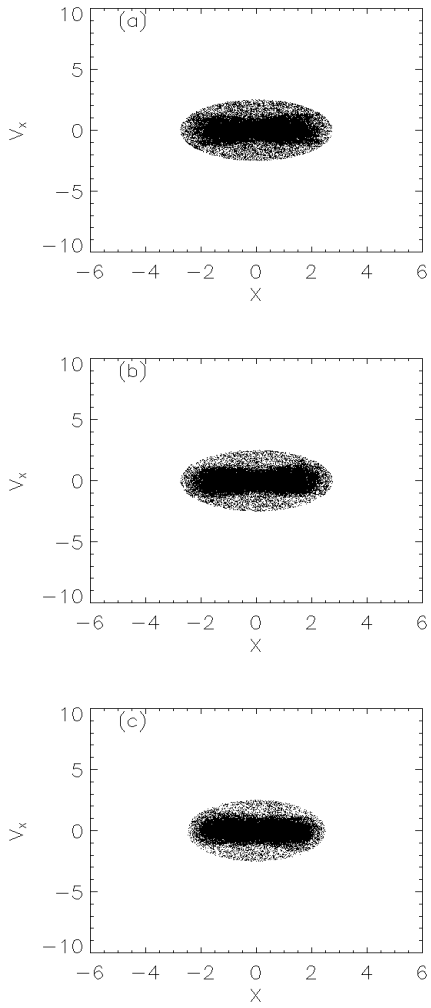

FIG. 10: Phase space distribution of particles just after collimation for a beam with nonlinear focusing for μ = (a)1.5, (b)1.35, (c)1.2

visually identified and collimated in phase space over an ellipse that satisfied the equation,

$$\frac{X^2+Y^2}{c^2}+\frac{V_x^2+V_y^2}{d^2}=1. \qquad (11)$$

The values of c and d are given in Table I. Care was taken so that the high density area constituting core was not scraped off by examination of enlarged figures of the distribution. The table also shows that the number of particles lost due to collimation reduces with reduced mismatch. Thus, having a small initial mismatch is still an advantage but this is not possible to achieve in most practicle applications.

Figure 9 shows the distribution of the particles just before collimation. The rms width of the beam was at a maximum for all the cases. Although the collimation was always perfomed when the rms beam width was a maximum, it has been shown previously in this paper that the phase of the oscillation is not a critical factor due to the nonlinear damping. The distribution of these particles are very similar to the ones seen in Fig.8 although they were taken at a much earlier stage after the damping. This shows that there is little change as the beam propagates once the damping has been achieved.

TABLE I: table specifying the parameters used for collimation of the beam

μ=1.5	c=2.75	d=2.5	particle loss = 15.15 %
μ=1.3	c=2.75	d=2.5	particle loss = 10.1 %
μ=1.2	c=2.5	d=2.5	particle loss = 6.4 %

Fig 10 shows the distribution just after collimatiom. This distribution shows the that core has been retained along with some particles surrounding it. For such particles lying close to the core, there is no existing method to identify those with stable motion and potential halo

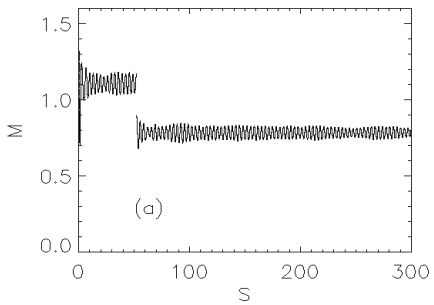

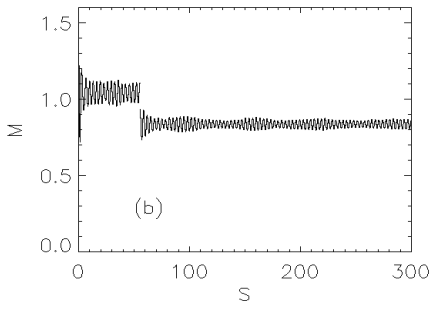

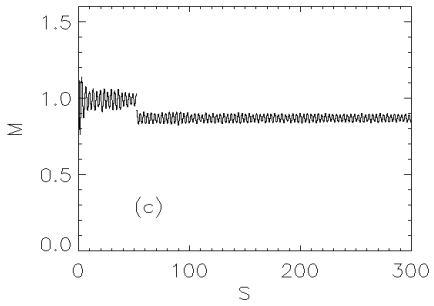

FIG. 11: Oscillation of the rms width of the beam with nonlinear focusing showing collimation for μ =(a)1.5,(b)1.35, (c) 1.2

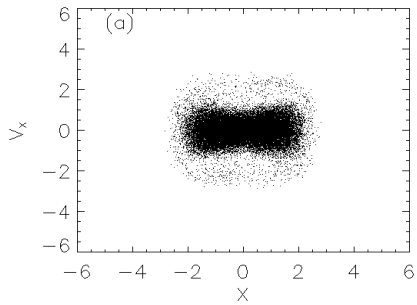

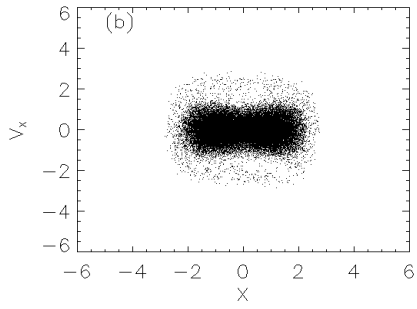

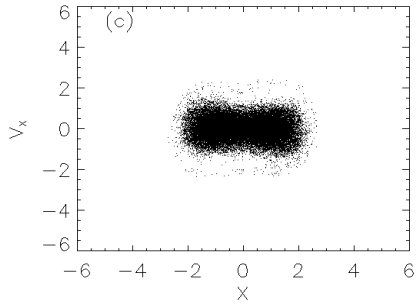

FIG. 12: Phase space distribution at the end of of oscillations shown in Fig. 11 for μ = (a)1.5, (b)1.35, (c)1.2

particles. We believe that sufficient number of these particles have been retained to allow this uncertainty.

Figure 11 shows the oscillation of the beam along with the collimation. The rms size of the beam abrubtly drops due to the elimination of particles far away from the center. It may be noticed that the damping is not affected and is sustained even after the collimation is performed which is an important phenomenon that ensures that the halo is not reproduced.

Figure 12 shows the distribution of particles at the end of the oscillations shown in Fig. 11 when the rms width was a maximum. It is clear that the particles that stray far away from the core are completely eliminated. These figures may be compared with the corresponding ones in the previous section for the same mismatch with linear focusing. Although the distributions were taken when the rms width was a maximum, this would not make a significant difference from another phase of the rms oscillation since their amplitudes are already well damped. The extent of the beam remains the same after this process regardless of the initial mismatch, while, the number of particles lost in the collimation increases with increased mismatch.

The large spread in velocity space which is a result of the nonlinear damping implies that more particles need to be collimated away if a small velocity distribution is desired. Despite this drawback, the absence of a halo would enable one to have a broader beam that would more than compensate for the additional loss in particles. For example, assume that particles cannot be allowed beyond a distance of $X = 3$. The particle distributions shown in Fig. 12 clearly satisfy the restrictions, while the ones shown in Figs. 4 and 5 do not because of the extended halo produced due to linear focusing. In addition to this, the core itself stretches to $X = 3$ for linear focusing as seen in Fig. 5 while Fig. 12 shows that even the at maximum rms width, the beam is restricted

to well within a distance of $X = 3$. All this implies that the initial beam will have to be considerably narrower in the case of linear focusing in order to restrict the halo to within a distance of $X = 3$ and thus allowing less particles in the channel. Another point to be noted is that the nonlinear focusing requires only a localized collimation system, while collimation with linear focusing will require repeated collimation due to the regeneration of the halo as already shown by Ikegami [23].

V. SUMMARY

In this paper, we have proposed a new method that combines nonlinear damping and beam collimation to control beam halos. Our results showed that particles oscillating with large amplitudes compared with the width of the core can be completely eliminated with this mechanism making the need for repeated collimation unnecesary.

Particle-core and PIC simulations showed that nonlinear focusing leads to damping thus reducing the beam mismatch. However, the damping was accompanied by the particle distribution spreading in the velocity space. This is a result of transfer of energy stored in the mismatch to the velocity distribution of the particles. The high velocity particles are prevented from straying far away from the beam due to the strong focusing force exerted by the nonlinear component at large radial distances. The beam was collimated soon after the nonlinear damping was achieved, and the damped oscillations prevented further halo formation. Results showed that the particles with large amplitude oscillations were completely eliminated. The apparent drawbacks of this process is the spread of particles in velocity space because of which the collimation process results in loss of particles. However, we argue that the knowledge that beam halos are controlled would enable one to extend the beam closer to the walls, thus increasing the beam current that would more than compensate for the loss in collimation.

It must be mentioned that the model used here was idealized in many respects because it had constant focusing and was purely radial. While this system is nearly integrable in the absence of space charge, this would not be true in real systems with nonlinear focusing components. This is because the Courant-Snyder invariants [32] are broken when nonlinear focusing components like sextupoles or octupoles are used. This will cause the orbits to be chaotic leading to poor confinement even in the absence of space charges. However, it has been shown that [33] it is possible to reduce the nonlinear system to an equivalent, continuous and radially focusing one upon averaging over the lattice period given that the nonlinear components are arranged in a specific manner along with an alternate gradient quadrupole focusing system. It has also been shown that this symmetry can be retained in the presence of space charge forces [34]. We propose the use of such a lattice for further study involving a two dimensional study.

Since the method proposed in this paper is not specific to a particular application, diffret applications will demand conditions that may be different to the ones used in this paper. For example, collimation of the halo is being studied for the SNS accumulator ring [35]. The collimators use scrapers and absorbers to clean the transverse halo. The accumulator ring already has a straight section dedicated to the collimation system. Applying the proposed method proposed to such a system will require more extensive study. This is beacause the tune depression in this ring is close to unity, in contrast to the ones chosen in this paper. In addition to this, including nonlinear components in a ring will not be straight forward due to the effect of resonances and beam instabilities. However, one of the advantages of the proposed method is the fact that the nonlinear damping is only a transient process. Once the collimation is achieved, the system may be adiabatically matched to a linear focusing system. The possibility of such a matching has been analyzed by Batygin [36] and could be considered in such a study.

Less effort has been spent in devising methods to eliminate beam halos when compared to the extensive study of the properties of halo production itself. This paper could be an important step toward this direction. The results are encouraging enough to perform simulations in higher dimensions using nonlinear focusing components such as sextupoles or octupoles along with realistic designs for collimators.

VI. ACKNOWLEDGMENTS

One of us (KS) wishes to thank Steve Lund and Alex Friedman for their input while writing the the radial PIC code. This work was supported by the U.S. Department of Energy under Grant No. DE-FG03-95ER40926.

[1] D. Jeon and et al, Phys. Rev. ST Accel and Beams **5**, 094201 (2002).
[2] R. L. Gluckstern, Phys Rev. Lett. **73**, 1247 (1994).
[3] J. S. O'Connell, T. Miller, R. S. Mills, and K. R. Crandall, *Proceedings of the 1993 Particle Accelerator Conferemce, Washington, DC, edited by S. T. Corneliussen* p. 3757 (1993).
[4] J. Lagniel, Nucl. Instrum. Methods Phys. Res, Sect A **345**, 405 (1994).
[5] J. Lagniel, Nucl. Instrum. Methods Phys. Res, Sect A **345**, 46 (1994).
[6] R. A. Jameson, los Alamos Report No. LA-UR-94-3753.
[7] T. P. Wangler, los Alamos Report No. LA-UR-94-1135.
[8] C. Chen and R. A. Jemeson, Phys Rev E **52**, 3075 (1995).

[9] R. D. Ryan and S. Habib, Part Accel **55**, 365 (1996).
[10] H. Okamoto and M. Ikegami, Phys Rev E **55**, 4694 (1997).
[11] R. L. Gluckstern, A. V. Fedotov, S. S. Kurennoy, and R. D. Ryne, Phys Rev E **58**, 4 (1998).
[12] A. V. Fedotov, R. L. Gluckstern, S. S. Kurennoy, and R. D. Ryne, Phys Rev ST Accel. Beams **2**, 014201 (1999).
[13] M. Ikegami, Phys Rev E **59**, 2330 (1999).
[14] T. Wang, Phys. Rev. E **61**, 855 (2000).
[15] T. Wangler, K. R. Crandall, R. Ryne, and T. S. Wang, Phys. Rev. ST Accel and Beams **1**, 084201 (1998).
[16] J. Qiang and R. Ryne, Phys. Rev. ST Accel and Beams **3**, 064201 (2000).
[17] R. L. Gluckstern, W.-H. Cheng, and H. Ye, Phys. Rev. Lett **75**, 2835 (1995).
[18] R. L. Gluckstern, W.-H. Cheng, S. S. Kurennoy, and H. Ye, Phys. Rev. E **54**, 6788 (1996).
[19] S. Strasburg and R. C. Davidson, Phys. Rev. E **61**, 5753 (2000).
[20] N. C. Petroni, S. D. Martino, S. D. Siena, and F. Illuminati, Phys. Rev. ST Accel and Beams **6**, 034206 (2003).
[21] C. K. Allen and et al, Phys. Rev. Lett **89**, 214802 (2002).
[22] M. Reiser and et al, Phys Rev. Lett. **61**, 2933 (1998).
[23] M. Ikegami and H. Okamoto, Jpn. J. Appl. Phys. **36**, 7028 (1997).
[24] Y. K. Batygin, Phys. Rev. E **57**, 6020 (1998).
[25] R. C. Davidson and H. Qin, Physics of Intense Charged Particle Beams in High Energy Accelerators(World Scientific, Singapore, 2001) (2001).
[26] T. P. Wangler, RF Linear Accelerators (Wiley Series in Beam Physics and Accelerator Technology) (1998).
[27] F. J. Sacherer, IEEE Trans. Nucl. Sci. **18**, 1105 (1971).
[28] C. K. Birdsall and A. B. Langdon, Plasma Physics via Computer Simulation (The Adam Hilger Series on Plasma Physics) (1991).
[29] I. Kapchinskij and V. Vladimirskij, *Proceedings of the International Conference on High Energy Accelerators and Instrumentation"* (CERN Scientific Information Services, Geneva 1959) p. 274 (1959).
[30] A. Friedman and S. Lund, private discussion.
[31] C. K. Allen and T. P. Wangler, Phys. Rev. ST Accel and Beams **5**, 124202 (2002).
[32] E. D. Courant and H. S. Snyder, Annals of Physics **3**, 1 (1958).
[33] K. G. Sonnad and J. R. Cary, Phys. Rev. E **69**, 056501 (2004).
[34] K. G. Sonnad and J. R. Cary, in preparation.
[35] N. Catalan-Lasheras, Y. Y. Lee, H. Ludewig, N. Simons, and J. Wei, Phys Rev. ST Accel and Beams **4**, 010101 (2001).
[36] Y. K. Batygin, Phys. Rev. E **54**, 5673 (1996).